5-2019

Defining Relationships Between Geometry and Behavior of Bistable Composite Laminates

Salil Abhijit Phatak
Clemson University, salil_170294@yahoo.co.in

DEFINING RELATIONSHIPS BETWEEN GEOMETRY AND BEHAVIOR OF BISTABLE COMPOSITE LAMINATES

A Thesis
Presented to
the Graduate School of
Clemson University

In Partial Fulfillment
of the Requirements for the Degree
Master of Science
Mechanical Engineering

---

by
Salil Abhijit Phatak
May 2019

Accepted by:
Dr. Oliver Myers, Committee Chair
Dr. Georges Fadel
Dr. Suyi Li

ABSTRACT

Bistability is exhibited by a composite laminate when it rests in two stable equilibrium states. Certain composite laminates exhibit bistability by having two stable curvatures of opposite sign with the two axes of curvature perpendicular to each other. These laminates can be actuated from one state to the other. The actuation from the original post-cure shape to the second shape is called as 'snap-through' and the reverse actuation is called as 'snap-back'. This phenomenon can be used in applications for morphing structures, energy harvesting, and other applications where there is a conflicting requirement of a structure that is load-carrying, light, and shape-adaptable. A number of researchers have tried to identify the key parameters affecting the behavior of such laminates. Geometric parameters such as stacking sequence, fibre orientation, cure cycle, boundary conditions, and force of actuation, have all been investigated. The objective of this research is to define relationships between the length, width and thickness of square and rectangular laminates required to achieve bistability. Using these relations, multiple bistable laminates up to 36 by 36 inch^2 are fabricated with varying thickness up to 30 CFRP layers. Further, for laminates that are bistable, it is necessary to be able to predict the curvature and force required for actuation. Therefore, a method is developed which allows us to predict the curvature of both stable shapes, as well as the force of actuation of laminates for which the thickness and dimensions are known. Finite Element Analysis is used to carry out the numerical calculations, which are validated by fabricating laminates. The curvature of these laminates is measured using a profilometer and the force of actuation is recorded using a universal test set-up.

DEDICATION

Dedicated to my family and friends.

ACKNOWLEDGMENTS

I would like to sincerely thank my advisor Dr. Oliver Myers for allowing me work on this project and for his guidance and support. I would also like to thank my committee members Dr. Suyi Li and Dr. Georges Fadel for their guidance and feedback, and especially Dr. Li for allowing me to use some of the equipment in his lab.

This work would not have been possible without the help from staff members in the Mechanical Engineering machine shop and the support and help from my fellow students doing research on the topic of bistable composites.

TABLE OF CONTENTS

Page

Table of Contents (Continued) Page

LIST OF TABLES

LIST OF FIGURES

List of Figures (Continued)

List of Figures (Continued)

List of Figures (Continued)

List of Figures (Continued)

Figure Page

List of Figures (Continued)

Figure Page

CHAPTER ONE

INTRODUCTION

Composite Materials

A composite is a structural material that consists of two or more combined constituents that are combined at a macroscopic level and are not soluble in each other [1]. A composite material usually consists of a matrix and a reinforcement. The reinforcing material is embedded inside the matrix material. The two constituent materials have different physical and/or chemical properties from each other and the composite material thus has a combination of properties which differs from the constituent materials. Some of the properties which can be improved by creating a composite material are strength, stiffness, fatigue life, corrosion resistance, weight, thermal insulation, and so on. The earliest form of a composite material was to combine mud and straws to form bricks. Today, composite materials are used in aircrafts, space shuttles, prosthetics, and in other demanding conditions where there are special requirements for a material.

Composite materials can be categorized based on geometry as 1. Fibrous composite materials – Fibers in a matrix, 2. Laminated composite materials – Layers of various materials, 3. Particulate composite materials – Particles in a matrix, 4. Combination of the above. Based on the matrix material, composites can be classified as 1. Polymer matrix composites, 2. Metal matrix composites, 3. Ceramic matrix composites, 4. Carbon composites. The presented research is focused on Laminated Fibre Reinforced Polymer Composites (CFRP).

CFRP Laminates

A lamina is a flat arrangement of unidirectional fibers or woven fibers in a matrix. CFRP Laminates consist of Carbon Fibers embedded into an epoxy matrix. For the material used in this research, the fibers are unidirectional inside the matrix as shown in figure 1.1.

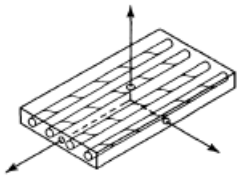

Figure 1.1 Lamina with unidirectional fibers [2]

A laminate is a bonded stack of laminae with various orientations of principal material directions in the laminae as shown in figure 1.2.

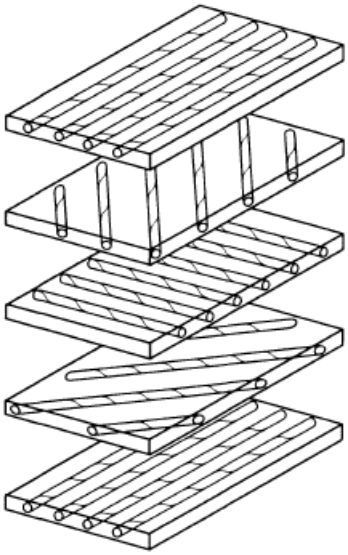

Figure 1.2 Exploded view of a laminate. [2]

The stress-strain relation of a laminate can be explained using the Classical Lamination Theory (CLT). The elastic constants for the laminate used in the CLT are found using three concepts: 1. Macromechanical behavior of a lamina, 2. Micromechanical behavior of a lamina, 3. Macromechanical behavior of a laminate.

Macromechanical behavior of a lamina

A lamina is the building block of a laminate. Macromechanical analysis of a lamina helps us understand the response of a lamina to an applied stress. The stress-strain relation of a lamina is developed in the following section. The stress-strain according to Hooke's law is written in contracted notation as follows:

$$\sigma_i = C_{ij}\varepsilon_j, \text{ where i,j = 1, 2,… 6} \tag{1.1}$$

Where σ_i are the stress components, C_{ij} is the stiffness matrix and ε_j are the strain components. These stress and strain components can be shown on a three dimensional cube as shown in figure 1.3.

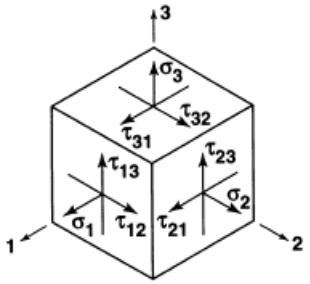

Figure 1.3 Stresses and strains on an element [2]

The contracted notations are defined in comparison with the usual tensor notation as given in table 1.1. The engineering shear strain γ_{ij} is equal to twice the tensor shear strain ε_{ij}. The stiffness matrix C_{ij} has 36 constants as per the contracted notation as shown in equation 1.2.

Stresses		Strains	
Tensor Notation	Contracted Notation	Tensor Notation	Contracted Notation
σ_{11} (σ_1)	σ_1	ε_{11}(ε_1)	ε_1
σ_{22} (σ_2)	σ_2	ε_{11}(ε_1)	ε_2
σ_{33} (σ_3)	σ_3	ε_{11}(ε_1)	ε_3
τ_{23} (σ_{32})	σ_4	$\gamma_{23} = 2\varepsilon_{23}$	ε_4
τ_{31} (σ_{31})	σ_5	$\gamma_{31} = 2\varepsilon_{31}$	ε_5
τ_{12} (σ_{12})	σ_6	$\gamma_{12} = 2\varepsilon_{12}$	ε_6

Table 1.1 Comparison between tensor notation and contracted notation for stresses and strains [2]

An anisotropic material is one that has different material properties in different directions. The stress-strain relation for an anisotropic material given by Hooke's Law, in matrix form thus becomes:

$$\begin{bmatrix}\sigma_1\\ \sigma_2\\ \sigma_3\\ \tau_{23}\\ \tau_{31}\\ \tau_{12}\end{bmatrix}=\begin{bmatrix}C_{11} & C_{12} & C_{13} & C_{14} & C_{15} & C_{16}\\ C_{21} & C_{22} & C_{23} & C_{24} & C_{25} & C_{26}\\ C_{31} & C_{32} & C_{33} & C_{34} & C_{35} & C_{36}\\ C_{41} & C_{42} & C_{43} & C_{44} & C_{45} & C_{46}\\ C_{51} & C_{52} & C_{53} & C_{54} & C_{55} & C_{56}\\ C_{61} & C_{62} & C_{63} & C_{64} & C_{65} & C_{66}\end{bmatrix}\begin{bmatrix}\varepsilon_1\\ \varepsilon_2\\ \varepsilon_3\\ \gamma_{23}\\ \gamma_{31}\\ \gamma_{12}\end{bmatrix} \tag{1.2}$$

For an orthotropic material, there are two orthogonal planes of symmetry. The number of constants in the stiffness matrix C_{ij} are then reduced to nine and the stress-strain relation is then given by equation 1.3

$$\begin{bmatrix}\sigma_1\\ \sigma_2\\ \sigma_3\\ \tau_{23}\\ \tau_{31}\\ \tau_{12}\end{bmatrix}=\begin{bmatrix}C_{11} & C_{12} & C_{13} & 0 & 0 & 0\\ C_{21} & C_{22} & C_{23} & 0 & 0 & 0\\ C_{31} & C_{32} & C_{33} & 0 & 0 & 0\\ 0 & 0 & 0 & C_{44} & 0 & 0\\ 0 & 0 & 0 & 0 & C_{55} & 0\\ 0 & 0 & 0 & 0 & 0 & C_{66}\end{bmatrix}\begin{bmatrix}\varepsilon_1\\ \varepsilon_2\\ \varepsilon_3\\ \gamma_{23}\\ \gamma_{31}\\ \gamma_{12}\end{bmatrix} \tag{1.3}$$

A unidirectional composite lamina is a transversely isotropic material, meaning that, at every point in the material there exists a plane in which the mechanical properties are equal in all directions. For example, if isotropy exists in the 2-3 plane then the subscripts 2 and 3 of the coefficients in the stiffness matrix are interchangeable. The number of constant is then reduced to five and the equation is given by equation 1.4.

$$\begin{bmatrix}\sigma_1\\ \sigma_2\\ \sigma_3\\ \tau_{23}\\ \tau_{31}\\ \tau_{12}\end{bmatrix}=\begin{bmatrix}C_{11} & C_{12} & C_{12} & 0 & 0 & 0\\ C_{12} & C_{22} & C_{23} & 0 & 0 & 0\\ C_{12} & C_{23} & C_{22} & 0 & 0 & 0\\ 0 & 0 & 0 & \dfrac{(C_{22}-C_{23})}{2} & 0 & 0\\ 0 & 0 & 0 & 0 & C_{66} & 0\\ 0 & 0 & 0 & 0 & 0 & C_{66}\end{bmatrix}\begin{bmatrix}\varepsilon_1\\ \varepsilon_2\\ \varepsilon_3\\ \gamma_{23}\\ \gamma_{31}\\ \gamma_{12}\end{bmatrix} \tag{1.4}$$

Usually, material characterization tests are performed with a known load. The resulting displacement is then measured and used to calculate the engineering constants. These constants are the components of the compliance matrix, which gives the strain-stress relation. Thus, since the compliance matrix is more directly obtained, the equation for strain-stress is used and is given in equation 1.5.

$$\begin{bmatrix} \varepsilon_1 \\ \varepsilon_2 \\ \varepsilon_3 \\ \gamma_{23} \\ \gamma_{31} \\ \gamma_{12} \end{bmatrix} = \begin{bmatrix} S_{11} & S_{12} & S_{12} & 0 & 0 & 0 \\ S_{12} & S_{22} & S_{23} & 0 & 0 & 0 \\ S_{12} & S_{23} & S_{22} & 0 & 0 & 0 \\ 0 & 0 & 0 & 2(S_{22}-S_{23}) & 0 & 0 \\ 0 & 0 & 0 & 0 & S_{66} & 0 \\ 0 & 0 & 0 & 0 & 0 & S_{66} \end{bmatrix} \begin{bmatrix} \sigma_1 \\ \sigma_2 \\ \sigma_3 \\ \tau_{23} \\ \tau_{31} \\ \tau_{12} \end{bmatrix} \tag{1.5}$$

The coefficients in the stiffness matrix are the slopes of a stress-strain curve or the slope of a strain-stress curve. These are written in terms of engineering constants and the equation for strain-stress of a lamina then becomes as given in equation 1.6.

$$\begin{bmatrix} \varepsilon_1 \\ \varepsilon_2 \\ \varepsilon_3 \\ \gamma_{23} \\ \gamma_{31} \\ \gamma_{12} \end{bmatrix} = \begin{bmatrix} \frac{1}{E_1} & -\frac{\nu_{21}}{E_2} & -\frac{\nu_{31}}{E_3} & 0 & 0 & 0 \\ -\frac{\nu_{12}}{E_1} & \frac{1}{E_2} & -\frac{\nu_{32}}{E_3} & 0 & 0 & 0 \\ -\frac{\nu_{13}}{E_3} & -\frac{\nu_{23}}{E_2} & \frac{1}{E_3} & 0 & 0 & 0 \\ 0 & 0 & 0 & \frac{1}{G_{23}} & 0 & 0 \\ 0 & 0 & 0 & 0 & \frac{1}{G_{31}} & 0 \\ 0 & 0 & 0 & 0 & 0 & \frac{1}{G_{12}} \end{bmatrix} \begin{bmatrix} \sigma_1 \\ \sigma_2 \\ \sigma_3 \\ \tau_{23} \\ \tau_{31} \\ \tau_{12} \end{bmatrix} \tag{1.6}$$

A lamina is generally considered to be under plane stress. This is because laminae cannot sustain high stresses in directions that are not parallel to the fibers and are therefore

not loaded in that manner. Thus, for a plane stress condition the strain-stress relation is given by equation 1.7.

$$\begin{bmatrix} \varepsilon_1 \\ \varepsilon_2 \\ \gamma_{12} \end{bmatrix} = \begin{bmatrix} \frac{1}{E_1} & -\frac{\nu_{21}}{E_2} & 0 \\ -\frac{\nu_{12}}{E_1} & \frac{1}{E_2} & 0 \\ 0 & 0 & \frac{1}{G_{12}} \end{bmatrix} \begin{bmatrix} \sigma_1 \\ \sigma_2 \\ \tau_{12} \end{bmatrix} \tag{1.7}$$

The stress-strain relation then becomes as shown in equation 1.8.

$$\begin{bmatrix} \sigma_1 \\ \sigma_2 \\ \tau_{12} \end{bmatrix} = \begin{bmatrix} Q_{11} & Q_{12} & 0 \\ Q_{12} & Q_{22} & 0 \\ 0 & 0 & Q_{66} \end{bmatrix} \begin{bmatrix} \varepsilon_1 \\ \varepsilon_2 \\ \gamma_{12} \end{bmatrix} \tag{1.8}$$

Q_{ij} are the reduced stiffness coefficients. They are found from the engineering coefficients given by equations 1.9 – 1.12.

$$Q_{11} = \frac{E_1}{1-\nu_{12}\nu_{21}} \tag{1.9}$$

$$Q_{22} = \frac{E_2}{1-\nu_{12}\nu_{21}} \tag{1.10}$$

$$Q_{12} = \frac{\nu_{12}E_2}{1-\nu_{12}\nu_{21}} = \frac{\nu_{21}E_1}{1-\nu_{12}\nu_{21}} \tag{1.11}$$

$$Q_{66} = G_{12} \tag{1.12}$$

In a single lamina, the fibers are oriented in a specific direction and the lamina has the potential to be under stress in the fiber direction. To have stiffness in other directions, a laminate is created such that other laminae have their fibers oriented in the direction of

stresses. In this way, the fibers can be orientated in all directions. Therefore, the equations in the local coordinates (1, 2, 3) need to be transformed into global coordinates (x, y, z). Let's consider a lamina with its fibers oriented at an angle θ. The reduced stiffness matrix [Q] is transformed to $[\bar{Q}]$ using the transformation matrix. The transformation matrix is given by equation 1.13.

$$[T] = \begin{bmatrix} \cos^2\theta & \sin^2\theta & 2\sin\theta\cos\theta \\ \sin^2\theta & \cos^2\theta & -2\sin\theta\cos\theta \\ -\sin\theta\cos\theta & \sin\theta\cos\theta & \cos^2\theta - \sin^2\theta \end{bmatrix} \tag{1.13}$$

$[\bar{Q}]$ is then found using equation 1.14.

$$\bar{Q} = [T]^{-1}[Q][T]^{-T} \tag{1.14}$$

We have thus found the stress-strain and the strain-stress relations for a lamina. In the following section, we will look at the micromechanical analysis of a lamina.

Micromechanical Analysis of a Lamina

In the previous section we defined the stress-strain relation for a lamina using the stiffness matrix and the strain-stress relation using the compliance matrix. The components of these two matrices are calculated using the modulus of elasticity, Poisson's ratio and the modulus of rigidity. These engineering constants are a function of the individual material properties and volume fractions of the two constituent elements. The individual material properties are denoted as:

E_f, E_m = Modulus of Elasticity of fiber and matrix respectively,

ν_f, ν_m = Poisson's ratio of fiber and matrix respectively,

G_f, G_m = Modulus of rigidity of fiber and matrix respectively.

The engineering constants for the lamina are then calculated using equations 1.15-1.18.

$$E_1 = E_f V_f + E_m V_m \tag{1.15}$$

$$E_2 = \frac{E_f E_m}{E_f V_f + E_m V_m} \tag{1.16}$$

$$\nu_{12} = \nu_f V_f + \nu_m V_m \tag{1.17}$$

$$G_{12} = \frac{G_f G_m}{G_f V_f + G_m V_m} \tag{1.18}$$

Where E_1 is the modulus of elasticity of the lamina in the direction parallel to the fibers and E_2 is the modulus of elasticity perpendicular to the fiber orientation.

Macromechanical Analysis of a Laminate

Having established the stress-strain relation for a lamina, in this section we will define the stress-strain relation for a laminate using the Classical Lamination Theory. The CLT is a linear theory and it has the following assumptions about a laminate [3]:

1. The displacements are continuous throughout the laminate.
2. The Kirchoff hypothesis regarding undeformed normals is assumed to be valid.
3. The strain-displacement relationship is linear.
4. The material is linearly elastic.

5. The through-the-thickness stresses are small in comparison to the in-plane stresses.

The implications of the Kirchoff hypothesis on the laminate displacement u, v, and w in the x, y, and z directions are shown in figure 1.4.

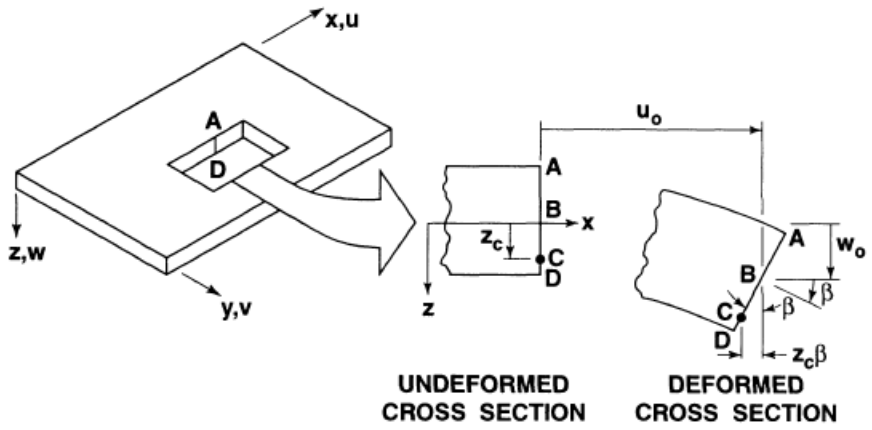

Figure 1.4. Geometry of deformation in x-z plane [2]

The displacements u, v, and w at any point z through the laminate thickness are,

$$u = u_0 - z\frac{\partial w_0}{\partial x} \tag{1.19}$$

$$v = v_0 - z\frac{\partial w_0}{\partial y} \tag{1.20}$$

$$w = w_0 - z\frac{\partial w_0}{\partial z} \tag{1.21}$$

Based on the assumptions, $\varepsilon_z = \gamma_{xz} = \gamma_{yz} = 0$. The remaining strain components are defined in terms of displacement as given by equations 1.22 – 1.24.

$$\varepsilon_x = \frac{\partial u}{\partial x} \tag{1.22}$$

$$\varepsilon_y = \frac{\partial v}{\partial y} \tag{1.23}$$

$$\gamma_{xy} = \frac{\partial u}{\partial y} + \frac{\partial v}{\partial x} \tag{1.24}$$

The strains associated with the derived displacements are then given by equation 1.25.

$$\begin{bmatrix} \varepsilon_x \\ \varepsilon_y \\ \gamma_{xy} \end{bmatrix} = \begin{bmatrix} \varepsilon_x^0 \\ \varepsilon_y^0 \\ \gamma_{xy}^0 \end{bmatrix} + z \begin{bmatrix} \kappa_x \\ \kappa_y \\ \kappa_{xy} \end{bmatrix} \tag{1.25}$$

Where ε_x^0, ε_y^0, and γ_{xy}^0 are the middle-surface strains and κ_x, κ_y are the curvatures of the plate due to bending and κ_{xy} is the curvature due to twisting. For a k[th] layer in a laminate, the stress-strain relation is given by equation 1.26 and equation 1.27.

$$\{\sigma\}_k = \left[\overline{Q}\right]_k \{\varepsilon\}_k \tag{1.26}$$

$$\begin{bmatrix} \sigma_x \\ \sigma_y \\ \tau_{xy} \end{bmatrix}_k = \begin{bmatrix} \overline{Q}_{11} & \overline{Q}_{12} & \overline{Q}_{16} \\ \overline{Q}_{12} & \overline{Q}_{22} & \overline{Q}_{26} \\ \overline{Q}_{16} & \overline{Q}_{26} & \overline{Q}_{66} \end{bmatrix}_k \left[\begin{bmatrix} \varepsilon_x^0 \\ \varepsilon_y^0 \\ \gamma_{xy}^0 \end{bmatrix} + z \begin{bmatrix} \kappa_x \\ \kappa_y \\ \kappa_{xy} \end{bmatrix} \right] \tag{1.27}$$

To obtain the forces and moments acting on a laminate, we integrate the stresses in each layer through the thickness. The forces and moments are given by equations 1.28 and 1.29 and are represented in figures 1.5 and 1.6.

$$\begin{bmatrix} N_x \\ N_y \\ N_{xy} \end{bmatrix} = \sum_{k=1}^{n} \int_{z_{k-1}}^{z_k} \begin{bmatrix} \sigma_x \\ \sigma_y \\ \tau_{xy} \end{bmatrix}_k dz \tag{1.28}$$

$$\begin{bmatrix} M_x \\ M_y \\ M_{xy} \end{bmatrix} = \sum_{k=1}^{n} \int_{z_{k-1}}^{z_k} \begin{bmatrix} \sigma_x \\ \sigma_y \\ \tau_{xy} \end{bmatrix}_k z dz \tag{1.29}$$

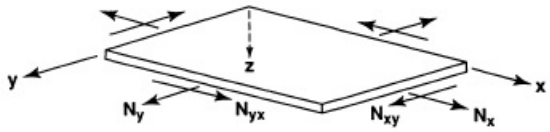

Figure 1.5 In-plane forces on a flat laminate [2]

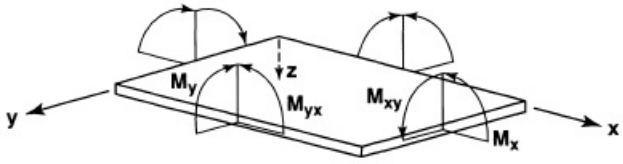

Figure 1.6. Moments on a flat laminate [2]

Substituting the equation for the stress components into equations 1.28 and 1.29 we get the forces and moments in expanded form as given in equation 1.30 and 1.31.

$$\begin{bmatrix} N_x \\ N_y \\ N_{xy} \end{bmatrix} = \sum_{k=1}^{n} \begin{bmatrix} \overline{Q}_{11} & \overline{Q}_{12} & \overline{Q}_{16} \\ \overline{Q}_{12} & \overline{Q}_{22} & \overline{Q}_{26} \\ \overline{Q}_{16} & \overline{Q}_{26} & \overline{Q}_{66} \end{bmatrix}_k \left[\int_{z_{k-1}}^{z_k} \begin{bmatrix} \varepsilon_x^0 \\ \varepsilon_y^0 \\ \gamma_{xy}^0 \end{bmatrix} dz + \int_{z_{k-1}}^{z_k} \begin{bmatrix} \kappa_x \\ \kappa_y \\ \kappa_{xy} \end{bmatrix} z dz \right] \tag{1.30}$$

$$\begin{bmatrix} M_x \\ M_y \\ M_{xy} \end{bmatrix} = \sum_{k=1}^{n} \begin{bmatrix} \overline{Q}_{11} & \overline{Q}_{12} & \overline{Q}_{16} \\ \overline{Q}_{12} & \overline{Q}_{22} & \overline{Q}_{26} \\ \overline{Q}_{16} & \overline{Q}_{26} & \overline{Q}_{66} \end{bmatrix}_k \left[\int_{z_{k-1}}^{z_k} \begin{bmatrix} \varepsilon_x^0 \\ \varepsilon_y^0 \\ \gamma_{xy}^0 \end{bmatrix} z dz + \int_{z_{k-1}}^{z_k} \begin{bmatrix} \kappa_x \\ \kappa_y \\ \kappa_{xy} \end{bmatrix} z^2 dz \right] \tag{1.31}$$

Keeping only the terms that are a function of z allows us to remove $\varepsilon_x^0, \varepsilon_y^0, \gamma_{xy}^0, \kappa_x$, κ_y , and κ_{xy} outside the summation.

$$\begin{bmatrix} N_x \\ N_y \\ N_{xy} \end{bmatrix} = \begin{bmatrix} A_{11} & A_{12} & A_{16} \\ A_{12} & A_{22} & A_{26} \\ A_{16} & A_{26} & A_{66} \end{bmatrix} \begin{bmatrix} \varepsilon_x^0 \\ \varepsilon_y^0 \\ \gamma_{xy}^0 \end{bmatrix} + \begin{bmatrix} B_{11} & B_{12} & B_{16} \\ B_{12} & B_{22} & B_{26} \\ B_{16} & B_{26} & B_{66} \end{bmatrix} \begin{bmatrix} \kappa_x \\ \kappa_y \\ \kappa_{xy} \end{bmatrix} \tag{1.32}$$

$$\begin{bmatrix} M_x \\ M_y \\ M_{xy} \end{bmatrix} = \begin{bmatrix} B_{11} & B_{12} & B_{16} \\ B_{12} & B_{22} & B_{26} \\ B_{16} & B_{26} & B_{66} \end{bmatrix} \begin{bmatrix} \varepsilon_x^0 \\ \varepsilon_y^0 \\ \gamma_{xy}^0 \end{bmatrix} + \begin{bmatrix} D_{11} & D_{12} & D_{16} \\ D_{12} & D_{22} & D_{26} \\ D_{16} & D_{26} & D_{66} \end{bmatrix} \begin{bmatrix} \kappa_x \\ \kappa_y \\ \kappa_{xy} \end{bmatrix} \tag{1.33}$$

$$\begin{aligned} A_{ij} &= \sum_{k=1}^{n} (\overline{Q}_{ij})_k (z_k - z_{k-1}) \\ B_{ij} &= \frac{1}{2} \sum_{k=1}^{n} (\overline{Q}_{ij})_k (z_K^2 - z_{K-1}^2) \\ D_{ij} &= \frac{1}{3} \sum_{k=1}^{n} (\overline{Q}_{ij})_k (z_K^3 - z_{K-1}^3) \end{aligned} \tag{1.34}$$

In equation 1.34, A_{ij} are the extensional stiffnesses, B_{ij} are the bending-extension coupling stiffnesses, and D_{ij} are the bending stiffnesses. If the matrix B_{ij} exists for a laminate, it implies coupling between bending and extension. Combining these three matrices, we get the ABD matrix which gives us the relation between forces and moments, and the strains and curvatures. It is given in equation 1.35.

$$\begin{bmatrix} N_x \\ N_y \\ N_{xy} \\ M_x \\ M_y \\ M_{xy} \end{bmatrix} = \begin{bmatrix} A_{11} & A_{12} & A_{16} & B_{11} & B_{12} & B_{16} \\ A_{12} & A_{22} & A_{26} & B_{12} & B_{22} & B_{26} \\ A_{16} & A_{26} & A_{66} & B_{16} & B_{26} & B_{66} \\ B_{11} & B_{12} & B_{16} & D_{11} & D_{12} & D_{16} \\ B_{12} & B_{22} & B_{26} & D_{12} & D_{22} & D_{26} \\ B_{16} & B_{26} & B_{66} & D_{16} & D_{26} & D_{66} \end{bmatrix} \begin{bmatrix} \varepsilon_x^0 \\ \varepsilon_y^0 \\ \gamma_{xy}^0 \\ \kappa_x \\ \kappa_y \\ \kappa_{xy} \end{bmatrix} \tag{1.35}$$

Thus using the Classical Lamination Theory, we can calculate the response of a laminate to an applied stress using the material properties of the constituents of a composite material.

Laminate Nomenclature and Special Types of Laminates

The behavior of a laminate can be controlled by altering the stacking sequence. Based on the stacking sequence, we can categorize laminates into a number of categories. To understand the stacking sequence, it is first necessary to understand the denotation of stacking sequences. A simple laminate with different angle orientations is denoted by listing their orientations such as [0/90/45]. If a specific orientation is repeated, then a subscript is used, for example, $[0_3/90_2]$. If a sequence is repeated, then the subscript is given to the entire bracket, $[0/90/45]_2$. If a laminate is symmetric about the middle surface, the subscript 's' is used, $[0/90/45]_S$. Finally, if there is no repetition or symmetricity, a subscript 't' is used to indicate total specification, $[0/90/45]_T$. The classification of laminates based on the stacking sequence is given below along with definitions and examples.

- Symmetric Laminates – A laminate is called symmetric if the material and geometric properties of laminas are the same above and below the mid-plane, $[0/90]_S$.
- Cross-Ply Laminates – A laminate is called a cross-ply laminate if only 0° and 90° plies are included in the laminate, $[0/90_2/0/90]$.
- Angle-Ply Laminate – A laminate is called an angle-ply laminate if the plies only orient at $+\theta$ and $-\theta$ alternatively, [-40/40/-40/40].

- Antisymmetric Laminates – A laminate is called antisymmetric if the ply orientations at the same distance above and below the mid-plane are negative of each other, [45/60/-60/-45].
- Balanced Laminate – A laminate is balanced if layers at angles other than 0° and 90° occur only as plus and minus pairs of +θ and –θ, [30/40/-30/30/-30/-40].

Bistability is observed in unsymmetric laminates and the subject of this research is on behavior of unsymmetric cross-ply laminates.

Unsymmetric Cross-Ply Laminates

Unsymmetric or nonsymmetric or asymmetric laminates are the most general class of laminates. An unsymmetric laminate is different from an anti-symmetric laminate in that the orientations above and below the mid-plane do not have to be exact opposites. For this research, the focus will be on unsymmetric laminates which have a stacking sequence of $[0_n/90_n]$.

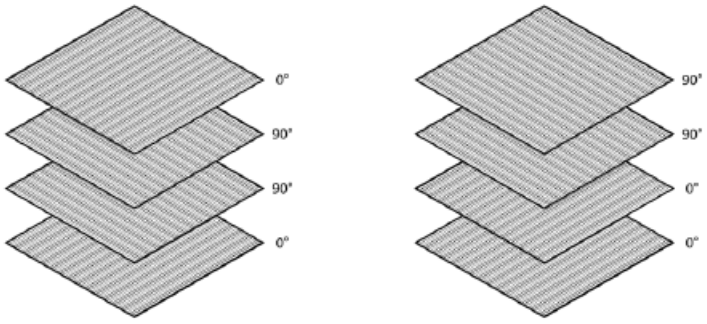

Figure 1.7 Symmetric (left) and asymmetric (right) cross-ply $[0_2/90_2]$ laminates

This laminate is fabricated by curing at an elevated temperature in order to activate the matrix material that bonds the fibers to ensure a strong structure. When the laminate is cooled from the elevated temperature, it goes from a 'stress free' state to a state with thermally induced residual stress. Since the coefficient of expansion is different for the matrix material and the fiber material, there is a difference in the coefficient of expansion in the overall laminate in the global 'x' and 'y' directions. This causes the laminate to curve and deform during the cooling process. This deformation depends on the stiffness matrix (ABD matrix) and the stiffness matrix depends on the stacking sequence. If the laminate is symmetric, the coupling between bending and extension gets eliminated and the B matrix becomes 0. Therefore, a symmetric matrix does not bend or twist when cooled from an elevated temperature. Since in most applications bending or twisting is not conducive, laminates are generally made symmetric. The CLT predicts the cured shape of unsymmetric cross-ply laminate to be a saddle shape ($K_x = - K_y$ or $-K_x = K_y$). But [4] found that the actual fabricated shape is a cylinder along with the existence of a second stable cylinder with a snap-through and snap-back phenomenon between them. The curvatures are either ($+K_x$, $K_y = 0$) or ($K_x = 0$, $+K_y$). This started the research in the area of 'bistable composites'.

Research Objectives

The objective of this research is to find four relations between the geometry and behavior of unsymmetric cross-ply laminates. These relations are as follows:

1. The relation between side length of a square laminate and its thickness required for achieving bistability.

2. The relation between length and width of a rectangular laminate required for achieving bistability.

3. For square and rectangular bistable laminates, the relation between the dimensions and thickness, and the curvature.

4. For square laminates, the relation between the side length and thickness, and the force of actuation.

Defining the first two relations allows us to predict whether an unsymmetric cross-ply laminate with a certain thickness and size is going to be bistable or not. For laminates that are bistable, the next two relations allow us to predict the magnitude of curvature exhibited by the two laminate shapes, and the force of actuation between the two shapes.

CHAPTER TWO

LITERATURE REVIEW

Bistability was first observed by [4] when he found that thin unsymmetric cross-ply laminates do not conform to the predictions of CLT. Since then, many researchers have studied different characteristics of bistable laminates in order to be able to find a usefulness to the phenomenon of bistability. The literature review provides the state of current research and is divided into the following sub-categories:

I. Development of analytical models
II. Development of finite element models
III. Inclusion of fabrication defects and environmental conditions into analytical and FEA models
IV. Studies on the relationship between the geometry of the laminate and its behavior, viz., a. Existence of bistability, b. Curvature, c. Snap-through force
V. Applications of bistable composites

I. Development of Analytical Models

Hyer [4] first observed bistability in laminates of different sizes, shapes, stacking sequences and orientations. He found that thin unsymmetric laminates do not conform to the predictions of CLT. The CLT predicts all unsymmetric laminates to be saddles with the two curvatures not necessarily of equal magnitude but definitely of opposite sign. While

Hyer reported the shapes of various laminates, of particular interest were two laminates with the same dimensions of 150 x 150 mm but different stacking sequences of $[0_2/90_2]$ (4 plies) and $[0_4/90_4]$ (8 plies). The thinner laminate exhibited bistability with two cylindrical shapes whereas the thicker laminate was a saddle shape as predicted by the CLT.

Since the CLT was unable to predict the shapes of some laminates, Hyer [3] developed a nonlinear theory known as the "Extended Classical Lamination Theory" (ECLT). A linear theory was ruled out because it would predict a unique shape instead of the observed two stable shapes. Since the out-of-plane deformation of the laminates were of the order of many laminate thicknesses, geometric nonlinearities were included through the strain-displacement relationship. The CLT assumes linear strain-displacement relationship as shown in equations 1.22 – 1.24. The ECLT assumes the strain-displacement relationship to be nonlinear as shown in equations 2.1 to 2.3.

$$\varepsilon_x = \frac{\partial u}{\partial x} + \frac{1}{2}\left(\frac{\partial w}{\partial x}\right)^2 \tag{2.1}$$

$$\varepsilon_y = \frac{\partial v}{\partial y} + \frac{1}{2}\left(\frac{\partial v}{\partial y}\right)^2 \tag{2.2}$$

$$\varepsilon_{xy} = \left(\frac{\partial u}{\partial y} + \frac{\partial v}{\partial x}\right) + \left(\frac{\partial w}{\partial x}\right)\left(\frac{\partial w}{\partial y}\right) \tag{2.3}$$

After a laminate cools from the elevated curing temperature, it can deform into one of the shapes shown in figure 2.1. Out of these shapes, the one that actually occurs is the one associated with the minimum total potential energy. A Rayleigh-Ritz technique was used for the minimization of the total potential energy. Hyer considered two laminates with stacking sequences of $[0_2/90_2]$ and $[0_4/90_4]$ and calculated the room temperature shapes by

increasing the side length of a square from 0 to 150 mm. He plotted the results on the graphs shown in figure 2.2. As seen, for smaller side length, only a single saddle shape exists. As the side length is increased, at a certain point, the graph bifurcates into three shapes – one saddle and two cylinders. When three such shapes are predicted it was found that the saddle shape was unstable and only the two cylindrical shapes existed. The side length represented by the bifurcation point is called as the critical length.

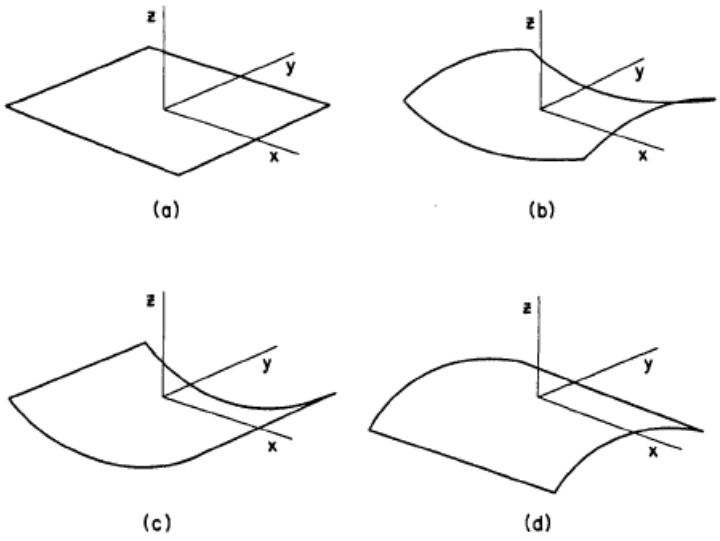

Figure 2.1: Laminate shapes: a. At elevated temperature, b. Saddle Shape, c and d, Two cylindrical shapes with opposite curvatures. [3]

Below this critical length, the laminate will be unique saddle shape whereas beyond this length bistability is exhibited. The critical length for the $[0_2/90_2]$ laminate was found to be 35mm and for the $[0_4/90_4]$ laminate it was 71mm. The comparison with the experimental data from fabrication of laminates was found to be fair. Hyer further noted that the effects of moisture absorption, viscoelastic relaxation, or any other mechanism that

alters the internal stress state of the laminate was felt to be an important factor for a laminate to be bistable. Because of these effects, a laminate sized just above the critical length could actually be sized just below the critical length. These time dependent effects would lead to strange behavior such as a laminate requiring no external force for a snap from one shape to the other.

Hyer [5] further modified the ECLT by considering polynomials that accounted for the in-plane displacements and found that the in-plane residual strain are compressive and practically independent of spatial locations. The limitation of this theory was that only orthotropic laminates were considered and thus the laminae only had orientations of 0° and 90°.

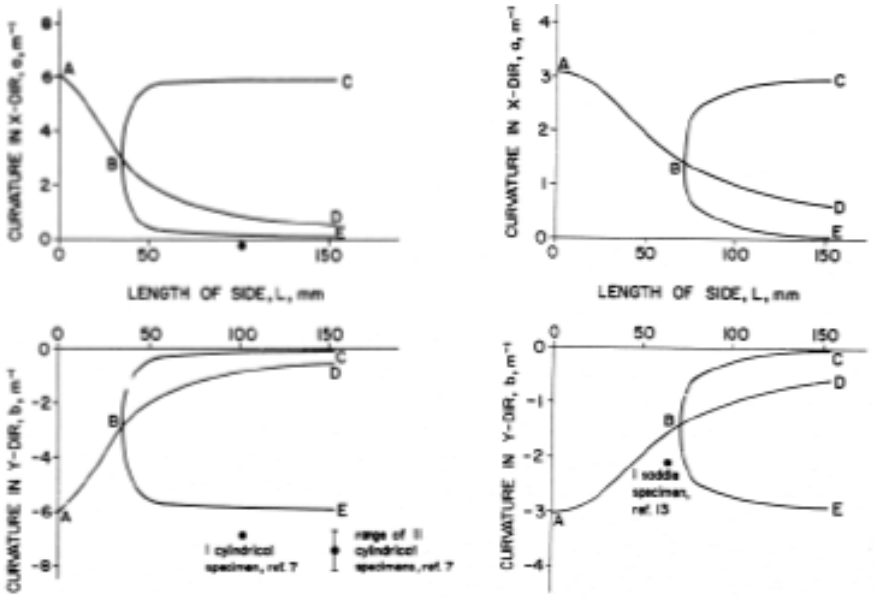

Figure 2.2: Room temperature shapes of square laminates, left: $[0_2/90_2]$ and right: $[0_4/90_4]$ [3]

Hamamoto and Hyer (Akira & Hyer, 1987) developed a non-linear theory to include geometric imperfections in order to achieve better comparison between theoretical predictions and fabricated results. Previous work consisted of examination of room temperature shapes of cross-ply laminates as a function of laminate geometry and stacking sequence. In this paper the size was fixed and the temperature was varied in order to predict the room temperature shape. Geometric imperfections resulting from hand lay-up and environmental conditions were the reasons for the mismatch between calculations and results.

Since Hyer considered only cross-ply laminates while developing his theory, (Dang, J. & Tang, 1986) modified it in order to calculate the shapes of laminates with angled plies. However, they assumed polynomial functions in such a way that only the sum of two unknown coefficients could be solved for. To correct this, Jun and Hong [8] and [9] modified Hyer's Extended Classical Lamination Theory and the work done by (Dang, J. & Tang, 1986) to enhance the accuracy by adding more polynomial terms and by including in-plane residual shear strains. The effects of width-to-thickness ratio, aspect ratio, number of layers, and stacking sequence on the shape of cross-ply laminates was also the subject of their work. The inclusion of residual shear strain to the ECLT led to more complex calculations and it was shown that in-plane shear strain was negligible for small or large length-to-thickness ratio but was considerable for medium length-to-thickness ratios. The investigation into effects of width-to-thickness ratio, aspect ratio, and number of layers will be discussed in a later section.

The assumed displacement function of Jun and Hong led to complex calculations and therefore, [10] modified their theory by including a complete set of third-order polynomials. They fixed the principal curvature at 45° from the edge for all laminates and compared it with a 30° angle-ply laminate. While the comparisons were reasonable, the experimental results were explained by manufacturing problems, material property uncertainties, and material inhomogeneities.

Later, the assumptions made by [10] were found to be incorrect by [11]. They found that principal curvature should not be assumed a priori and in fact, should be considered as a variable. They used a structural coordinate system which eliminated the need to find the direction of principal curvature and developed a comprehensive model for general unsymmetric laminates by using the Rayleigh-Ritz minimization of Total Potential Energy to predict the deformation behavior. Instead of approximating the displacements, their theory approximated the mid-plane strain, hitherto considered state-of-the-art. They also conducted some limited Finite Element Analysis for comparison. The laminates in consideration belonged to three families: $[-\theta_4/\ \theta_4]$, $[(90 - \theta)_4/\ \theta_4]$ and $[(\theta - 90)_4/\ \theta_4]$. The temperature-curvature relation for them is presented in figures 2.3, 2.4 and 2.5.

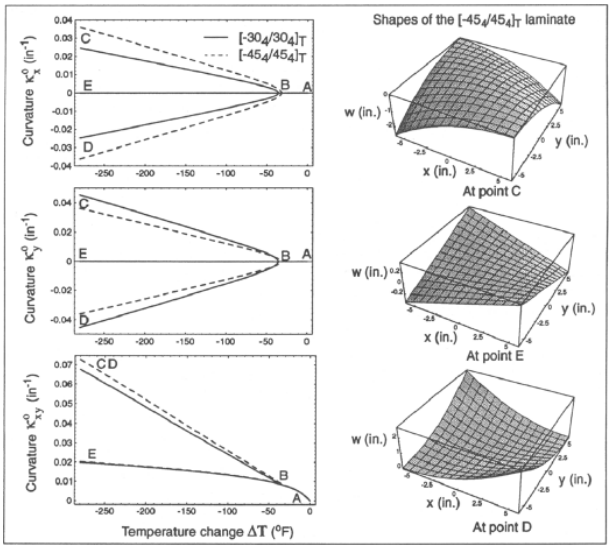

Figure 2.3. Temperature-curvature relations for [-θ$_4$/ θ$_4$] laminates [11]

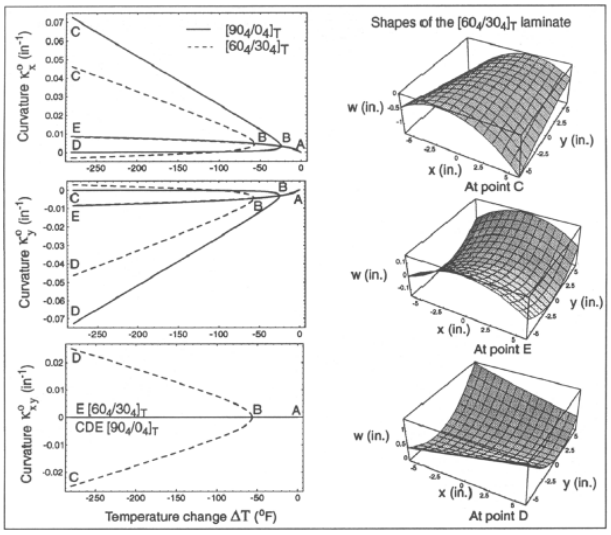

Figure 2.4. Temperature-curvature relations for [(90 – θ)$_4$/ θ$_4$] laminates [11].

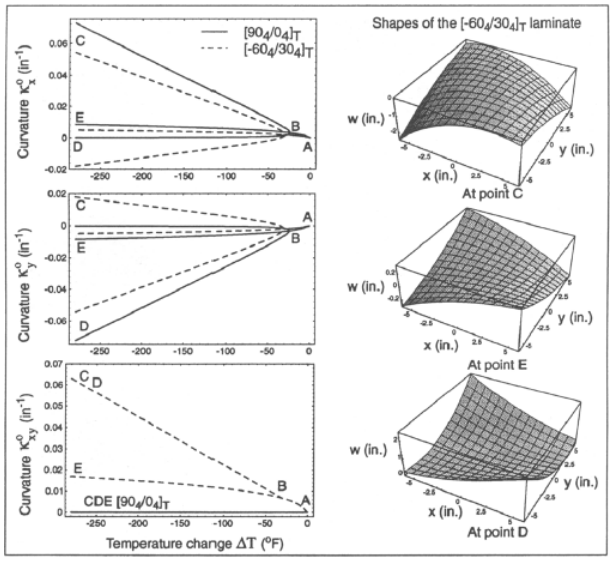

Figure 2.5. Temperature-curvature relations for $[(\theta - 90)_4/ \theta_4]$ laminates [11].

The comparison between results obtained for a $[0_2/30_2]$ laminate by [11] with the results obtained by [8] is given in figure 2.6. ABAQUS software was used to perform the Finite Element Analysis for the cooling of the laminate from the cure temperature to the room temperature.

In Abaqus, as the bifurcation temperature is reached, there are multiple equilibrium configurations and the simulation must be coaxed to follow a certain path. This was done by introducing an imperfection in the initial shape of the laminate. Without this imperfection, the solution converged to an unstable shape. The results obtained from the FEA model matched fairly well with the results obtained from the Rayleigh-Ritz model, and previous Jun & Hong model. The results also matched with the fabricated laminates.

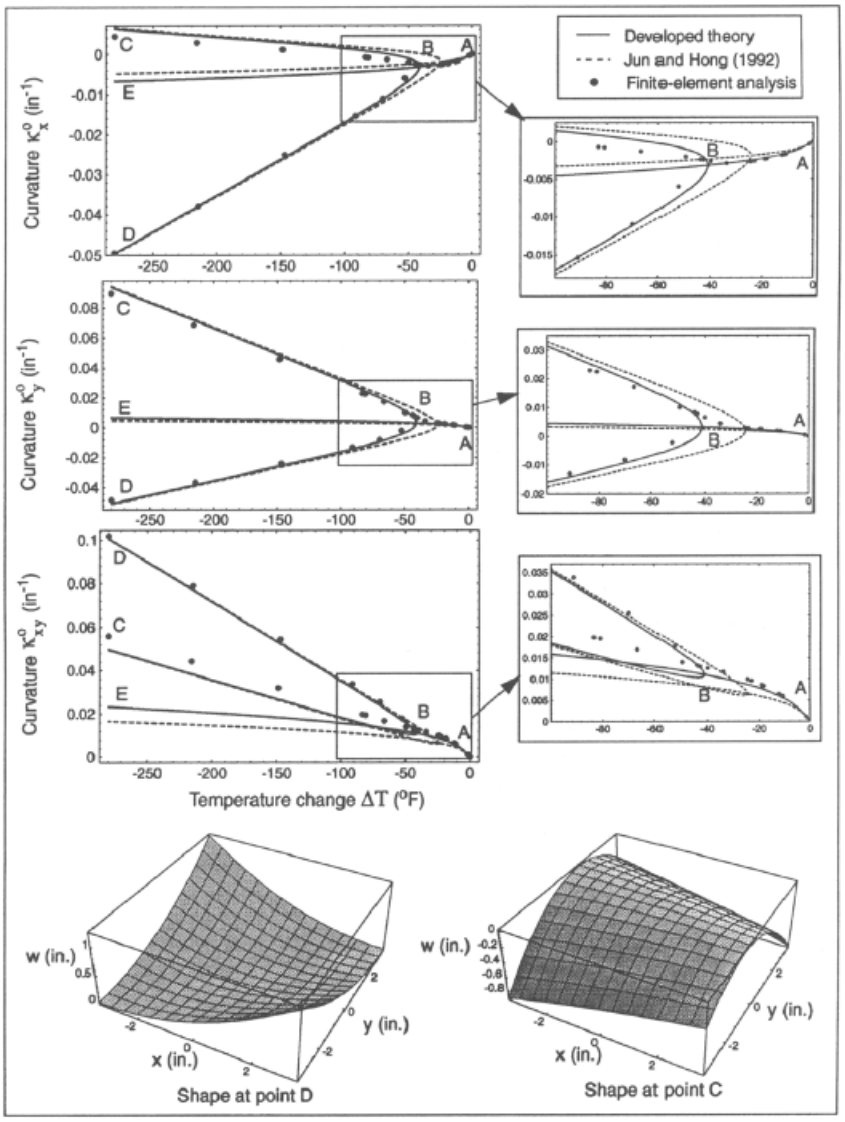

Figure 2.6. Comparison between results obtained by [11] and [8]. [11].

The model presented in [11] was considered to be the most comprehensive and straightforward analytical model for studying the behavior of bistable laminates. However, the model assumes a constant curvature throughout the domain and thus fails to predict the free edge effects that are observed in fabricated laminates.

To model the displacement at the edges of a laminate more accurately, [12] modified Hyer's out-of-plane displacement function. Hyer's displacement function assumed a constant curvature throughout the domain and is given in equation 2.4.

$$w(x, y) = -\frac{1}{2}(w_{20}x^2 + w_{02}y^2 + w_{11}xy) \tag{2.4}$$

To model boundary conditions that are not free edges, the assumption of constant curvature was eliminated. In order to do this, a fourth order displacement function was chosen as the product of two parabolas, given in equation 2.5.

$$w(x, y) = P(x).G(y) \tag{2.5}$$

Where,

$$\begin{aligned} P(x) &= p_0 + p_1x + p_2x^2 \\ G(y) &= g_0 + g_1y + g_2y^2 \end{aligned} \tag{2.6}$$

Thus the displacement function takes the form shown in equation 2.6

$$\begin{aligned} w(x, y) = w_{00} + w_{10}x + w_{01}y + w_{20}x^2 + w_{02}y^2 + w_{11}xy + \\ w_{12}xy^2 + w_{21}x^2y + w_{22}x^2y^2 \end{aligned} \tag{2.7}$$

Keeping the other assumptions made by Hyer to be the same, this new function leads to 20 unknown coefficients. A comparison between the new model, Hyer's model and an FEA model is given in figure 2.7. The laminate is a 180mm square plate with a stacking sequence of $[0_4/90_4]$.

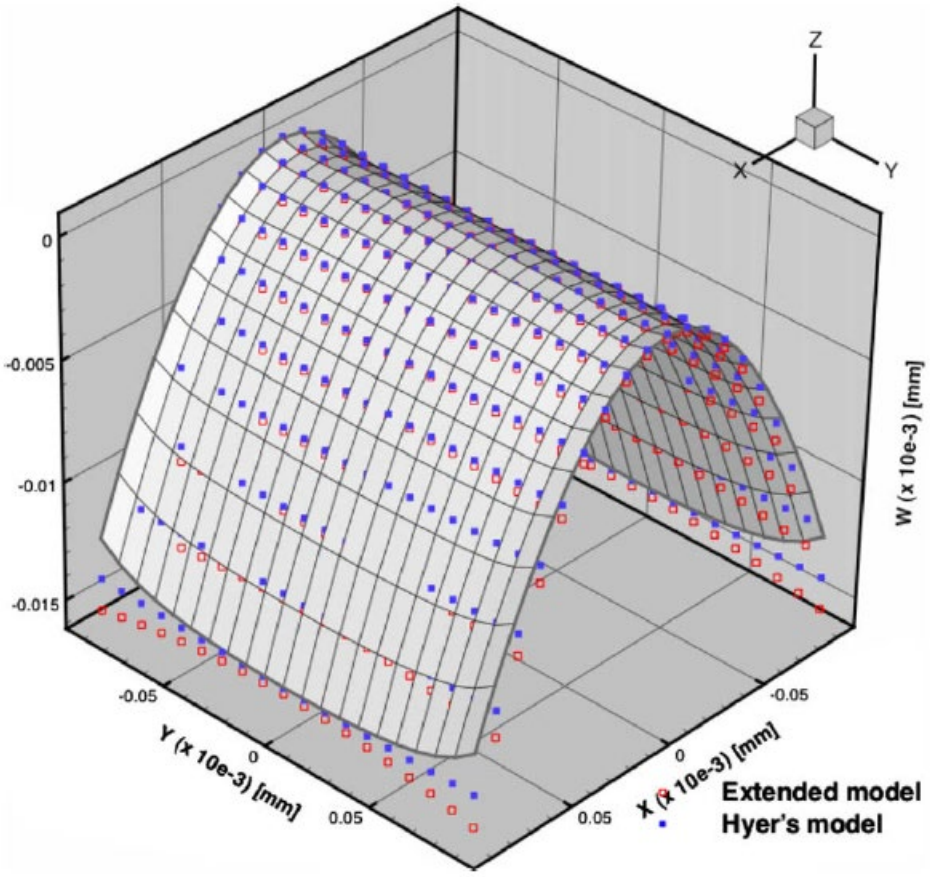

Figure 2.7 Hyer's model and the extended model overlaid on an FEA model. [12]

As can be seen, Hyer's model exhibited a perfectly flat edge whereas Mattioni's extended model showed a slight parabolic variation. The Finite Element model shows the edge to be flat in the center and more curved toward the corners. It is seen that the meshless models developed by Hyer and Mattioni are not able to describe the local displacements toward the edges as accurately as the FEA model. However, Mattioni's model was able to predict the displacement at the edges more accurately than Hyer by eliminating the assumption of constant curvature and by assuming a displacement function with a higher

order polynomial. Using the new model, he was able to study a laminate with piecewise variation of layup shown in figure 2.8.

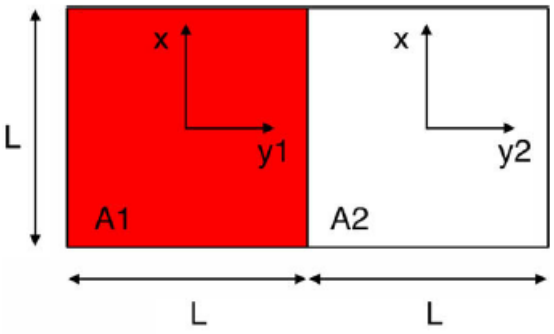

Figure 2.8. Geometry of a laminate with piecewise variation of layup. [12]

The section denoted as 'A1' is a symmetric layup whereas section 'A2' is unsymmetric. For this type of laminate, the boundary conditions between the two sections need to take into account non free-edge assumptions and therefore, Mattioni's model is better for modelling such a laminate.

[13] tried to improve the shortcomings of analytical models by coupling the analytical models with path-following algorithms. Doing this allowed them to have an increase in the order of the polynomial interpolation up to 11^{th} order. The results were better when compared to Hyer's 3^{rd} order model, however, FEA was still found to be better suited for simulating the displacement at the edges. The error between the model at order 11 and FEA is shown in figure 2.9.

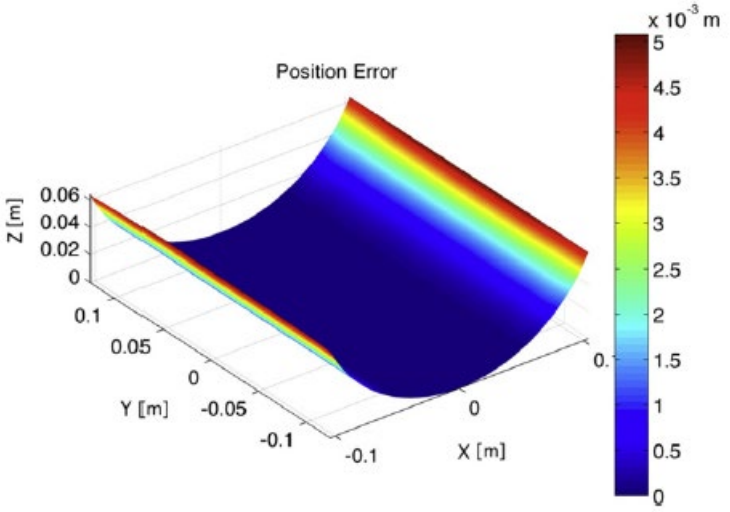

Figure 2.9. Difference between model at order 11 and FEA model. [13]

The reason for FEA being more accurate was that it had a larger number of degrees of freedom. Also, FEA updates the stiffness matrix at each step. However, the model at order 11 was found to be significantly better than previous models and matched fairly well with FEA results. They used this model to study the bifurcation process, snap-through load, and the relation between plate size and aspect ratio.

As has been established so far, FEA methods are better suited for the analysis of bistable composites, and hence, the next section reviews the literature on FEA models.

II. Development of FEA models

[14] used the FEA program MARC to simulate the curing process of unsymmetric laminates and also developed a method for testing the stability of a second shape. They

studied laminates with various stacking sequences and compared the results with the ones found using Hyer's ECLT. The stacking sequences were $[0_2/90_2]$, [90/0/90/90], and [0/90/0/90]. Only FEA was used to predict room temperature shapes of laminates with angle plies such as [0/-45/+45/0], and [0/-45/90/0] since an analytical model had not been developed to include angle plies at that time. All laminates were of 140 x 140 mm dimensions and were simulated using 196 8-node bilinear shell elements. The laminates were cooled down from a temperature of 177°C to 157°C in steps of 2°C followed by steps of 5°C down to 20°C. Temperature dependent thermal properties were used, however using temperature dependent mechanical properties was found to be unnecessary. Both the analytical and FEA results were compared with fabricated laminates by measuring the displacements in the Z direction. It was seen that both methods gave similar results, however, FEA was able to clearly show edge effects. It was also noted that FE was able to deal with different classes of unsymmetric laminates. However, FEA calculations took a long time and there was a need for more powerful workstations.

The snap-through effect was studied by [15] using FEA. First, the room temperature shape was calculated using the previous model and then the four corner nodes were moved in the direction of the supposed second shape. The reaction force at the center node was recorded. The snap-through force was positive at first and kept increasing until snap-through, beyond which it started to decrease and became negative. After the snap-through the boundary conditions were changed to the old configuration of a fixed center. This was done to check the stability of the second shape.

Laminates with various stacking sequences were studied and in addition, a circular laminate was also studied. The mesh used for the circular laminate was different than for square laminates. It had quadratic elements in the center region and the other elements were arranged radially. The center node was fixed during the curing step. A saddle shape was predicted for this configuration, however, by forcing the laminate into a cylindrical shape by applying a force perpendicular to the laminate on four nodes on the circumference, a cylindrical shape was obtained. The second shape was obtained by moving the same four nodes in the opposite direction. Calculations were also performed for a circular laminate with a stacking sequence of $[0/90_2/60]$. It was found that such a laminate with a fixed center predicted a cylindrical shape without the use of any other boundary conditions. The conclusions were that FEA showed better edge effects, was able to calculate shapes of square laminates with arbitrary layups, and it was also able to calculate the shape of a circular laminate. Again, the drawback long processing time and the need for a powerful workstation.

[16] studied the loss of bifurcation in laminates due to asymmetric thickness ratios and with an increase in aspect ratio using Abaqus FEA software. The calculations were performed using S4R, 4-node general purpose reduced integration shell elements, which allowed shear deformation. Geometric nonlinear algorithms were used by activating the 'NLGEOM' option. It was found that a perfectly square plate always deformed into a saddle shape upon curing. However, introducing a small imperfection by modelling the plate to be 100 x 99 mm gave a cylindrical shape as the result. They also verified Hyer's previous finding that below a certain critical length, both perfectly square plates and plates

with slight imperfections deformed into a single saddle shape without bistability. The importance of including in-plane residual shear strain found by [8] was also verified. Comparison between the Abaqus model with the presence of the shear modulus G_{12} and a Ritz model without in-plane residual shear strain was done and it was found that the results from Abaqus were better. However, when negligible in-plane shear strain was employed in Abaqus using a very high shear modulus G_{12}, the results from Abaqus matched with the Ritz model. It was also found that Abaqus was able to predict the anticlastic effect toward the laminate edges, which the CLT and the Ritz model failed to do. The relation between thickness ratio, and aspect ratio, on the shapes of the laminate will be reviewed in a later section.

Abaqus was used by (Filippo Mattioni et al., 2006) to carry out FEA analysis of variable sweep wing, shown in figure 2.10

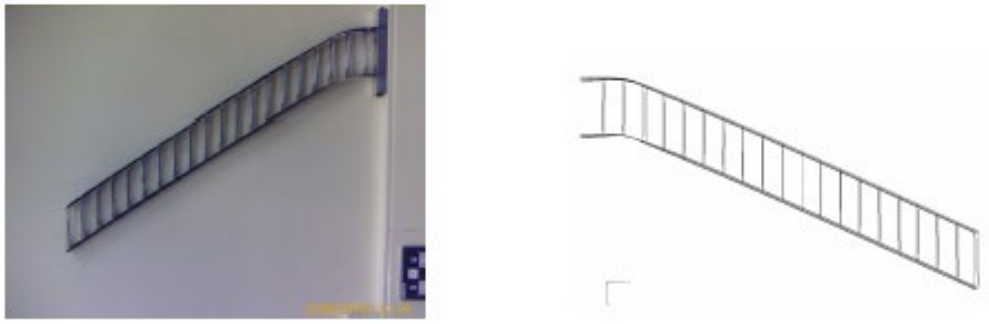

Figure 2.10 Swept wing configuration. Left: Experimental, Right: FEA model. [17]

S4R shell elements were used to model the composite material. To simulate the curing process, a nonlinear static analysis was performed whereas a Newton-Raphson scheme with a volume proportional damping was used to simulate the snap-through. The

'STABILIZE' option in Abaqus introduces the damping effect in order to control the local instabilities. To ensure accuracy, the energy fraction was set equal to 5×10^{-11}, representing the lowest value where convergence was still achieved. Results from experiment matched fairly well with FEA results.

A comprehensive FEA model was built by (Tawfik et al., 2007) to study the relation between the geometry and behavior of unsymmetric laminates. The FEA model was also used to find the force required for snap-through. These relations will be reviewed in a later section. The FEA model was built in Abaqus. The plates were modelled using 400 4-node, S4R, doubly curved, reduced integration shell elements. The total number of nodes were 441 with 2646 degrees of freedom. As has been established so far, a perfectly square laminate always deforms to a saddle shape as per FEA. To overcome this, imperfections are introduced to the model to perturb the geometry. This was done by first solving the linear eigenvalue buckling problem for the unsymmetric laminate under thermal load. Once the eigenmodes are obtained, they are superimposed onto the perfect laminate using the 'IMPERFECTION' command in Abaqus. The snap-through step was then carried out by restricting the movement of corner nodes in the Z-direction and then applying a concentrated force at the middle point using the STATIC, STABILIZE procedure, as shown in figure 2.11. After the laminate snaps, the force is removed and the laminate is checked for stability in the second shape. To calculate the snap-back force, the load is reversed in direction with the same boundary conditions, and again, the force is removed to check for stability.

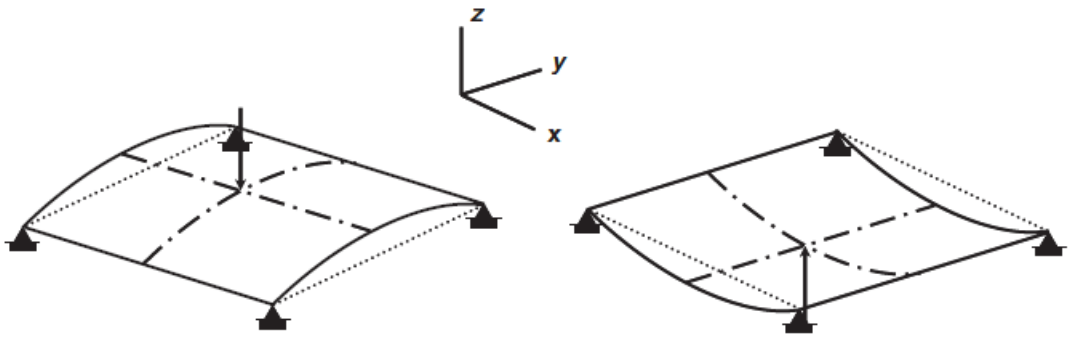

Figure 2.11. Boundary conditions for snap-through and snap-back. [18]

The results compared well with results obtained from Hyer's ECLT and with Hyer's experimental data, as shown in figure 2.12.

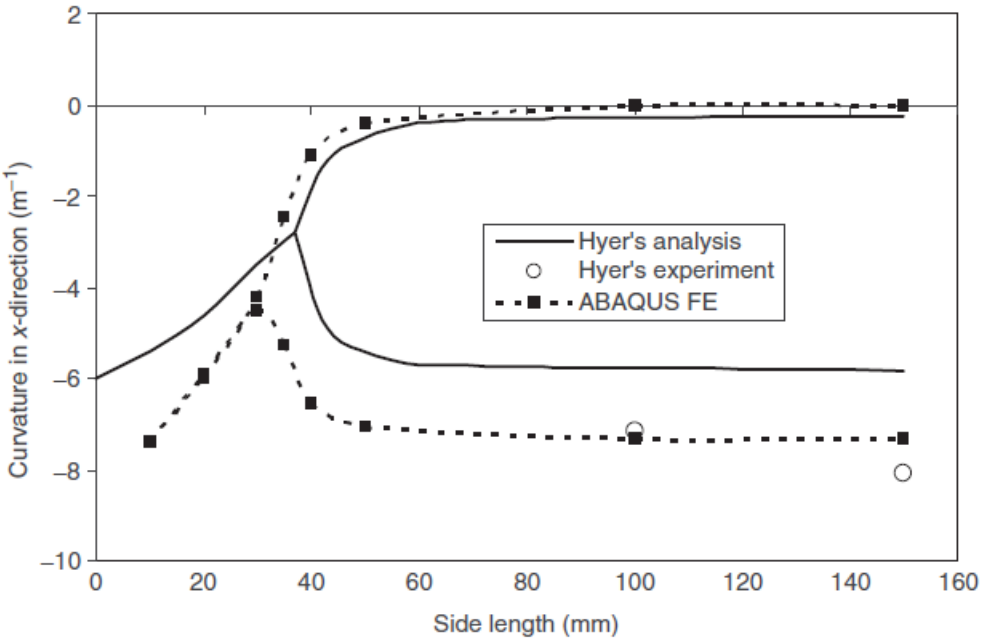

Figure 2.12. Comparison between FEA model and Hyer's ECLT. [18]

Mattioni used a pseudo-dynamic FEA model to simulate the cooling and snap-through of a laminate with piecewise variation in layup (Filippo Mattioni, 2007), (F. Mattioni et al., 2008), and [12]. Since the physical process of curing takes a considerable time (a few hours), it was considered to be quasi-static. Mechanical stresses are developed due to temperature differences, and since no external loads are applied, significant velocities are not developed. Therefore, the process can be modeled either statically or dynamically. As the bifurcation is reached, there are multiple possible shapes and a dynamic problem will always converge to a stable shape. However, this was computationally expensive and therefore a pseudo-dynamic procedure was employed. This consisted of an automatic stabilization step that adds viscous forces to damp the local instabilities. The panel was modelled using 800 4-node shell elements (S4R) with 861 nodes and 5166 degrees of freedom. An initial temperature of 140°C and a final temperature of 0°C was applied to all nodes. The snap-through was modelled by restricting the movement of four corners nodes in the Z direction and applying a perpendicular force in the center. The comparison between the FEA model and the analytical model are given in figure 2.7.

[21] developed an FEA model to analyze the morphing of a bistable laminate using piezoelectric patches. They introduced an imperfection into the square plate by modelling the geometry to be 151 x 149 mm. They found that using an explicit method or an implicit direct-integration dynamic method allowed even a perfectly square laminate to converge into a stable cylinder. However, the computational time of modelling an explicit method is high, and the results are fairly accurate with an implicit model with geometric

imperfections. The snap-through loads applied by the piezoelectric patches were recorded and by including the environmental effects in the FEA model, they correlated well with the experimental data.

[22] studied the morphing of composite plates using thermal gradients. They noted that while the FEA model with perfectly symmetric geometry converged to an unstable saddle shape upon curing, applying a through-the-thickness thermal gradient allowed the solution to start its way to a stable equilibrium. Subsequently, the thermal gradient was removed and the laminate stabilized to a cylindrical shape.

Recently, [23] modified the boundary conditions developed by [18] to simulate the snap-through and snap-back effect. He modelled laminates with various geometries where sometimes, a combination of triangular and quadrilateral elements was used. Depending on the post-cure curvature of a rectangular laminate, the snap-through and snap-back forces were applied as shown in figure 2.13

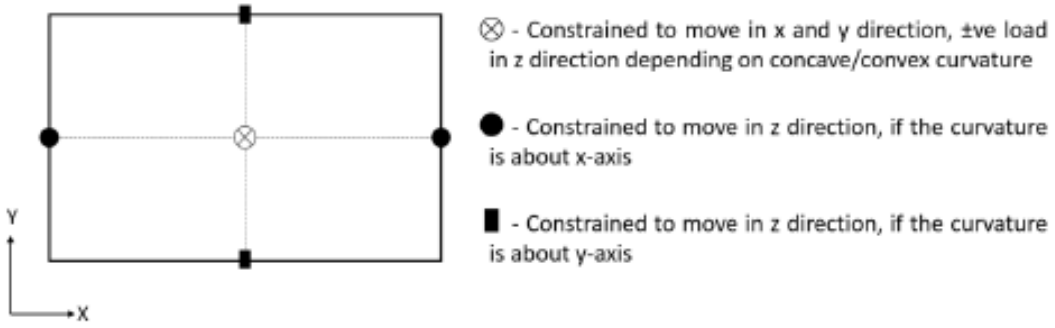

Figure 2.13. Loading and Boundary Conditions for Snapping [23].

As shown, the force is always applied in the center perpendicular to the laminate, and on the side that has a convex curvature. The boundary conditions are to restrict the

centers of two opposite edges such that the edges are curved pre-snapping and flat post-snapping.

The literature review on analytical and FEA models presented so far assumes perfect geometry, lamina orientation, uniform thickness, and ignores the effects of environmental conditions and fabricating defects. In the next section, literature review is presented on the inclusion of these effects.

III. Inclusion of fabricating defects and environmental conditions

Irrespective of whether the calculations are performed analytically or numerically, fabrication defects and environmental conditions play a role in the behavior of unsymmetric composite laminates.

(Akira & Hyer, 1987) modelled a 125 x 125 mm $[0_4/90_4]$ AS4/1908 laminate using the CLT and compared it with a fabricated laminate. The results are shown in figure 2.14. It was evident that there was a clear difference between theoretical and experimental results. The reason for this difference is that the CLT assumes an ideal laminate whereas there are imperfections in the experimentally obtained results. There are various assumptions made by the CLT which are not applicable for experimental results, listed below:

1. The CLT assumes that the material properties are uniform throughout the laminate
2. It assumes that all the different layers of laminae have the same properties as each other
3. It assumes the angles of the laminate to be exactly 0° or 90°

4. It does not take into account the fact that often, the fibers in the lamina are curved, twisted, and misaligned

5. It does not consider the existence of a temperature gradient in the laminate thickness or surface

6. A thermal gradient will lead to non-uniform curing as well as a difference in epoxy flow from point to point.

7. The CLT assumes a uniform thickness, which is not accurate

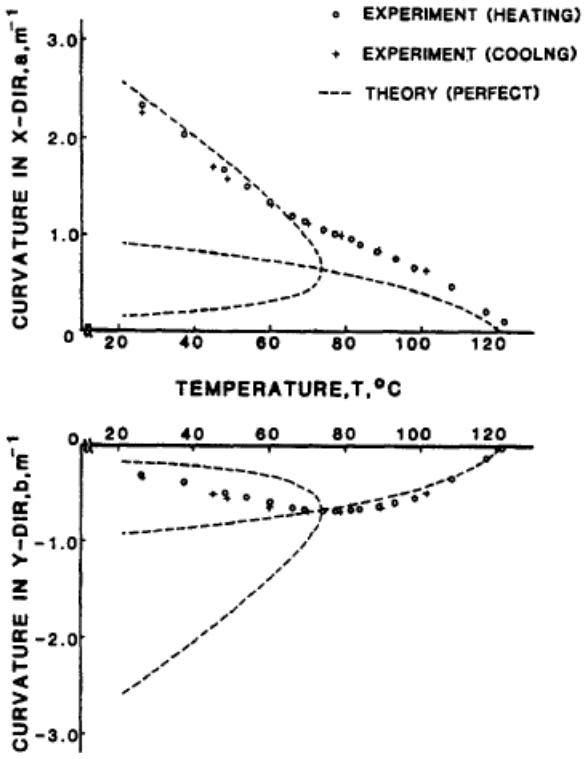

Figure 2.14 Comparison between theory and experiment for a 125 x 125 mm [$0_4/90_4$] AS4/1908 laminate. (Akira & Hyer, 1987)

As an example, they modelled the same laminate such that the laminae with the 0° orientation were 1% thicker and the laminae with the 90° orientation were 1% thinner than the quoted thickness of 0.175 mm. As shown in figures 2.15 and 2.16, this small imperfection gave completely different results for the temperature-curvature relationship.

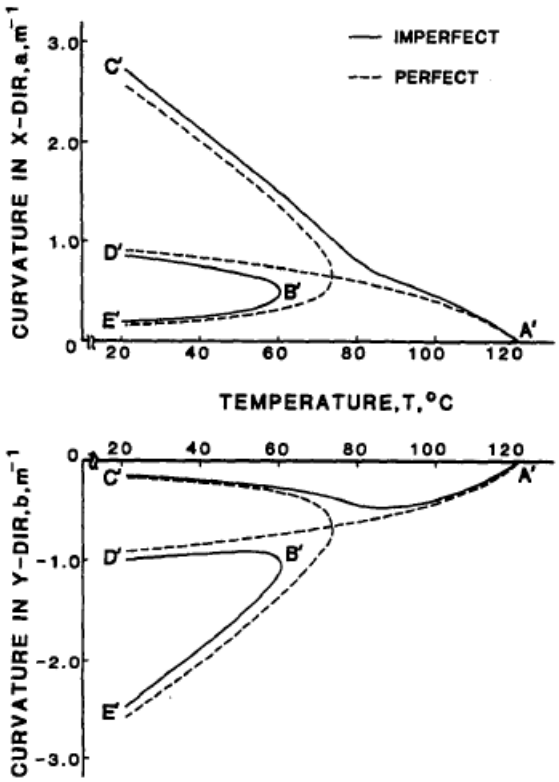

Figure 2.15. Comparison between a perfect laminate and a laminate with thickness variation. (Akira & Hyer, 1987)

As shown in figure 2.15, a thickness variation eliminated the presence of a bifurcation point, and also changed the magnitude of curvature in the laminate. When compared with the experimental results (figure 2.16), there was a better correlation with the imperfect laminate than with the perfect laminate shown in figure 2.14. This study

showed the importance of including geometric imperfections. Obviously, a thickness variation was not the only imperfection present in the laminate, and perhaps even the thickness variation was not of the same nature or magnitude. However, this gave an indication that including imperfections in the analytical and numerical models was necessary.

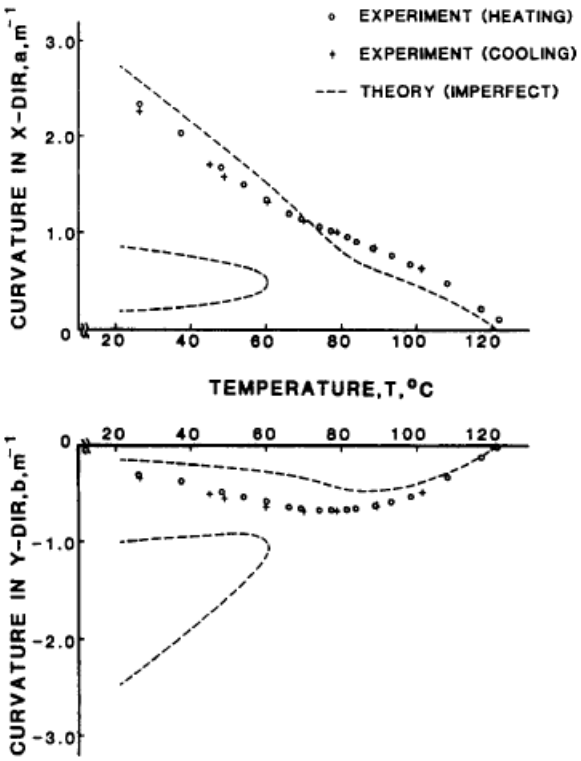

Figure 2.16. Comparison between a laminate with thickness variation imperfection and experimental results. (Akira & Hyer, 1987)

[21] analyzed the morphing of bistable laminates using piezoelectric patches. They noted that moisture absorption creates a stress field not unlike the one created by thermal stresses. The effect of this hygroscopic stress is to reduce the curvature of the laminate by

relaxing the internal stresses. A reduction in curvature also leads to a reduction in the force required for snap-through. The effect of moisture absorption was included in the FEA model, which was used for calculating the required force for snap-through. By calculating the weight gain of a laminate, the moisture content can be calculated. The force vs displacement graph (displacement of the geometric center, where a concentrated force is applied) was plotted for three techniques: one measured with a 'dry' laminate in FEA, one with a 'moist' laminate in FEA, and one measured experimentally. The results are shown in figure 2.17.

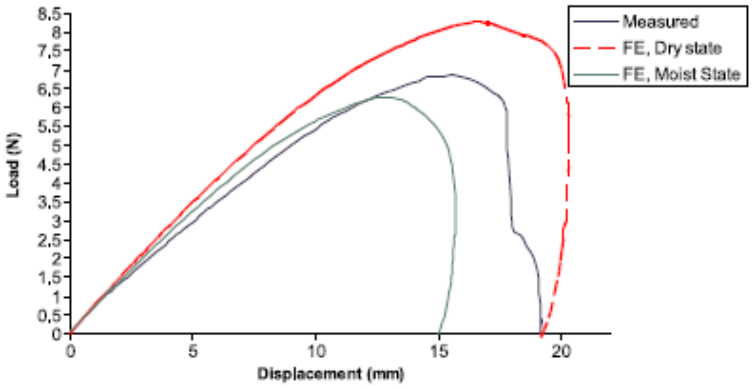

Figure 2.17 Comparison between force vs displacement of a 150 x 150 mm [0/90] AS4/8552 laminate.[21]

The assumption that moisture absorption leads to a reduction in snap-through force was thus confirmed. A moisture content of 1.2% was arbitrarily chosen, and thus, a variation of snap-through force with respect to other values of moisture content was not presented.

An experimental study on loss of curvature and reduction in snap-through load was done by (Etches et al., 2009). The experiments were done on panels of 200 x 200mm, [0/90], AS4/8552 laminates with a thickness of 0.25mm. The samples were maintained at a temperature of 20±1°C and 65±2% relative humidity. The change in the 'chord length' and 'height' of the laminate (definition of terms presented in figure 2.18) over a period of 8 days is given in figure 2.19.

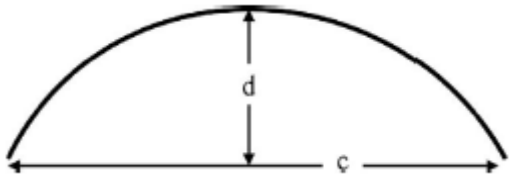

Figure 2.18. C = Chord Length, d = Height [24]

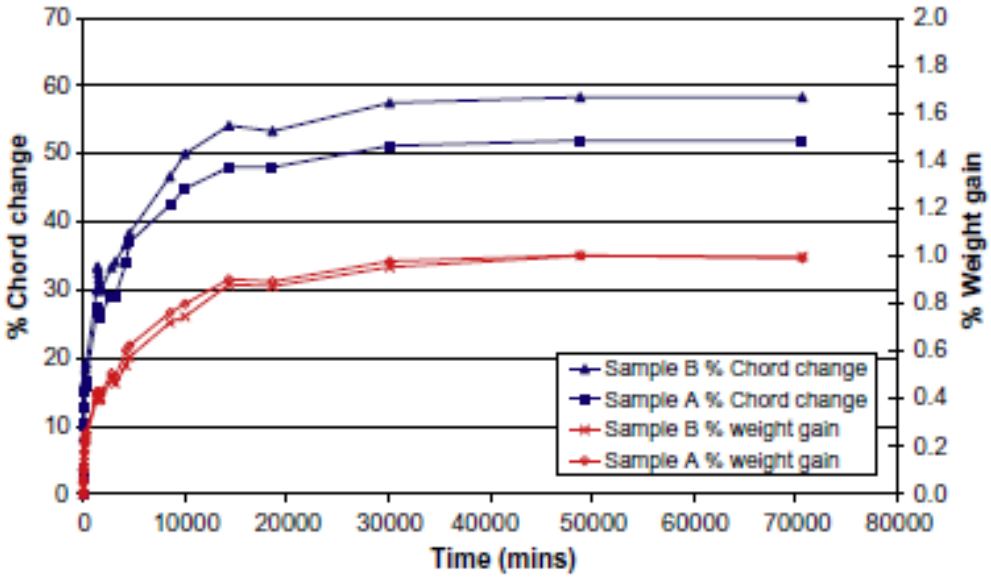

Figure 2.19. Change in shape of a laminate due to moisture absorption. [24]

The force for snap-through was measured using a Instron 3343 test machine. The laminate was simply supported and the force was applied on the geometric center using a rounded indenter of 10 mm diameter. The experiment was repeated over 7 days and the results are shown in figure 2.20. The effect of moisture absorption is clearly evident. However, it was noted that the experiments were performed on a thin laminate, which reach the limit of moisture absorption very quickly. For thicker laminates, reaching the maximum moisture content would take a much longer time.

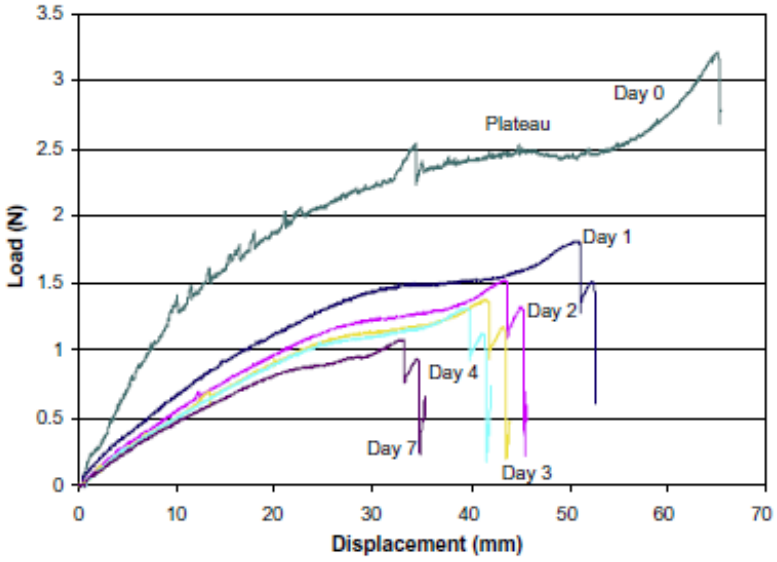

Figure 2.20. Load vs Displacement of a laminate measured over a period of 7 days [24]

(Giddings et al., 2010) used optical microscopy and digital image processing to investigate the effect of a resin layer on the surface of two laminates, one a [0/90], 75 x 75 mm laminate and the other a [-30/60], 150 x 150 mm laminate. It was found that the thickness of the individual plies and the total laminate deviated by up to 6%. The effect of the resin layer was captured, and it was found that the curvature of the laminate when the

resin layer is on the concave side is more than the curvature of the laminate when the resin layer lies on the convex side. By including the effect of the resin layer into the FEA model, the error between the two states was reduced from 7% and 73% for the idealized laminate to 3% and 7% for the laminate with a resin layer.

(Betts et al., 2010) used three-dimensional motion analysis techniques to measure the out-of-plane deformation of five laminates (total of 10 shapes) and compared it to the results obtained from Hyer's model. The laminates had stacking sequences of [-45/45], [-30/60], [-15/75/, [30/60], and [45/90]. It was found that the error between predicted and measured deflection was between 2.5% and 16.7%. Error caused by the existence of a resin layer was about 5%. A variation of 5°C lead to a change of 3% in the displacement of the laminate.

(Brampton et al., 2013) conducted a detailed sensitivity analysis of bistable laminates. The change in curvature with a variation in various material properties was studied. The calculations were done using Hyer's ECLT model [11]. First the material property values at room temperature were used and varied by ±5%, to identify which properties the laminate is most sensitive to. The results are shown in table 2.1.

From these results it was clear that the laminate was most sensitive to the Young's moduli (E_{11} and E_{22}), transverse thermal expansion coefficient (α_{22}), ply thickness (t), and temperature change from cure (ΔT). In an additional study, the effect of temperature changes on the material properties themselves, and consequently a change in laminate curvature was done. The temperature itself was varied from 13.05°C-28.95°C. It was observed the material properties E_{22} and α_{11} were most sensitive to temperature change

with a variation of -7.91% to 9.21%, and -44.44% to 50.69% respectively. Subsequent change in curvature was then found to be 3.66% to -3.51% for E_{22} and -5.29% to 4.63% for α_{11}.

Material Property	Room Temperature Value (T = 294K)	Percent change in curvature with ±5% change in variable	
		-5%	+5%
Longitudinal Young's modulus, E_{11}	146 GPa	2.16	-2.08
Transverse Young's modulus, E_{22}	11.7 GPa	-2.18	2.05
Poisson's ratio, ν_{12}	0.308	0.27	-0.27
Shear modulus G_{12}	6.95 GPa	-0.01	0.01
Longitudinal thermal coefficient of expansion, α_{11}	2.48×10^{-6} °C^{-1}	0.52	-0.52
Transverse thermal coefficient of expansion, α_{22}	2.65×10^{-5} °C^{-1}	-5.55	5.55
Single ply thickness, t	0.25 mm	5.32	-4.82
Moisture content, m	0 wt	0.0	-89.07
Temperature change from cure, ΔT	-180 °C	-5.03	5.03

Table 2.1. Maximum change in curvature for a ±5% change in variable, as L/t increases. [27]

[28] studied the temperature dependence of bistable laminates and the effect of a resin layer on the snap-through and snap-back force. They built 4 different FEA models with the presence/absence of temperature dependence, resin layer, and thickness variation. Considering temperature dependence improved the predictions of maximum deflection by 26.2% for [0/90] laminates, 24.1% for [-20/70] laminates, and 25.2% for [-30/60] laminates. Optical microscopy was used to measure the thickness of the resin layer, and by including the effect into the FEA model, accuracy was improved by 7.6-8.9% for the laminate deflection. Investigation of snap-through and snap-back forces revealed that the snap-through force was greater than the force required for snap-back. This was primarily because of the presence of resin layer, which cause unsymmetric stiffness properties for the two different shapes of the laminate.

From this section, it is evident that environmental effects with respect to moisture absorption and change in temperature play a big role in the behavior of bistable laminates. Improper assumptions of material properties also lead to discrepancy between theory and experiment. However, measuring material properties of the composite material is difficult in some cases, which meant that the experimental results never perfectly match with theory. In the next section, a literature review of the relation between laminate geometry and the presence or loss of bistability, relation between geometry and curvature, and the relation between the geometry and force of actuation is presented.

IV. Relationship between the geometry of the laminate and its behavior

As established in the introduction, this research is aimed at investigating different relations between geometry and behavior of a laminate through theoretical and experimental approaches. Hence, this part of the literature review is also divided into three sections:

1. Relation between the length/thickness ratio and length/width ratio on the presence/absence of bistability,
2. Relation between side length and curvature,
3. Relation between side length and snap-through force

1. Relation between length/thickness and length/width on the presence of bistability: While developing the first ECLT, Hyer [3] found that the critical length for a T300/5208 graphite-epoxy laminate with a stacking sequence of $[0_2/90_2]$ was 35mm, whereas the critical length for a $[0_4/90_4]$ laminate was 71mm. Thus, it was proved that as the number of plies is increased, the critical length necessary for achieving bistability must also be increased. It was also observed that the curvature for the thicker laminate was less than the curvature for the thinner laminate.

[8] also found that as the number of layers were increased, the curvature decreased, the bifurcation point was obtained at the constant value of W/T of 84. It is important to note that Hyer found that the critical length increased with an increase in thickness, whereas Jun and Hong found that the bifurcation point remained constant when plotted against the

ratio of W/T. [9] conducted further studies on various angle-ply laminates, but the scope of this research is limited to cross-ply laminates, and hence those results are not presented here.

[16] proved that there exists a non-dimensional critical length for square plates beyond which bistability exists, by plotting the non-dimensional curvatures of two perpendicular sides against an increase in the non-dimensional side length of squares. The results are shown in figure 2.21. The non-dimensional parameters were:

$$\text{Curvature, a}^* = \frac{aL^2}{t} \tag{2.8}$$

$$\text{Curvature, b}^* = \frac{bL^2}{t} \tag{2.9}$$

$$\text{L}^* = \frac{L^2}{t^2}\alpha\Delta T \tag{2.10}$$

Where, L is the side length, t is the thickness, and α is the difference between the transverse and the longitudinal coefficients of thermal expansion and ΔT is the temperature differential.

They further studied the loss of bifurcation induced by a change in thickness ratio of the 0° layers to the 90° layer, and the loss of bifurcation induced by a change in the aspect ratio between length and width. As the ratio t_0/t_{90} is reduced; 0.93, 0.78, and 0.51, the value of the non-dimensional critical length L_A^* keeps increasing; 25, 42, and 143. The following relationship was established:

$$(L_A^*).(t_0/t_{90})^3 = \text{constant} \tag{2.11}$$

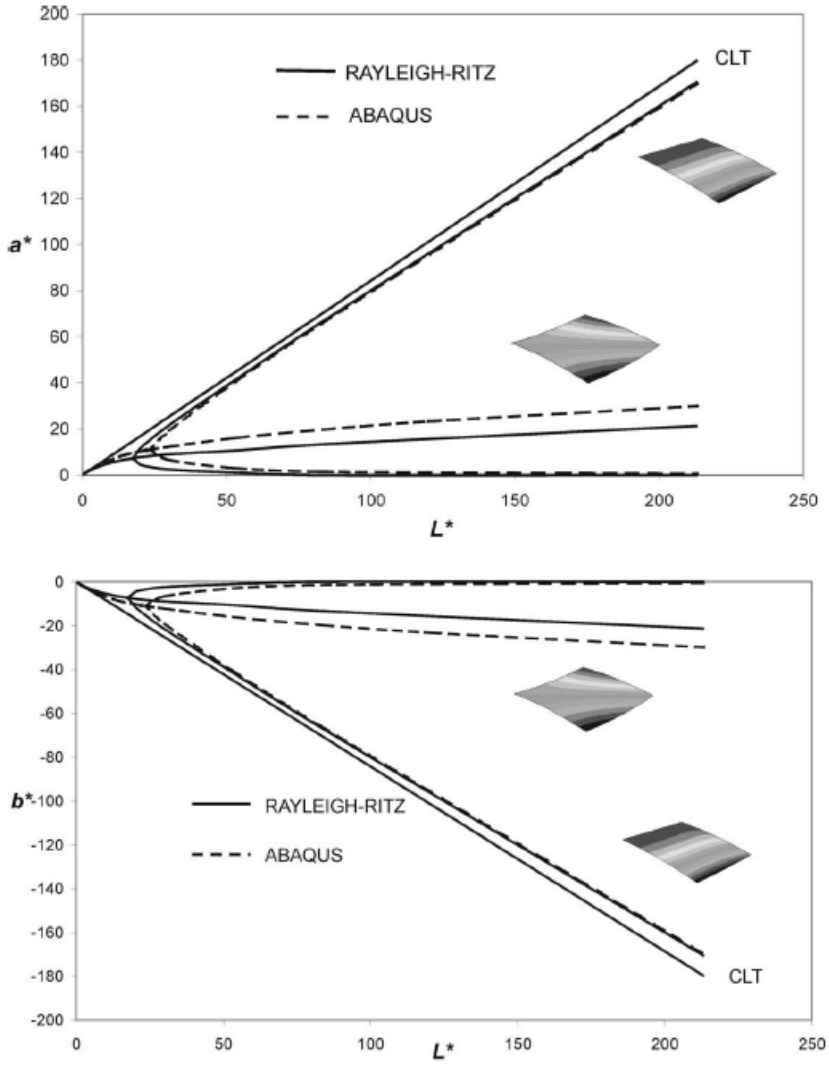

Figure 2.21. Non-dimensional curvatures predicted by Abaqus and Rayleigh-Ritz. [16]

By changing the Aspect Ratio from 1, 2, 3 up to 10, it was found that the Rayleigh-Ritz method and Abaqus gave different results. The Rayleigh-Ritz predicted that as the aspect ratio was increased, the bifurcation point was reached at higher values of side length. However, results from Abaqus show that there is no existence of bifurcation as the aspect ratio is changed from 1. The range of values of side length for which multiple solutions got

reduced as the aspect ratio was increased, and for an aspect ratio of 10, the multiple solutions were not found for the range of side lengths being studied.

(S. A. Tawfik et al., 2011) inspected the bifurcation graph of curvature vs side length for different number of plies. After including non-dimensional for length and curvatures, it was evident that the curves collapsed into a single graph and the non-dimensional critical length L_C was equal to 82.88. The graph is shown in figure 2.22.

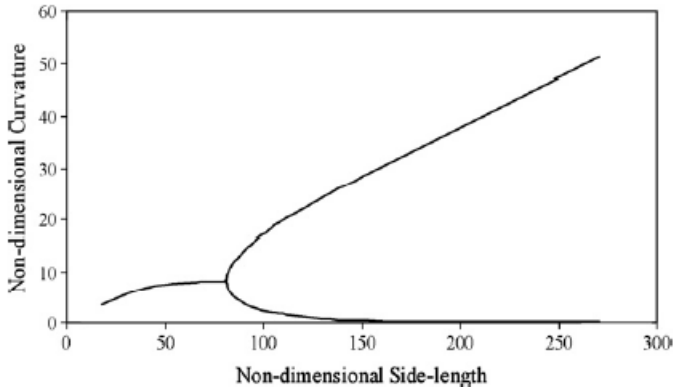

Figure 2.22. Bifurcation of non-dimensional curvature vs non-dimensional side-length for square laminates. [29]

The non-dimensional parameters were:

$$L^* = \frac{L}{t}, \text{ where L is the length and t is the thickness} \quad (2.12)$$

$$K^* = K \times L \times \frac{180}{\pi}, \text{ where K is the curvature} \quad (2.13)$$

Using this graph, it is possible to predict the critical length for a given number of plies. Obviously, this specific graph is for the specific material, IM7/851-7 Graphite/Epoxy prepreg. For different material properties, the non-dimensional critical length will have a different value. A numerical study of the force required for snap-through and snap-back

with an increase in aspect ratio of the laminate found that a laminate with an aspect ratio of 8 was not bistable. One side of the laminate was kept constant at 150mm, and starting with an aspect ratio of 150mm, the other side was decreased up to an aspect ratio of 8.

2. Relation between side length and curvature: The primary geometries being considered in the current research are squares and rectangles. For bistable laminates, by definition, there exist two curvatures that are perpendicular to each other and opposite in sign. The relation between the size of two laminates and its curvature are well understood based on the bifurcation graphs shown in figure 2.21 and 2.22. However, there is not a lot of research available on the relation between the curvature associated with the length and widths of rectangular laminates.

3. Relation between side length and force for snap-through: [30] studied the response of unsymmetric laminates to simple applied forces. The ECLT was used to predict the force of actuation for a 250 x 250 mm, $[0_2/90_2]$ laminate and it was verified with a simple experiment. The force was applied experimentally by adding water to a container tied to the laminate, and by measuring the weight of the water, the force was measured. The force was predicted to be 22.5N by ECLT and it was found to be just above 23N by experiment.

(Potter et al., 2007) conducted experimental tests to study the snap-through of [0/90] square laminates of different sizes. The laminates were placed on a polished 5mm thin aluminum plate and the force was applied with a 10mm diameter hardened steel ball. The typical load-displacement curve observed for the laminates is shown in figure 2.23.

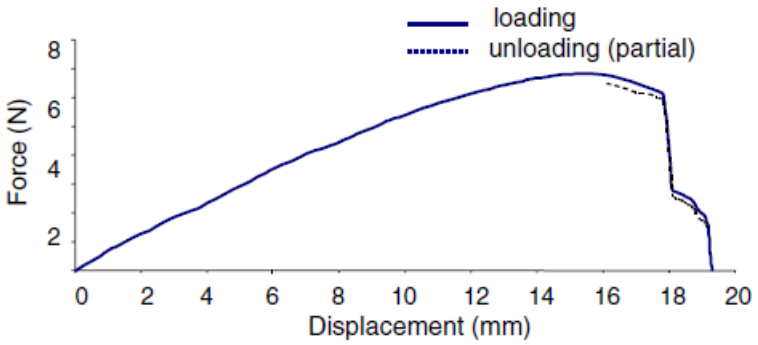

Figure 2.23. Load vs displacement of a 150 x 150 mm, [0/90] laminate. [31]

The tests were performed for square laminates with sizes of 70, 80, 90, 100, 110, 120, 130, 140, and 150 mm. The peak load for each laminate is given in table 2.2. For the results presented here, the force was applied in the geometric center of the laminate. The point of application of force was varied and it was found that the minimum peak load was at the center of the laminate.

Side Length (mm)	Peak Load (N)
70	4.2
80	5.1
90	5.8
100	6
110	6.6
130	7
140	7.3
150	7.1

Table 2.2. Side Length Vs Peak Load before snap-through for [0/90] laminates. [31]

[18] found the force for snap-through and snap-back for laminates with varying aspect ratio (length-to-width). The laminates were manufactured using Hexcel IM7/8551-7 graphite/epoxy prepreg with a stacking sequence of $[0_2/90_2]$. The aspect ratio was varied by maintaining one side at 152.4mm and reducing the other one. The Instron Microstester 5548 machine was used with a 25mm wide plunger to measure the experimental loads. The theoretical forces were obtained from FEA. There was a difference between the results primarily because of a difference in boundary conditions between the experiments and FEA. In FEA, the corner nodes were restricted to move in the z direction whereas in the experiment the two opposite straight edges of the laminate were sliding against a flat surface. The results are presented in table 2.3. It was observed that laminates with aspect ratio of 8 did not snap-through and it was concluded that bistability ceased to exist beyond an aspect ratio of 8.

[20] found the snap-through force for laminates with variation in the lay-up experimentally and theoretically, whereas (Diaconu et al., 2009) developed a dynamic model to calculate snap-through force.

Aspect Ratio	Snap-through load			Snap-back load		
	Experiment	FEA	Difference	Experiment	FEA	Difference
1.0	2.37	2.55	7.59	2.37	2.55	7.59
1.2	1.96	2.03	3.78	2.41	3.13	30.06
1.5	1.27	1.49	16.75	2.45	3.03	23.86
2.0	0.86	1.04	21.13	2.69	2.97	10.74
3.0	0.46	0.67	46.20	2.18	2.79	27.86
6.0	0.28	0.29	5.78	-	0.56	-
8.0	-	-	-	-	-	-

Table 2.3. Comparison between experimental and FEA results for snapping forces with varying aspect ratio. [18]

Research reviewed in this section thus gives us an understanding of various methods that have been developed to calculate the force for snap-through including some relations between geometry and force for snap-through.

V. Potential applications of Bistable Composites

In this section research on potential applications of bistable composites is presented. The uniqueness of bistable composites is that they can remain stable in two

shapes with large out of plane deformation. This characteristic can be used for shape-morphing applications.

[33] developed an airfoil-like active bistable twisting structure consisting of two curved shells. Several proof-of-concept models were built using bistable composites and steel. Finite Element Analysis was used to compare the predicted shapes with the experimental shapes. The devices were built using two rectangular cylindrical shells that were combined in such a way as to form a bistable assembly; one with a positive twist and one with a negative twist. Piezoelectric actuators were bonded to the inside of the constituent shells and were used for actuation between two shapes.

[34] manufactured and performed aeroelastic analysis of a bistable structure for a helicopter rotor blade. The manufactured structure is shown in figure 2.24. It consists of six, 100 x 100 mm, [0/90/90/0], Hexcel 913 laminates. The bistable laminates were attached at one end to a spar. A deflection of 10° was achieved through actuation. The maximum actuator work needed for snap through was found to be 4.01 J/m.

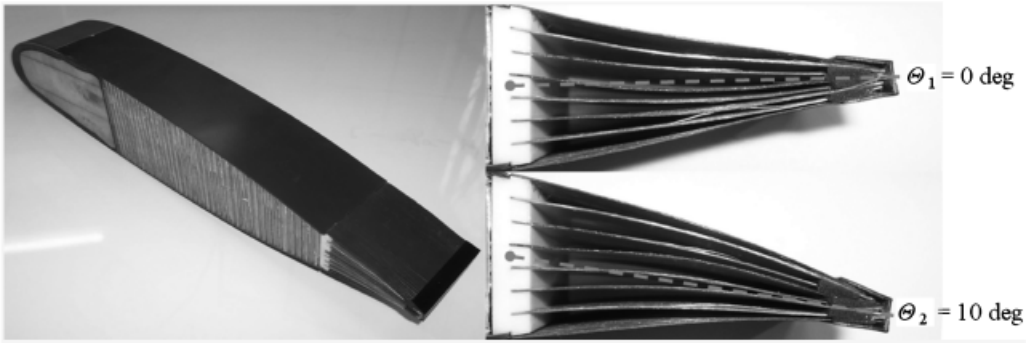

Figure 2.24. Rotor blade section with bistable flap [34]

(Mattioni et al., 2008) presented three possible applications for morphing aircraft structures, namely, a variable sweep wing, bistable blended winglets, and a variable camber trailing edge. These are shown in figures 2.25 – 2.28.

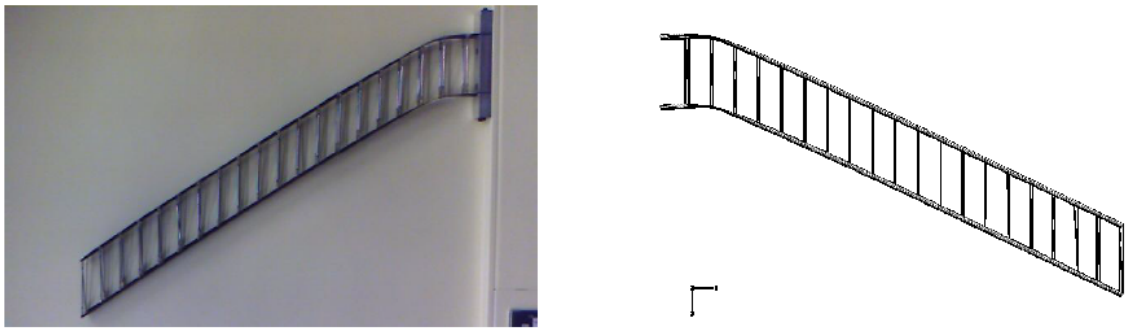

(a) Experimental model (b) Numerical Model

Figure 2.25. Variable sweep wing [35]

The variable sweep wing consists of two spars with an interconnected truss-rib structure. The load for actuation was found to be 70.3N by clamping the wing-box.

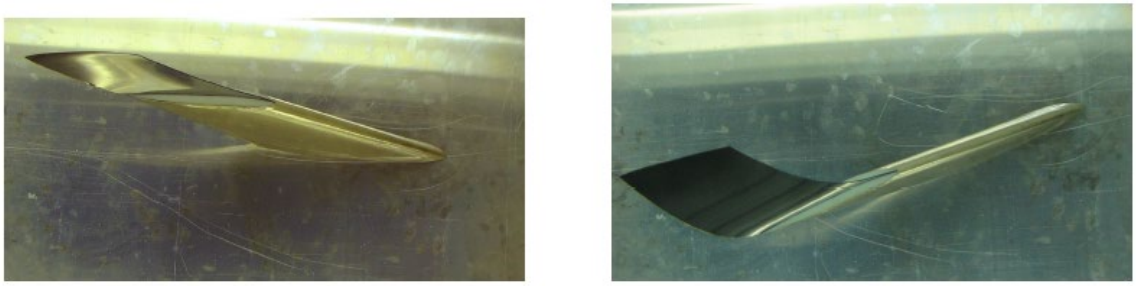

(a) Extended configuration (b) Deployed Configuration

Figure 2.26. Bistable blended winglet [35]

The purpose of the bistable blended winglet was that when the panel is flat, the wing span was extended thus increasing the lift, whereas in the deployed state, it optimized

the aerodynamic performance for cruise flight. The stacking sequence for the bistable blended winglet is shown in figure 2.27.

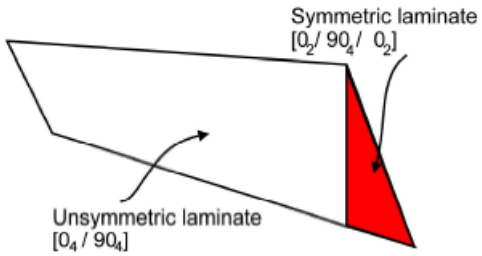

Figure 2.27. Stacking sequence for bistable blended winglet (Mattioni et al., 2008)

Figure 2.28. Variable camber trailing edge [35]

The variable camber trailing edge is shown in figure 2.28. It consisted of bistable laminates with variable stacking sequences such that the laminate was continuous when going from the upper skin to the lower skin. Four configurations are possible with the two skins, with two of them being useful. It was found that the deployed configuration had higher stiffness and therefor generate higher aerodynamic forces and structural loads.

(Arrieta et al., 2010) conducted experiments on bistable laminates for nonlinear energy harvesting. Testing was done on $[0_2/90_2]$, 200 x 200 mm laminates with four PZT-5A piezoelectric patches bonded to the plate. It was found that a very high electric power output was obtained for intermittency and large amplitude limit cycle oscillations giving 34 mW and 27 mW respectively.

[37] provided an experimental study of bistable piezoelectric-composite plates as well. They found that power outputs were large during snap-through with power being generated at the order of 3.2mW. (D. N. Betts et al., 2012) optimized the bistable piezoelectric-composite plates by varying the aspect ratio, thickness, stacking sequence, and piezoelectric area. It was found that square, cross-ply, $[0^P/0/90/90^P]$ laminates offered the largest energy output, since the laminate curvatures aligned with the piezoelectric polarization axis. A local solution was also found for $[0^P/90/0/90^P]$ laminates with optimal piezoelectric alignment but reduced laminate curvature. (David N Betts et al., 2012) analyzed the problem using static and dynamic analysis. The dynamic analysis revealed that thicker laminates produced higher levels of energy, however, the force range in which snap-through occurred was more limited than for the less optimal thinner laminates.

CHAPTER THREE

SIMULATION AND EXPERIMENTS

As established in the literature review, Finite Element Analysis is found to be very accurate at predicting the post-cure shape of bistable laminates including the displacement near the edges. In this research, Abaqus software is used for all FEA calculations with post-processing of data being done on Matlab. The results are then validated by fabrication and testing of laminates. Laminates are manufactured using a vacuum bagging technique, curvatures of laminates are measured using the Nanovea ST500 profilometer and the force for snap-through is measured using an ADMET Expert 5601 universal testing system with an MTESTQuattro Controller. This chapter is divided into five sections;

I. The first describes the FEA model, the vacuum bagging technique, the profilometer set-up, and the universal test set-up.
II. Relation between length and thickness of square laminates for bistability.
III. Relation between length and width of rectangular laminates for bistability.
IV. Prediction of curvature for bistable laminates
V. Prediction of snap-through force for bistable laminates

I. FEA model, Vacuum Bagging Technique, Profilometer, and Universal Test Set-Up

In this section, the FEA model used for all calculations is described. The FEA analysis is verified by fabricating laminates and the vacuum bagging technique used for

fabrication is explained. The shape of the fabricated laminates is scanned using a Nanovea Profilometer and the snap-through force is measured using the ADMET universal test set-up. Both these set-ups are also detailed.

FEA Model

The Abaqus FEA model described by [18] and [23], is modified and used in this research. Since only simple geometries (square and rectangles) are being considered, the part geometry is modelled in Abaqus itself. For more complicated geometries, a CAD software can be used for generating the part file and then analyzing it in Abaqus. The material being used is DA 409U/G35 150 unidirectional carbon epoxy prepreg. The only material properties available for this material were its tensile modulus (18.8 msi) and flexural modulus (17.9 msi). These values are very close to those of AS4/8552 as shown in table 3.1. Therefore, the properties of AS4/8552 are used, which are given in table 3.2.

Property/Material	DA 409U/G35-150	AS4 – 8552
Tensile Modulus	18.8 msi	19.6 msi
Flexural Modulus	17.9 msi	18.4 msi

Table 3.1. Comparison of material properties of AS4/8552 and DA 409U/G35-150.

Property	Value
E_1	135GPa
E_2	9.5GPa
ν_{12}	0.3
G_{12}	5GPa
G_{13}	7.17GPa
G_{23}	3.97GPa
α_1	$-2x10^{-8}$/°C
α_2	$-3x10^{-5}$/°C
Ply Thickness	0.15mm

Table 3.2. Material properties for AS4/8552.

The ply thickness and orientation are assigned using the 'section' tab, with orientation being either 0° or 90°. Thick shell S4R elements are used for meshing the laminates. Mesh convergence information provided by [18] was used for reference and a convergence study was carried out. Since the laminate size is altered on each simulation, a constant number of elements equal to 900, corresponding to 961 nodes is chosen. This corresponded to a global element size of 1 mm^2 for a square laminate of 30 x 30 mm dimensions. This ratio is kept constant in order to have the same number of elements for laminates of different sizes. For rectangular laminates, the same ratio of side length-to-global element size is maintained with respect to the smaller side. So for example, a 150 x

150 mm square laminate has a global element size of 5 mm^2, whereas a rectangular laminate with dimensions of 90 x 150 mm has a global element size of 3 mm^2.

The bistability of laminates is tested in several 'steps' in Abaqus:

1. Initial condition: The initial elevated curing temperature of 121°C is applied to the entire laminate in the 'predefined field' tab. The initial boundary condition is slightly different for square laminates and rectangular laminates. For rectangular laminates, the node coinciding with the geometric center is fixed in all degrees of freedom. As established in the literature review, an FEA simulation of perfectly square laminates always deforms into an unstable shape unless a slight imperfection is introduced in the geometry or by applying a small force at the start of the cool down step. Therefore, for square laminates, the initial boundary condition is applied to two nodes at the center of two opposite sides as shown in figure 3.1. The displacement in z direction, as well as all rotational degrees of freedom are fixed. The boundary conditions for square (150 x 150 mm), and rectangular (50 x 100 mm), [0/90] laminates are shown in figure 3.1.

2. Cooling: The initial boundary condition is propagated, whereas the 'predefined field' temperature of 121°C is modified to 21°C (room temperature). This is a 'static, general' step with the 'NLGEOM' function turned on. It is important to note that without the 'NLGEOM' function, Abaqus assumes a linear stress-displacement relation and predicts a saddle shape similar to the one predicted by the linear CLT. A small constant damping factor of $2.5e^{-7}$ is used in order to make the step pseudo-dynamic. This helps the

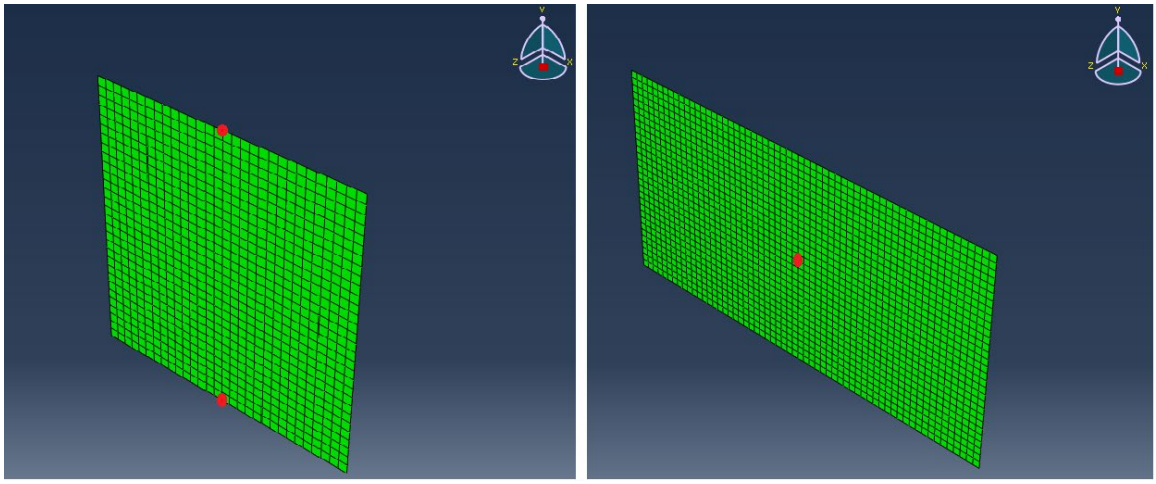

Figure 3.1. Initial boundary condition for a square and rectangular laminates.

convergence of the model as described in [13]. At the end of this step, the laminates cool down to the post-cure room temperature as shown in figure 3.2.

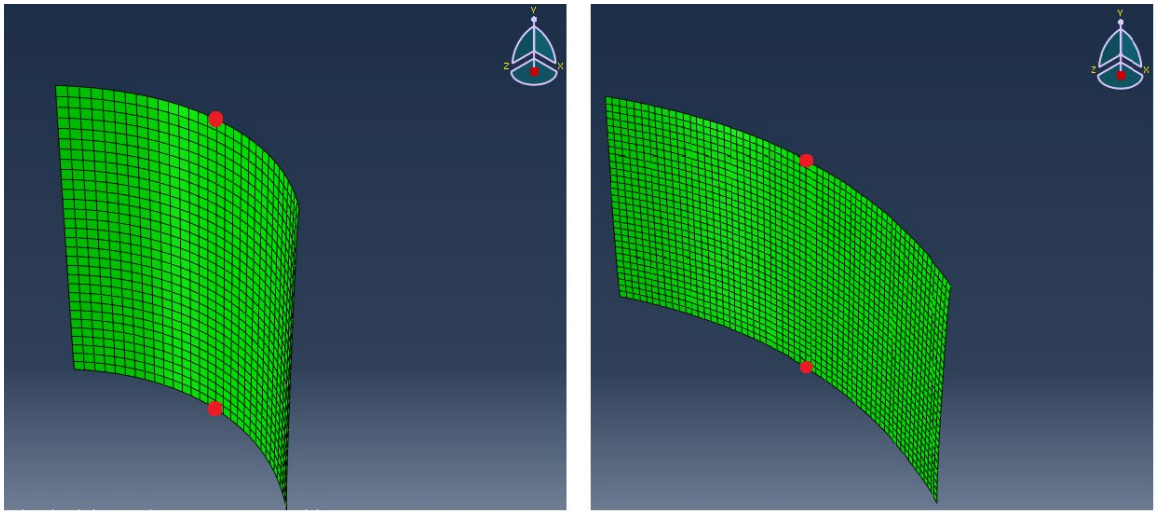

Figure 3.2. Post cure shape of square and rectangular laminates.

3. Snap-Through: Once the laminate cools down, the snap-through is initiated by applying a concentrated force in the geometric center of the laminate. The force is applied perpendicular to the laminate in the positive z direction which is approximately higher than the snap-through force. The boundary conditions for both square and rectangular laminates are the same from this step onwards and for this step, they are applied to the two nodes shown in figure 3.2. The two nodes are restricted to move in z direction and all rotational degrees of freedom are suppressed.

4. Unloading step: After the application of force, the laminate deforms into an unstable shape with the curvature opposite to the post-cure shape. To test whether the laminate stabilizes back into the original shape or a secondary stable shape, a neutral, unloading step is applied. The force is deactivated and the central node is fixed in all degrees of freedom. If the laminate is bistable, it stabilizes into the shapes show in figure 3.3. If the laminate is not bistable, it stabilizes back to the original shape shown in figure 3.1.

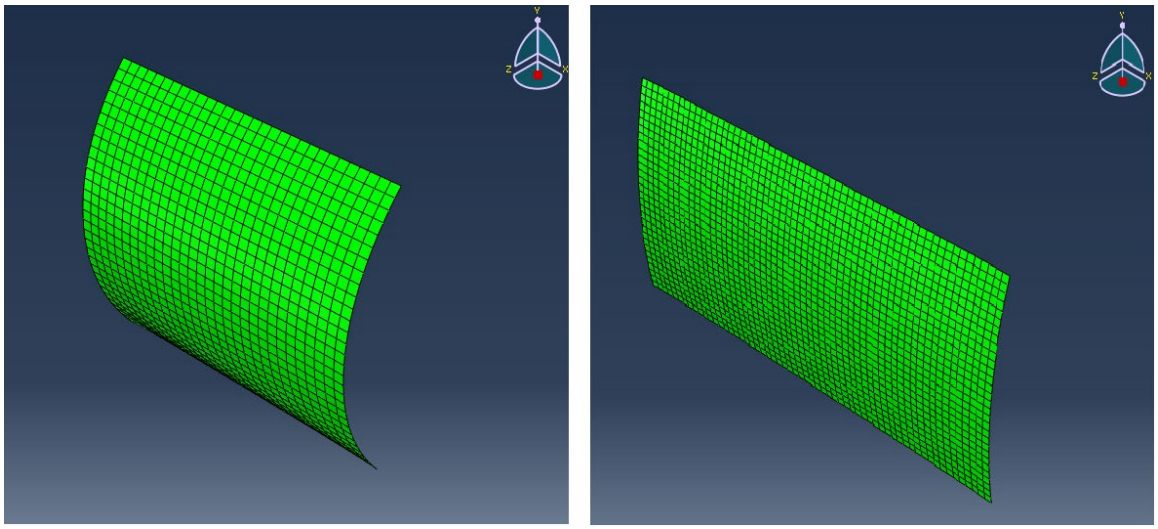

Figure 3.3. Post snap-through shape of bistable, square and rectangular laminates.

The post-processing of FEA results is done in MATLAB. The nodal displacements are exported and the curvatures are calculated using the formula given in equation 3.1.

$$\kappa = \frac{1}{R} = \frac{8d}{C^2 + 4d^2} \tag{3.1}$$

Where K is the curvature, R is the radius of curvature, d is the out of plane deformation, and C is the chord length.

Experimental Set-Up

A standard vacuum bagging technique is used for manufacturing the laminates. The material for vacuum bagging and the prepreg is purchased from Rock West Composites, Inc. and Fibre Glast Developments Corporation. The vacuum bagging technique involves an application of pressure on the laminates while curing using a vacuum pump which is explained on the Fibre Glast website. Applying this pressure serves various purposes. First; it removes the trapped air between the layers of the laminate. Second, it compacts the fibre layers and prevents shifting of the fibre orientation. Third, it reduces humidity. Finally, it also optimizes the fibre-to-resin ratio by squeezing out excess resin. The fabrication process begins by cutting the required geometry from the prepreg material and laying up the laminate according to the required stacking sequence. A quarter inch aluminium plate is used for curing the laminate. First, a 'mold release' (FibRelease 1153, purchased from Fibreglast) is applied on the aluminium plate and allowed to evaporate. This avoids the laminate from sticking to the plate after curing. Then, the laminate is placed on the plate and it is covered by a perforated release film and a peel ply. The perforation in the release film helps to squeeze out the excess resin and the peel ply provides a smooth finish to the

laminate surface. Both these layers are covered by a breather material which helps in uniform distribution of pressure over the surface of the laminate. A 'thru-bag vacuum connector' is placed on top of the breather material which allows the air to be sucked out from the vacuum bag. Finally, the vacuum bag is used along with double sided sealant tape to create a vacuum using a vacuum pump.

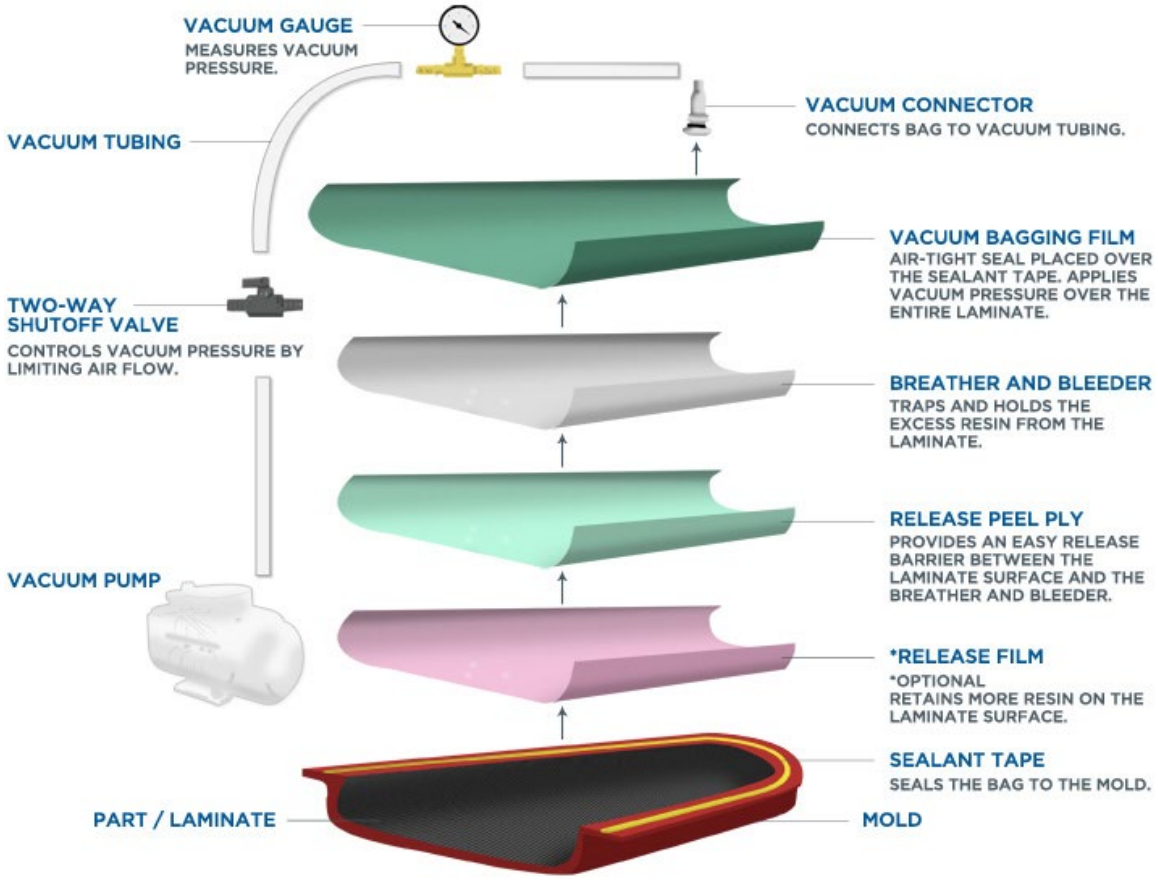

Figure 3.4 Vacuum Bag Apparatus [40].

The entire vacuum bag is placed in an oven at 275F for one hour, after which the oven and the vacuum pump are shut off. The laminate is allowed to cool down to room

temperature naturally and is retrieved from the vacuum bag after cooling. The vacuum bagging apparatus taken from the Fibre Glast website is shown in figure 3.4.

The Nanovea ST500 profilometer is used to scan the top surface of the laminate and 'Expert 3D software' is used to measure the deformation and curvature of the scanned shape. The approach used in the post-processing of the FEA model is also used while measuring the curvature of the fabricated laminate. Figures 3.5 shows a 3D scan of a 3 x 3 in^2, [0/90] laminate in one of its stable configurations

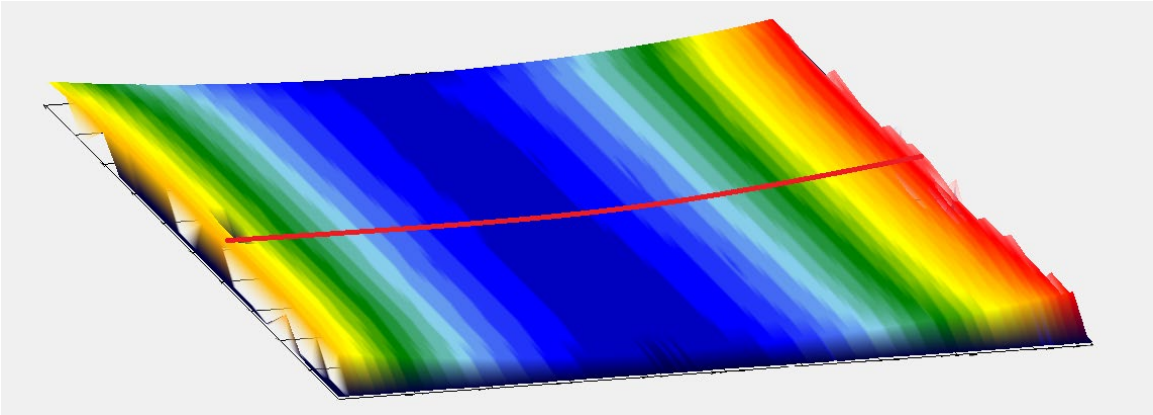

Figure 3.5. A 3D scan of a 3 x 3 in^2, [0/90] laminate in its post-cure configuration.

The post-processing of this 3D scan is done in Expert 3D software. The out of plane deformation of a horizontal line (red colour line in figure 3.5), coincident with the X axis (geometric center being the origin in a Cartesian coordinate system) is recorded. The X axis is chosen such that it is perpendicular to the axis of curvature for the laminate in its post-cure shape. First, a 2D profile is extracted as shown in figure 3.6. Then, using the distance measurement tool, the out-of-plane deformation of both edges is recorded, and the

curvature is calculated using equation 3.1 by taking an average of the two deformations, indicated by 'height difference' in figure 3.6. Thus, the curvature of a line coincident with the X axis for the laminate shown in figure 3.5 is found to be 0.0038 mm^{-1}.

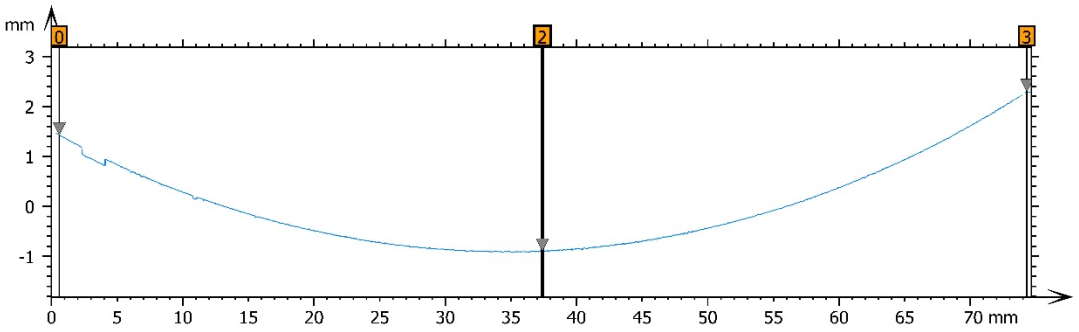

Parameters	Unit	0-1	2-3
Horizontal distance	mm	36.794	36.913
Height difference	mm	-2.324	3.192

Figure 3.6. 2D profile of horizontal line coincident with the X axis for the laminate shape shown in figure 3.5.

The ADMET Expert 5601 universal testing system is used to measure the force for snap-through. The boundary conditions from the FEA model are replicated by using two hinge supports on two opposite edges with an application of force in the center. The test set up is shown in figure 3.7. The load is applied using displacement control and the screw used for application of force travels at a rate of 0.25mm/sec. The reaction load is recorded at every step by the software and the peak load is observed at the moment of snap-through. The peak load is considered to be the force required for snap-through. The load-displacement curve is similar to the one found by [31], shown in figure 2.23. The test is repeated five times for each laminate and an average is taken.

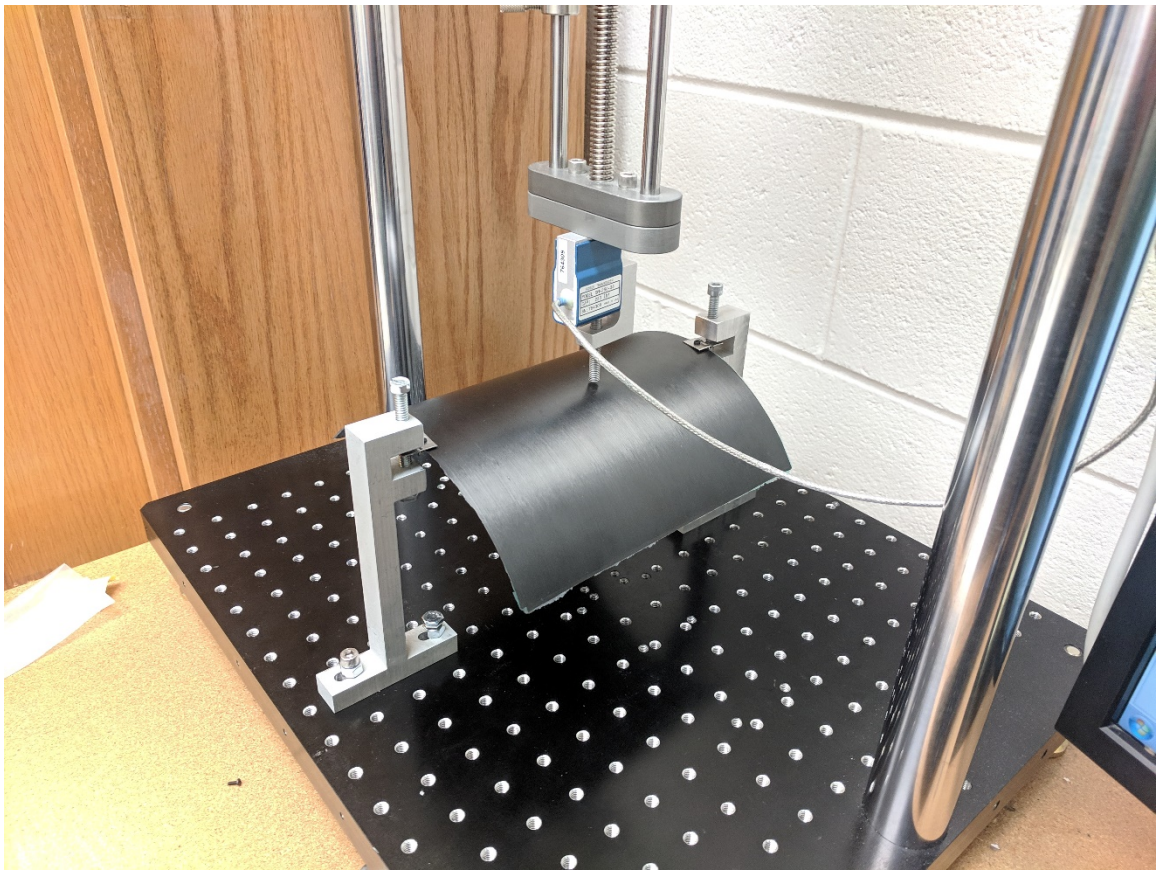

Figure 3.7. Set-up for measurement of force for snap-through. Figure shows an 8 x 8 in^2, [0/90] laminate.

I. Relation between length and thickness of square laminates for bistability

The relation between side length and thickness of square laminates necessary to achieve bistability is first studied using FEA, which is then followed by experimental validation. Using these results, large bistable structures are fabricated. The results from both are compared and the similarities and differences are discussed.

FEA Approach

Work presented by [29] showed that there exists a non-dimensional critical length for square laminates of all thicknesses such that laminates with a greater side length are bistable, whereas smaller laminates have one unique shape. This is shown in figure 2.22. However, no experimental data was presented to validate the results. Also, the results were limited to thin laminates with 2 or 4 layers. The purpose here is to fabricate laminates of different thicknesses in order to validate the existence of a single non-dimensional critical length that is valid for all laminates. Further, a thick and large bistable laminate is fabricated. Before proceeding to the experimental results, first, the work done by [29] is replicated for the material properties presented in table 3.2.

The use of FEA to test the bistability was presented in the previous section. While the examples presented in figures 3.1 - 3.3 are clearly bistable, smaller laminates near the bifurcation point are not bistable visually. This is because the two curvatures are so small that it is difficult to notice a difference. Therefore, the deformation in the z direction of the laminates is plotted after the first and last step of the FEA model. If the laminate is bistable, any node on the laminate other than the central node will have two different deformations in the z direction. If the laminate is not bistable, it will come back to the original shape after the last step, and the deflection will be the same for both stages. A node on the edge of the laminate is chosen for this purpose, which is shown in figure 3.8. A major difference between the experimental measurement of curvature and the FEA model is that the FEA model has symmetry about the X and Y axis (geometric centre being the origin). As a

result, unlike the experimental measurement using the profilometer where an average of out of plane deformation of two opposite edges was needed, in the FEA model, only one edge is sufficient.

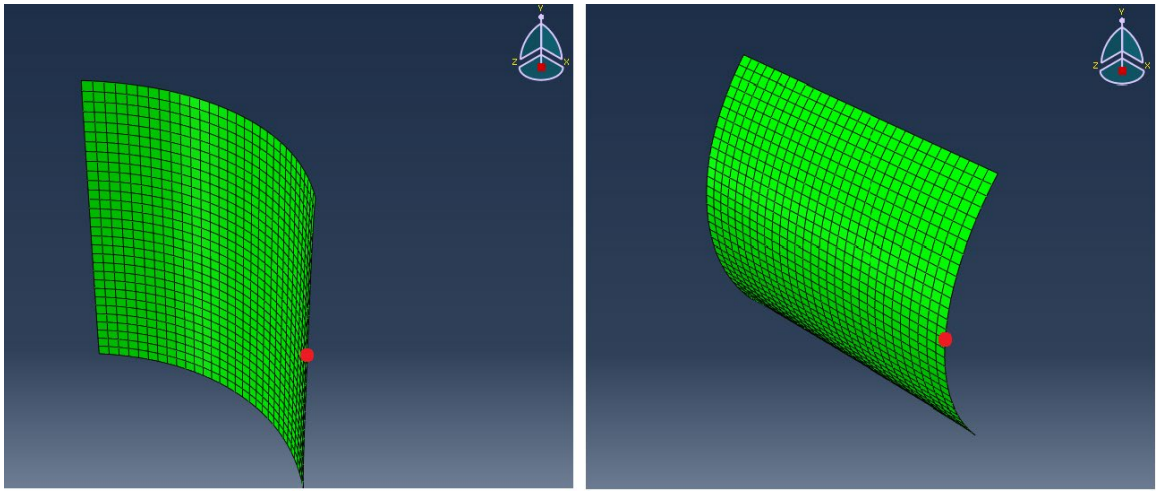

Figure 3.8. Difference in deformation in z direction of a node on the edge of the laminate.

The size of the laminate is increased from 10mm, in increments of 10mm for all thicknesses. For the first few sizes, the two deflections are equal, indicating monostability. As the size is increased, the graph bifurcates into two curves. For example, for laminates with two plies, i.e., a stacking sequence of [0/90], a 20mm laminate is monostable, but a 30mm laminate is bistable, indicating that there is a bifurcation between 20mm and 30mm. To get the specific critical length, the length is then varied in increments of 1mm within this 10mm interval. This gives us a critical length of 23mm as shown in figure 3.9.

The same process is repeated for laminates with 4 plies, i.e., a stacking sequence of $[0_2/90_2]$ and the bifurcation length is found to be 46mm. For 6 plies, the bifurcation is found

to be 69mm. By introducing non-dimensional parameters, a single non-dimensional critical length can be found.

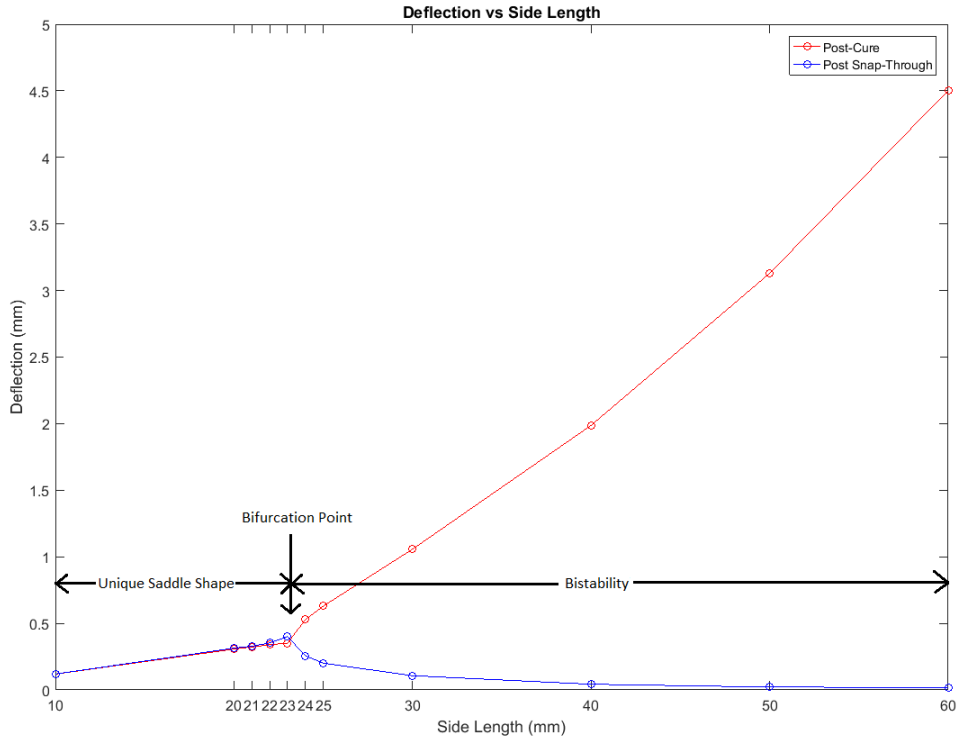

Figure 3.9. Critical length for [0/90] laminates indicated by bifurcation at 23mm.

The side length on the X axis is divided by the thickness. The out-of-plane deformation on the Y axis is used as the out of plane deformation to calculate the curvature using equation 3.1. This curvature is then multiplied by the side length. This is given in equation 3.2 and 3.3.

$$L^* = \frac{L}{t} \tag{3.2}$$

$$K^* = K \times L \tag{3.3}$$

Where L* is the non-dimensional side length, t is the thickness, K is the curvature, and K* is the non-dimensional curvature.

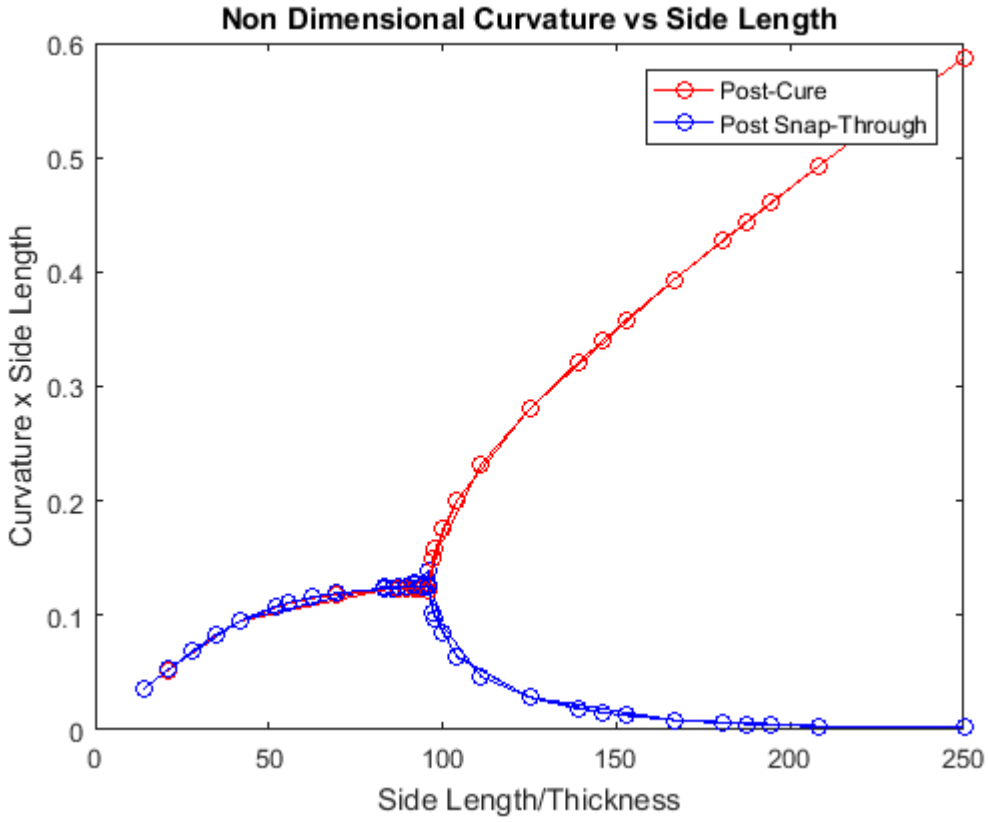

Figure 3.10. Non-dimensional bifurcation graph for laminates with 2 plies, 4 plies, and 6 plies (FEA).

By plotting the bifurcation graph for laminates with 2 plies, 4 plies, and 6 plies with non-dimensional parameters, we get a single curve shown in figure 3.10. The non-dimensional critical length is found to be 95.833. Using this non-dimensional critical length, the critical length for any number of plies can be predicted. For example, a laminate

with 50 plies would have a thickness of 6mm. Substituting in equation 3.2, the critical length for a laminate with 50 plies would be 575mm (22.63 inches).

Experimental Approach

The same approach is followed experimentally. Square laminates with 2, 4, and 6 plies are fabricated with an increase in side length such that smaller laminates were monostable and larger laminates are bistable with a bifurcation in between the two sizes.

2 Plies	**4 Plies**	**6 Plies**
25.40 mm (1.00 in)	57.15 mm (2.25 in)	101.60 mm (4.00 in)
31.75 mm (1.25 in)	63.50 mm (2.50 in)	107.95 mm (4.25 in)
38.10 mm (1.50 in)	69.85 mm (2.75 in)	114.30 mm (4.50 in)
44.45 mm (1.75 in)	76.20 mm (3.00 in)	120.65 mm (4.75 in)
50.80 mm (2.00 in)*	82.55 mm (3.25 in)	127.00 mm (5.00 in)
57.15 mm (2.25 in)*	88.90 mm (3.50 in)	133.35 mm (5.25 in)
63.50 mm (2.50 in)*	95.25 mm (3.75 in)	139.70 mm (5.50 in)
76.20 mm (3.00 in)*	101.60 mm (4.00 in)*	146.05 mm (5.75 in)
	107.95 mm (4.25 in)*	152.40 mm (6.00 in)*
	114.30 mm (4.50 in)*	165.10 mm (6.50 in)*
	120.65 mm (4.75 in)*	171.45 mm (6.75 in)*
	127.00 mm (5.00 in)*	177.80 mm (7.00 in)*

Table 3.3. Results from fabricated laminates. * indicates that laminate is bistable.

The sizes are increased from least to maximum in increments of 0.25 in (6.25 mm). The range of sizes were 1 - 3 in (25.4 – 76.2 mm) for 2 plies, 2 – 5 in (50.8 – 127 mm) for 4 plies, 4 – 7 in (101.6 – 177.8 mm) for 6 plies. It should be noted that the unit for the size of the laminates in the FEA analysis is millimeters. This is because Abaqus does not consider units, and it is the responsibility of the user to convert all properties into a consistent set of units. Since all the material properties are available in Newton and millimeters, the dimensions for the geometry were given in millimeters. However, since the fabrication is done by hand lay-up, it is not possible to have accuracy for a least count as small as millimeters. Therefore, inches are the chosen unit for convenience. The results from fabricated laminates are shown in table 3.3. It is found that the bifurcation points are found at 2 in (50.8 mm) for 2 plies, 4 in (101.6 mm) for 4 plies, and 6 in (152.4 mm) for 6 plies.

The out of plane deformation is scanned using the profilometer for each laminate. For non-bistable laminates, only one shape and the corresponding deformation is measured. For bistable laminates, the out-of-plane deformation is measured for both stable shapes. For a [0/90], 3 x 3 in^2 laminate for example, the two stable shapes are as shown in figures 3.11 and 3.13. The profile of a line coincident with the X axis is shown in figures 3.12 and 3.14.

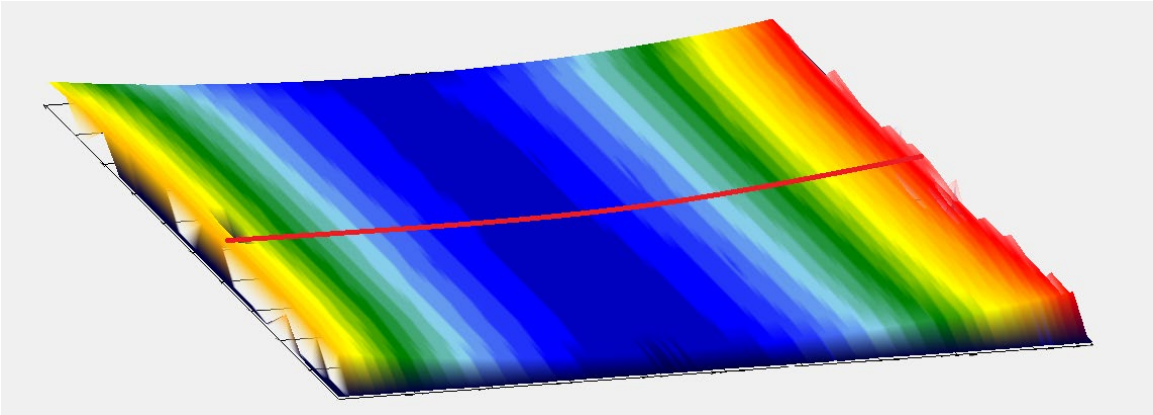

Figure 3.11. Post-cure shape of a [0/90], 3 x 3 in^2 laminate.

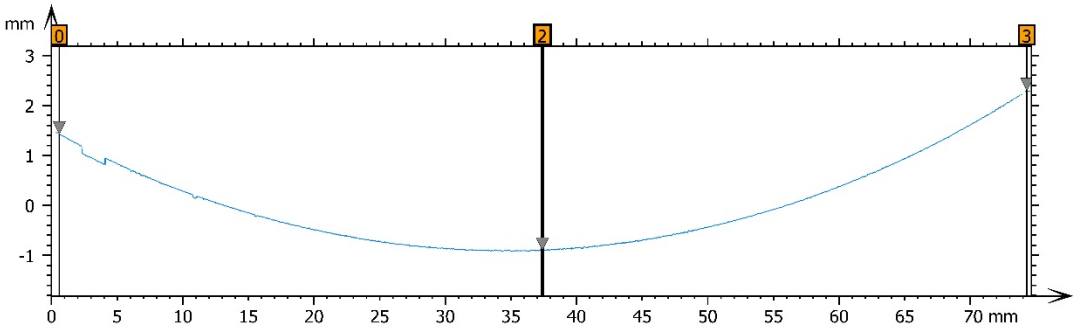

Parameters	Unit	0-1	2-3
Horizontal distance	mm	36.794	36.913
Height difference	mm	-2.324	3.192

Figure 3.12. Curvature of X axis for laminate shown in figure 3.11 (red line).

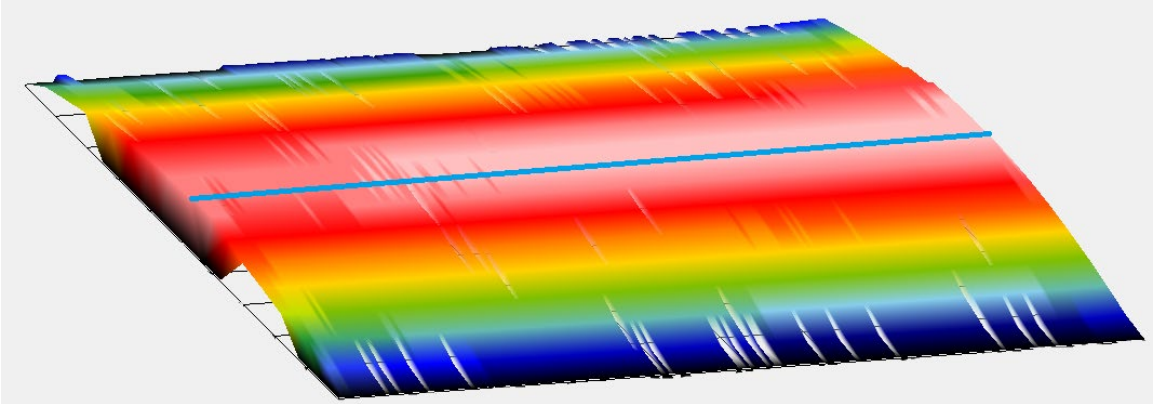

Figure 3.13. Post snap-through shape of a [0/90], 3 x 3 in^2 laminate.

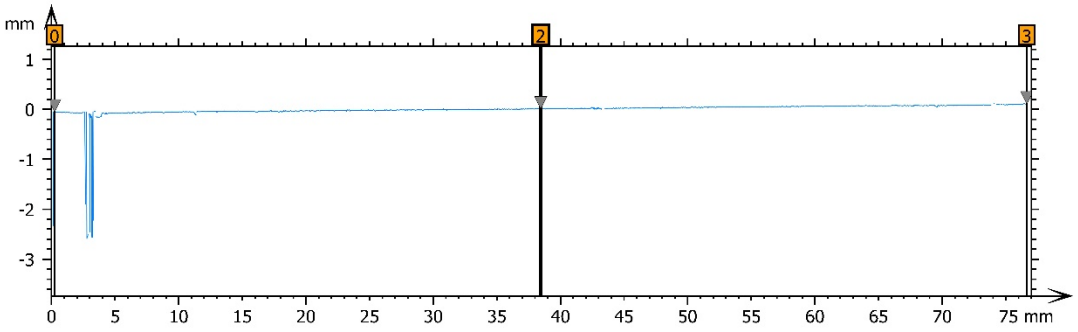

Parameters	Unit	0-1	2-3
Horizontal distance	mm	38.203	38.203
Height difference	mm	0.058	0.100

Figure 3.14. Curvature of X axis of laminate shown in figure 3.13 (blue line).

Using the out of plane deformation (denoted as 'height difference' in figure 3.12 and 3.14), the curvature can be calculated using the formula given in equation 3.1. Thus we get two curvatures for the two shapes with values of 0.0038 mm^{-1} and 1.0884e-04 mm^{-1}. The curvatures and side lengths are then converted into non dimensional parameters using the equations 3.2 and 3.3. The results for 2, 4, and 6 plies are then plotted as shown in figures 3.15-3.17, whereas the non-dimensional parameters are plotted in figure 3.18.

The non-dimensional critical length is found to be 185.2 for 2 plies, 211.7 for 4 plies, and 202.84 for 6 plies. The average non dimensional critical length is therefore 199.9. Using this length, a square laminate with 8 plies would have to be above 191.9mm, or 7.55in to be bistable. Two square laminates with stacking sequences of $[0_4/90_4]$ and side lengths equal to 7 in and 8 in were fabricated. It was found that the 7in laminate was not bistable whereas the 8in laminate was bistable. Thus, from this data, it was concluded that the critical ratio between number of plies and length in inches was 1:1, i.e., a square laminate with 'X' number of plies would have to have a side length of 'X' inches to be bistable.

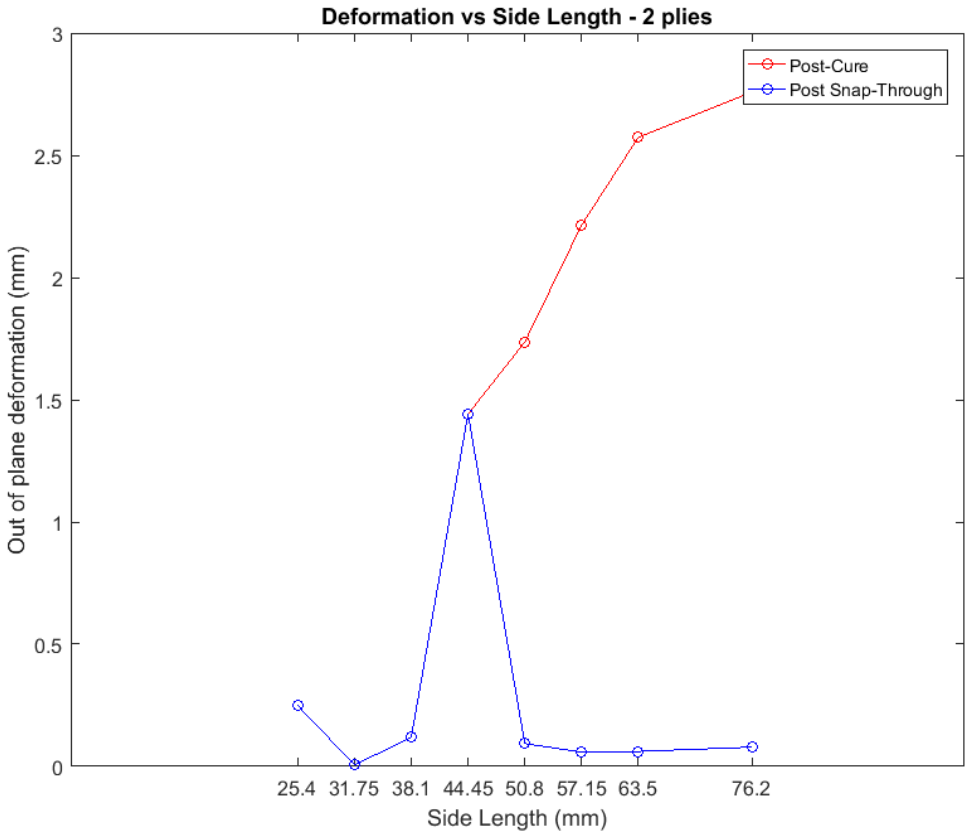

Figure 3.15. Out of plane deformation vs side length for [0/90] square laminates.

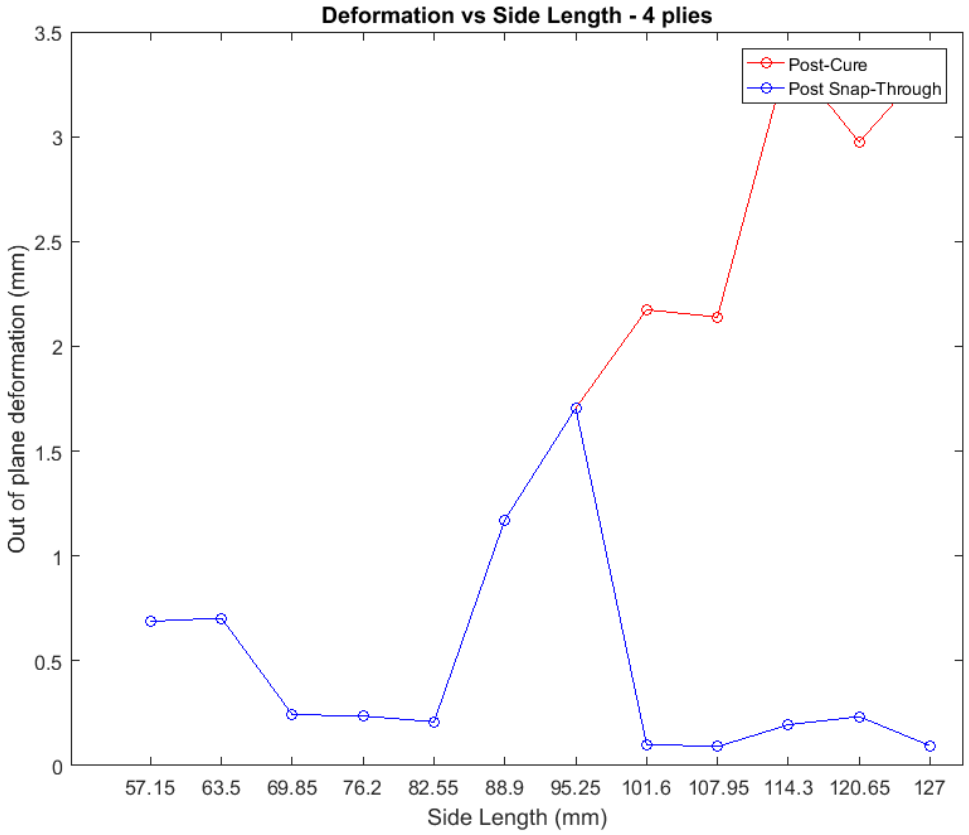

Figure 3.16. Out of plane deformation vs side length for $[0_2/90_2]$ square laminates.

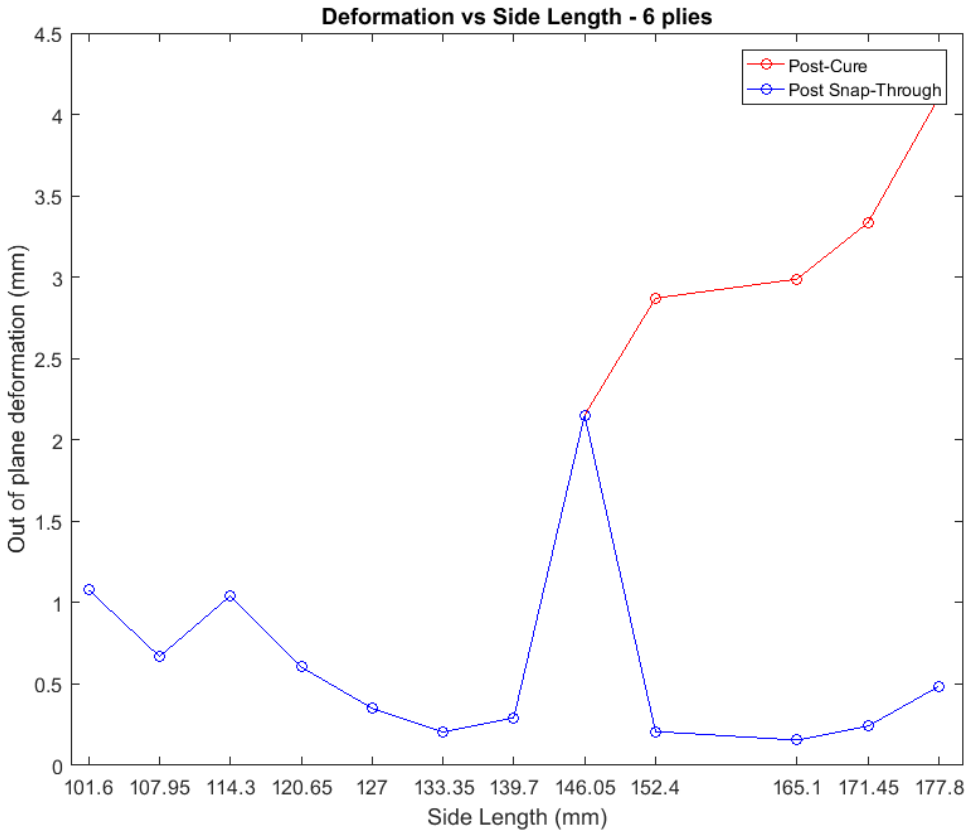

Figure 3.17. Out of plane deformation vs side length for $[0_3/90_3]$ square laminates (variations caused by manufacturing defects of hand lay-up)

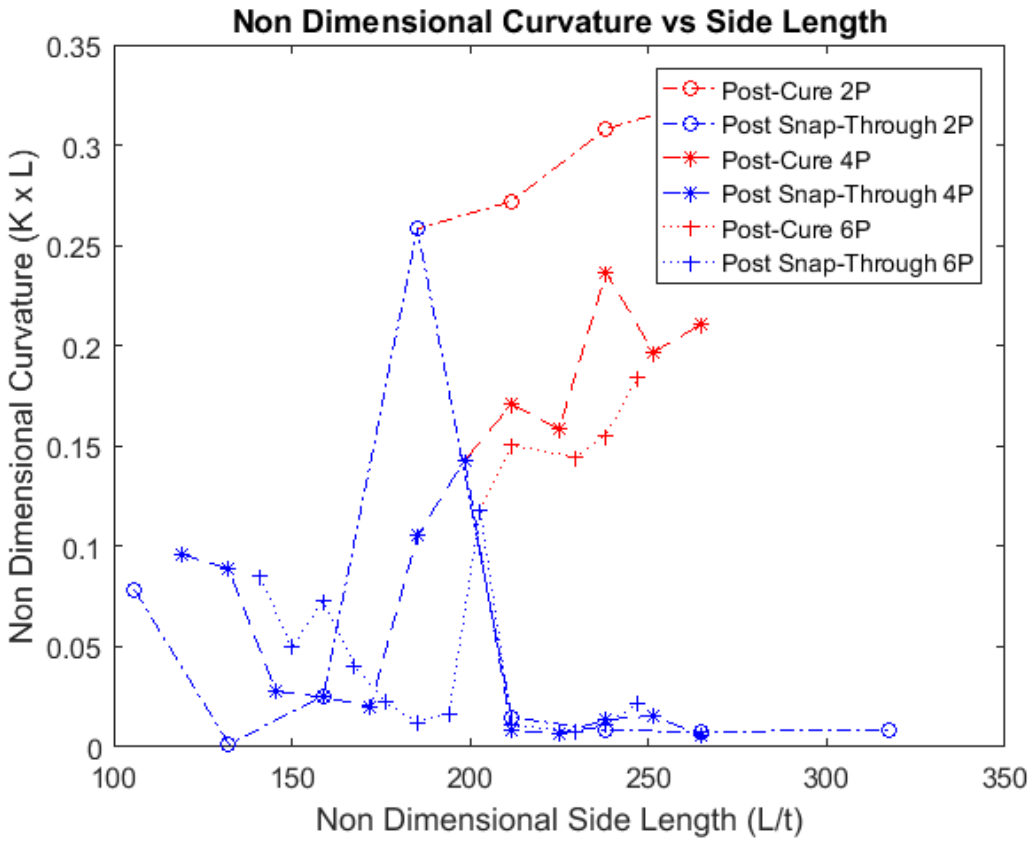

Figure 3.18. Non-dimensional bifurcation graph for laminates with 2 plies, 4 plies, and 6 plies (Experiment)

As established in the literature review, moisture absorption plays a huge role in the reduction of curvature of composite laminates due to a relaxation of internal stresses. The loss in curvature was recorded by [24]. This phenomenon is observed, which results in a loss of bistability of laminates just above the bifurcation point. It was found that the bifurcation length was increased because of moisture absorption, and the bifurcation length for 2, 4, and 6 plies, after a period of one month is given in table 3.4.

Thickness	Critical length without moisture absorption	Critical length after a period of 1 month
2 plies	2 inches (50.8 mm)	2 inches (50.8 mm)
4 plies	4 inches (101.6 mm)	6 inches (152.4 mm)
6 plies	6 inches (152.4 mm)	8 inches (203.2 mm)

Table 3.4. Increase in critical length due to moisture absorption.

The effect of moisture absorption on the bifurcation point is shown in figures 3.19 and 3.20. It can be seen that the bifurcation is found at a greater value of side length.

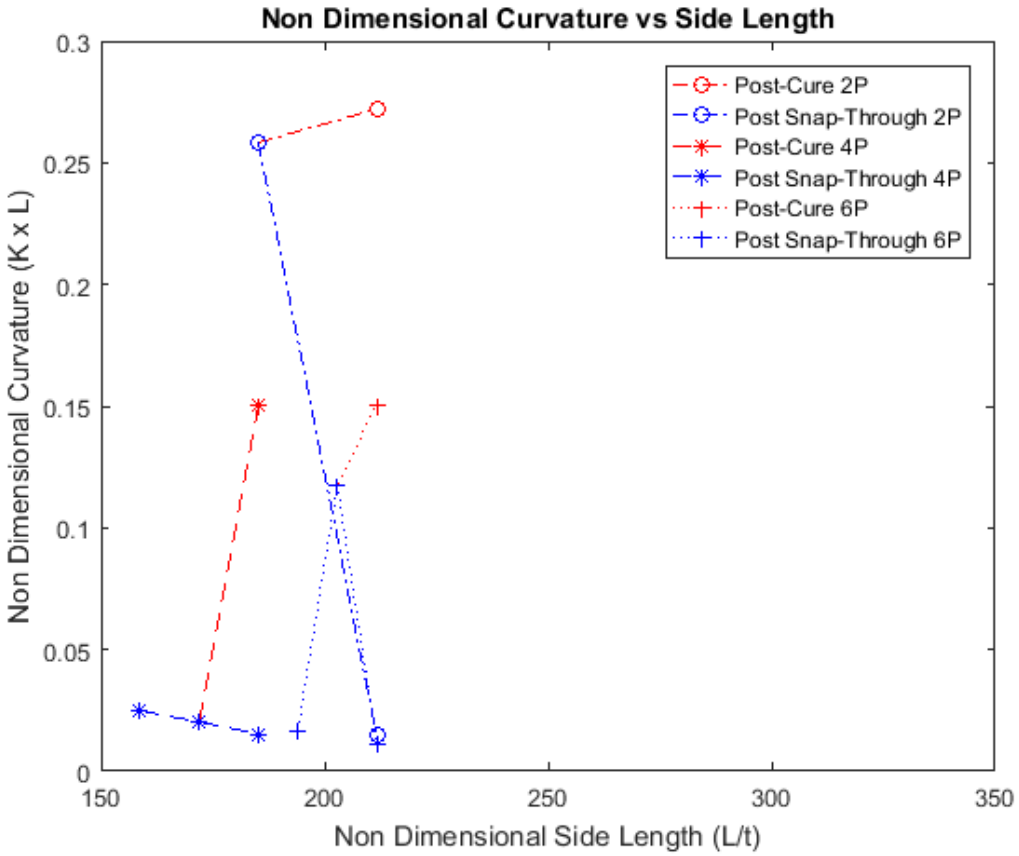

Figure 3.19. Original bifurcation points for 2, 4, and 6 plies.

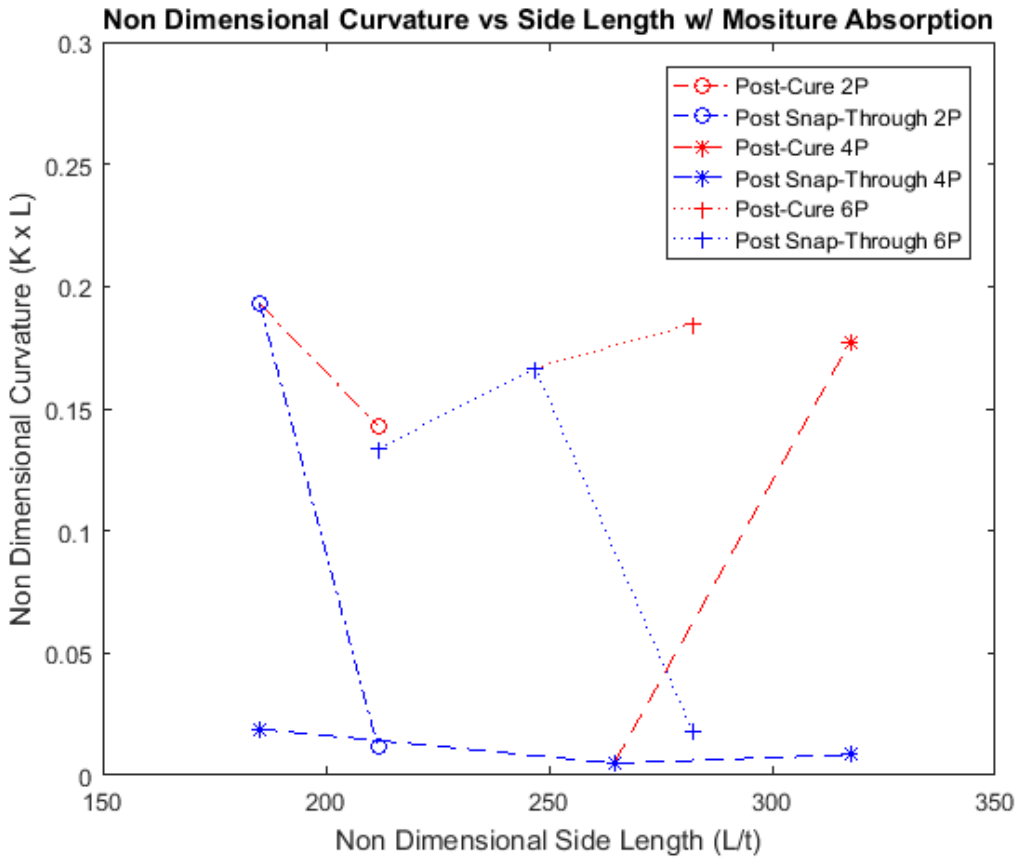

Figure 3.20. Bifurcation points for 2, 4, and 6 plies after a period of one month.

Comparing the bifurcation points in figure 3.19 and 3.20 shows that moisture absorption increases the critical length. Based on the data given in table 3.2, a number of plies-to-side length ratio of 1:1.2 was used for fabrication of large bistable laminates, meaning that a non dimensional critical length was placed at a value of 254. First, a laminate with 10 plies and side length of 12 inches was fabricated, which is bistable as shown in figure 3.21.

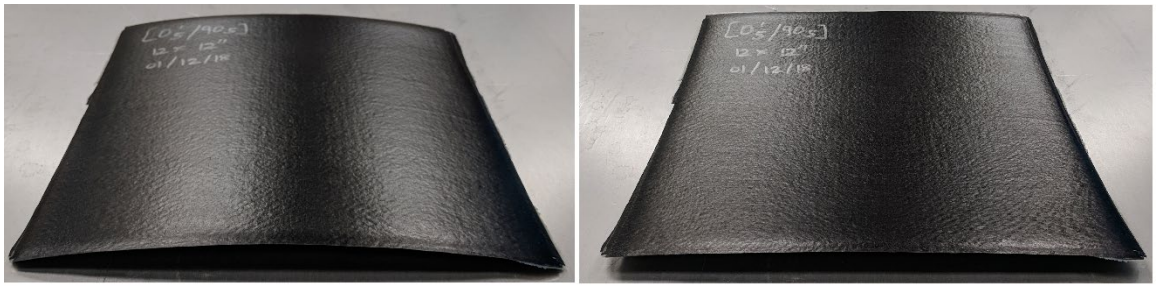

Fig 3.21. Bistable [$0_5/90_5$], 12 x 12 in^2 laminate.

The length and number of plies was further increased and a bistable laminate with 20 plies and side length of 24 inches was fabricated, shown in figure 3.22.

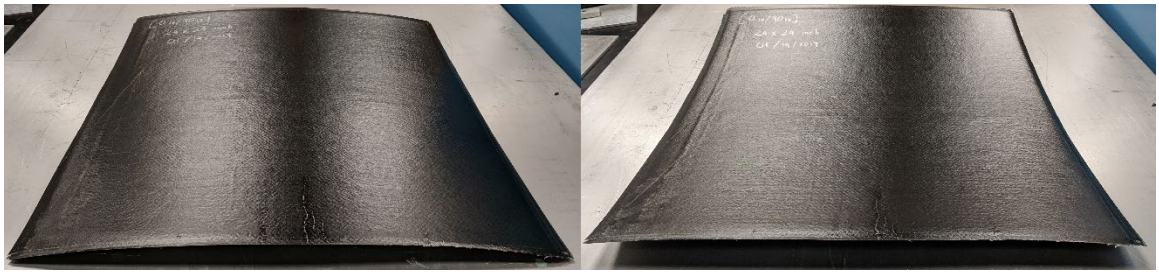

Fig 3.22. Bistable [$0_{10}/90_{10}$], 24 x 24 in^2 laminate.

Finally, a bistable laminate with 30 plies and a side length of 36 inches was fabricated, shown in figure 3.23. There was a limitation on the maximum side length for the laminate because the oven was 40 x 40 in^2 in dimension.

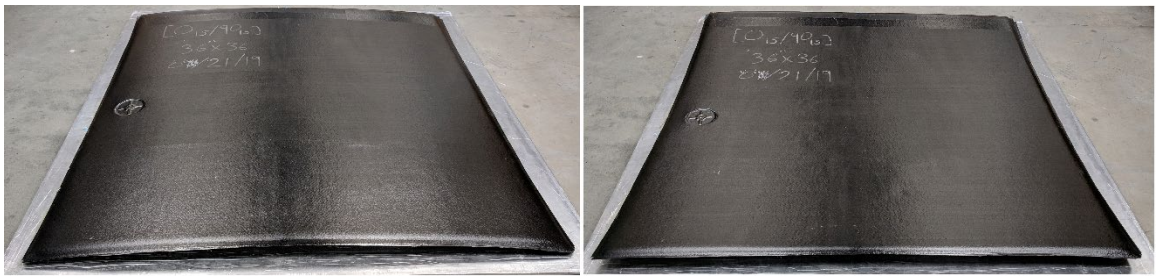

Fig 3.23. Bistable [$0_{15}/90_{15}$], 36 x 36 in^2 laminate.

Discussion

While the work presented by [29] showed that a single non-dimensional bifurcation point exists for square laminates of all sizes, the results were not validated by experiment. First, a non dimensional critical length was found to be 95.833 from the FEA analysis. During the experimental validation, a different value was found for this non dimensional critical length which was equal to 199.9. The possible reasons for this difference are that:

a. The material properties of AS4/8552 were used for the FEA simulation, whereas the actual material being used was DA 409U/G35 150. This was because all of the necessary material properties were not provided by the manufacturer of DA 409U/G35 150.

b. The experimental fabrication was done using hand lay-up. This introduces various defects such as fibre misalignment, difference in lamina sizes, inaccurate stacking of different layers on top of each other causing inaccurate stacking sequence toward the edges and variation in the $[0_n/90_n]$ lay-up, introduction of air bubbles within lamina layers, and so on.

c. There exists a variation in the epoxy content of each laminate. This variation exists because of non-uniform distribution of pressure and heat during vacuum bagging, material aging, and use of different batches of prepreg rolls for different laminates.

d. Several other factors presented by [27] play a role in causing mismatch between the ideal FEA simulation and fabricated laminates.

Using the non-dimensional critical length found from laminates with 2, 4, 6, and 8 plies, larger laminates were fabricated. However, it was seen that due to moisture

absorption, laminates near the bifurcation point lost their bistability over a period of time. While the bistability was regained upon reheating, it would not have been practical to reheat larger structures. Therefore, the average non dimensional critical length of 254 was used to fabricate large bistable laminates, one, a $[0_{10}/90_{10}]$ 24 x 24 in^2 laminate and two, a $[0_{15}/90_{15}]$ 36 x 36 in^2 laminate.

To get a better correlation between theory and experiment, the material properties that affect the curvature the most were varied. As found by [27], the two material properties affecting the curvature the most were E_{22} and α_{22}. The curvature of a 3 x 3 inch, [0/90] laminate is therefore studied as an example.

The curvature of the 3 x 3 inch laminate found from fabrication was 2.758m^{-1} and from FEA it was found to be 7.22m^{-1}. The original values of E_{22} and α_{22} were 9.5GPa and -3 x 10^{-5} /°C. The effect of variation in these values on the curvature found from FEA is given in table 3.5.

Parameter & Value	-5%	-10%	-15%	-20%	-25%
E_{22} (GPa)	9.025	8.55	8.075	7.6	7.125
α_{22} (/°C)	-2.85x10^{-5}	-2.7x10^{-5}	-2.55x10^{-5}	-2.4x10^{-5}	-2.25x10^{-5}
Curvature (/m)	6.71	6.20	5.70	5.20	4.72

Table 3.5. Change in curvature due to variation in material properties.

As seen from the data, reducing the values of E_{22} and α_{22} gave better correlation between theory and experiment.

III. Relation between length and width for bistability

In the previous section the relation between the side length and thickness for square laminates, necessary for achieving bistability was found. In this section, the relation between length and width is found by keeping thickness constant.

FEA Approach

The aspect ratio is varied by keeping one side constant and increasing the other one. In the previous section it was found that square, [0/90] laminates with side length less than 24mm (0.95 in) were not bistable. For rectangular laminates, a similar trend was observed - laminates with one side less than 24mm (0.95 in) were not bistable. Therefore, the side that is kept constant is given a value of 24mm (0.95 in), and the other side is increased in magnitude starting from 24mm such that the aspect ratio is varied as given in equation 3.2.

$$AR = 1:2^{i}, \text{ where } i = 0, 1, 2...\infty \quad (3.2)$$

Using the previously described FEA model, the simulations showed that laminates with AR equal to 1, 2, and 4 (laminate sizes being 24x24 mm^2, 24x48 mm^2, 24x96 mm^2) were bistable. However, the FEA model did not allow the laminate with an AR of 8 (24x192 $mm^{2)}$ to be snapped through. This is because the post-cure curvature was so high (shown in figure 3.24) that an application of a point force did not allow the snap-through to be propagated to the entire laminate, as shown in figure 3.25.

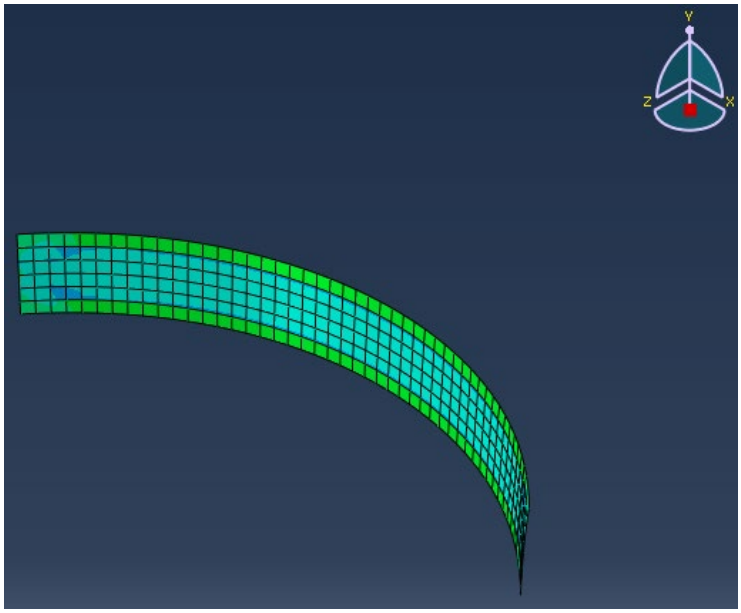

Figure 3.24. Post cure shape of a 24x192 mm^2, [0/90] laminate.

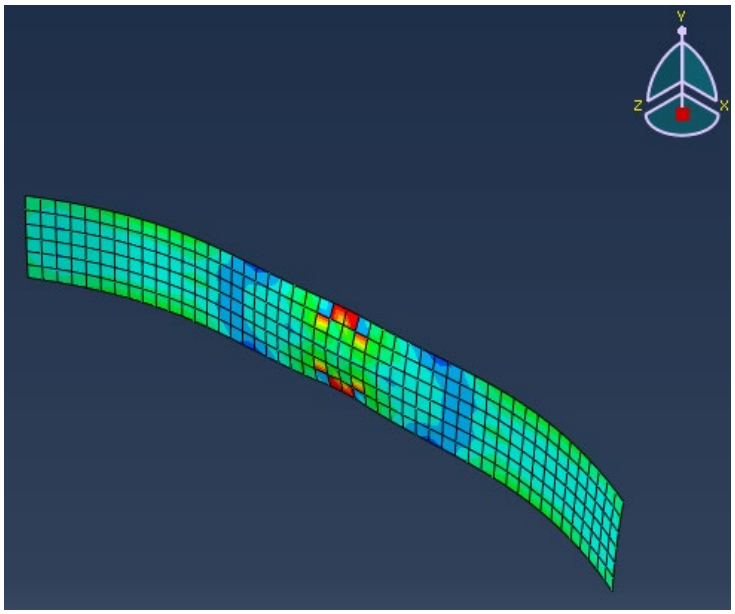

Figure 3.25. Failure of snap-through propagation of 24x192 mm^2, [0/90] laminate.

The application of force was therefore modified such that it was applied in two steps. First, a force is applied on two opposite edges, such that the laminate is ‘opened’ like

a newspaper, then a point force is applied in the center. The post snap-through shape obtained using this snap-through process is shown in figure 3.26.

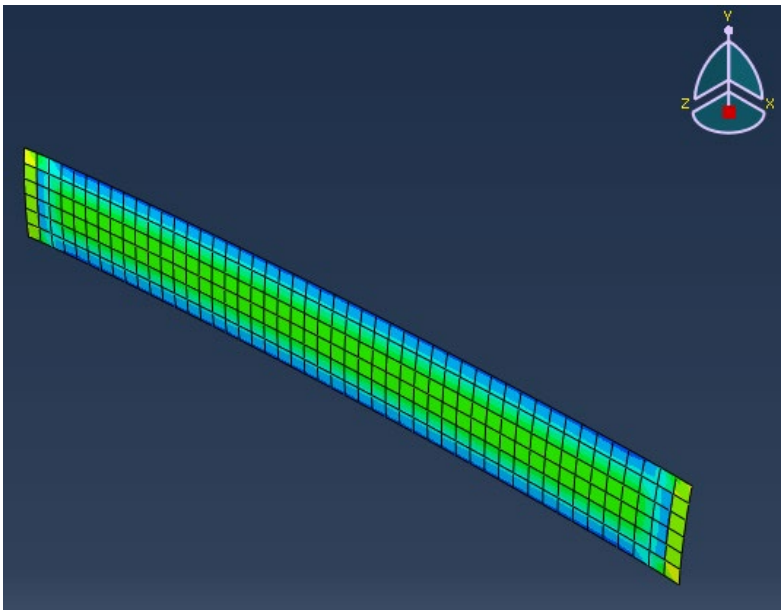

Figure 3.26. Post snap-through shape of [0/90], 24 x 192 mm^2 laminate.

The same process is used for a laminate with an AR of 1:16 and it was found that the laminate was bistable. An increase in AR beyond 1:16 was not possible as the laminate became an extremely thin strip and the FEA stopped converging within a reasonable processing time. The post-cure shape for all rectangular laminates is such that the longer side is curved and the shorter side has a nearly straight edge, as shown in figure 3.24, and the post snap-through shape is as shown in figure 3.26. An increase in out of plane deformation with an increase in AR was observed for the post-cure shape, whereas the out of plane deformation post snap-through remained fairly constant, with a slight increase. This is shown in figure 3.27

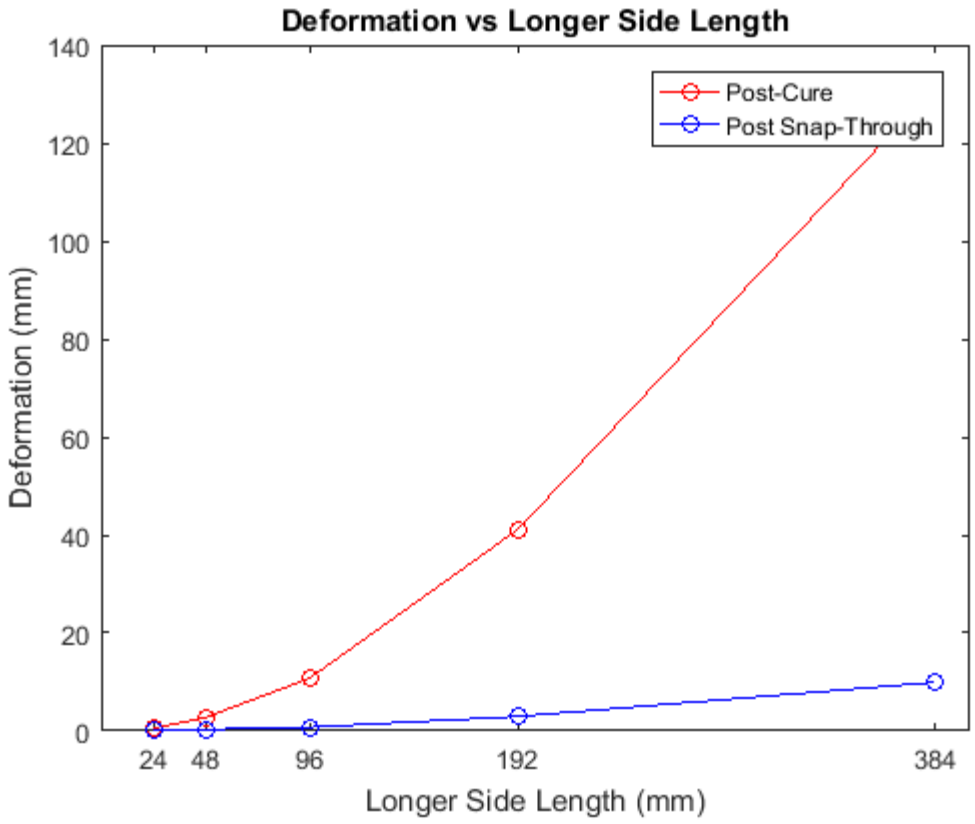

Figure 3.27. Out of plane deformation post curing and post snap-through with increase in AR.

For a laminate to lose bistability, the out of plane deformation would have to reduce with an increase in AR, with a loss in bifurcation at a certain point. The data obtained thus far shows that an increase is AR will not cause a loss in bistability, since there is an increase in out of plane deformation for both shapes. In simpler words, it is observed the longer side is curved post-curing and this curvature significantly increases with an increase in side length. The out of plane deformation of the post snap-through shape is not affected by an

increase in AR, except for a marginal increase, meaning that a post snap-through shape will always exist, no matter how much the AR is increased.

Experimental Approach

Four laminates with varying AR's were fabricated with stacking sequences of [0/90]. The sizes were 6 x 36 in^2, 4 x 32 in^2, 3 x 45 in^2, and 2 x 50 in^2, i.e. AR's of 1:6, 1:8, 1:15, and 1:25. All laminates were bistable, as shown in figure 3.28 and 3.29.

Figure 3.28. (From right) Post cure shape of laminates with AR's 1:6, 1:8, 1:15, and 1:25.

Figure 3.29. (From top) Post snap-through shape of laminates with AR's 1:6, 1:8, 1:15, and 1:25.

To fabricate the laminate with the largest AR of 1:25, data obtained in previous sections is used. The minimum side length for a square, [0/90] laminate to be bistable was 2 inches. With one side constant at 2 in, the other side was fabricated to be 50 in. This was the maximum length that could fit inside the dimensions of the curing oven.

Discussion

Using the FEA model, it was possible to prove that a [0/90] laminate with an aspect ratio of 1:16 (24 x 384 mm^2) was bistable. It was not possible to simulate a laminate with higher aspect ratios since the FEA stopped converging. Further, it was seen that the curvature did not reduce with an increase in aspect ratio, indicating that laminates with even higher aspect ratios would be bistable. This was proven using fabricated laminates. A [0/90], 2 x 50 in^2 laminate with an aspect ratio of 1:25 was fabricated and shown to be bistable. Therefore, we can conclude that a rectangular laminate will not lose bistability for any aspect ratio as long as both sides are above the critical length.

IV. Prediction of curvature for bistable laminates

The previous two sections outlined the necessary geometric conditions for achieving bistability in square and rectangular laminates. For laminates that fit inside these geometric constraints, it is important to be able to predict the curvature of the laminates for both shapes. This is the subject of this section.

FEA Approach

For square bistable laminates, assuming an ideal geometry and lay-up, the curvatures for both shapes is predicted to be equal using the FEA model. This non dimensional curvature (curvature x side length) varies with respect to the non-dimensional side length (side length/thickness) as shown in figure 3.30. The graph includes laminates with 2 plies, 4 plies, and 6 plies. Note that the curve represents the post-cure part of the bifurcation graph shown in figure 3.10.

As shown in figure 3.10, the bifurcation is found at a non dimensional critical length of 95.833. This is also seen in figure 3.30, where a change is seen in the curvature as the non-dimensional side length reaches a value of 95.833. Below this magnitude of non-dimensional side length, only one unique shape exists, and above this value, two shapes exist with equal curvatures as shown. Therefore, using this graph, it is possible to predict the curvature of square laminates.

For rectangular laminates, let us say that one side has a dimension of ‘X’ units and the other side has a dimension of ‘Y’ units. In the previous section it was seen that keeping the ‘X’ side constant at 24mm and varying the ‘Y’ side in magnitude did not affect the out of plane deformation of one of the laminate shapes. This shape was the one in which the side ‘X’ (24 mm) was curved and side ‘Y’ was straight.

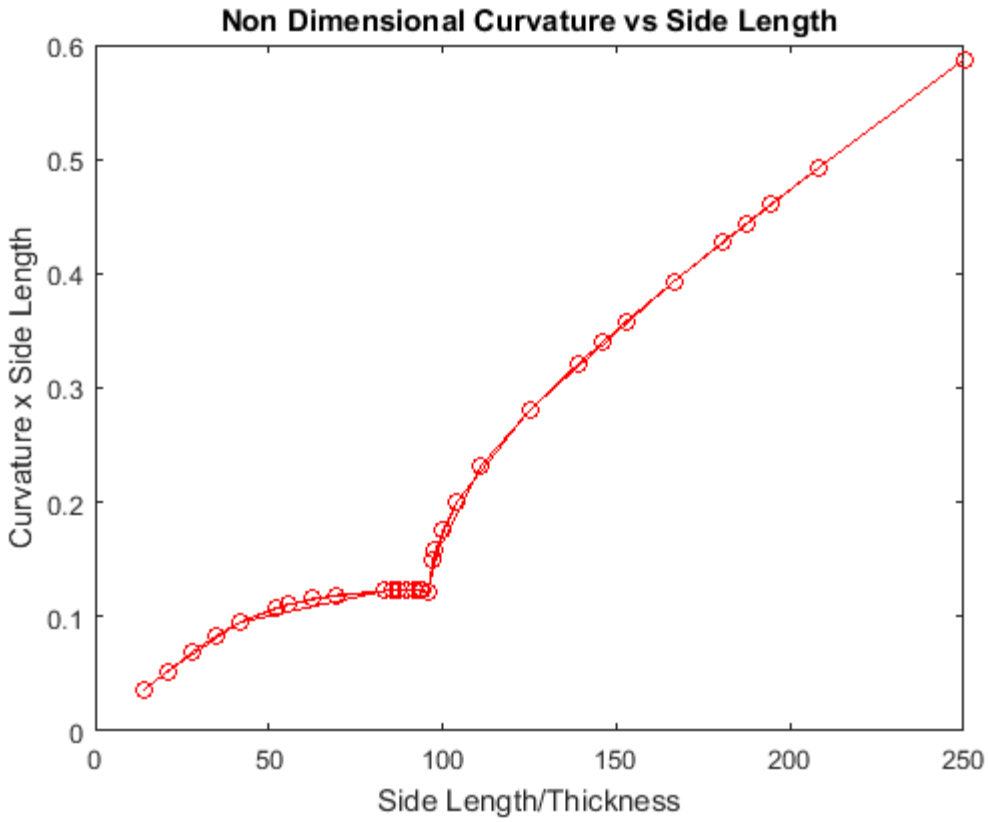

Figure 3.30. Non Dimensional Curvature Vs Side Length for square laminates.

For further examples, consider the rectangular laminates with dimensions ‘X by Y’ given in table 3.5. Every laminate is bistable and has two shapes. For ease of explanation, let us say that the shape where side X is curved is called as a ‘X by Y’ laminate whereas the shape where side Y is curved is called a ‘Y by X’ laminate. Therefore, a ‘50mm x 100mm’ laminate means that the side with a value of 50mm is curved and the 100mm side is straight. For a ‘100mm x 50mm’ laminate, the 100mm side is curved and the 50mm side is straight.

50 x 50	60 x 50	70 x 50	80 x 50	90 x 50	100 x 50
50 x 60	60 x 60	70 x 60	80 x 60	90 x 60	100 x 60
50 x 70	60 x 70	70 x 70	80 x 70	90 x 70	100 x 70
50 x 80	60 x 80	70 x 80	80 x 80	90 x 80	100 x 80
50 x 90	60 x 90	70 x 90	80 x 90	90 x 90	100 x 90
50 x 100	60 x 100	70 x 100	80 x 100	90 x 100	100 x 100

Table 3.6. List of rectangular laminates for FEA (All dimensions in mm)

Plotting the out of plane deformation for each of these shapes gives us the result shown in figure 3.31. It can be seen that the out of plane deformation remains approximately constant for all shapes in which the dimension X remains constant with variation in Y. Therefore, it can be concluded that for a rectangular laminate 'X by Y', the two shapes will be as following:

1. The side 'X' will be curved and side 'Y' will be straight, and the magnitude of curvature will be equal to that of a square 'X by X' laminate.

2. The side 'Y' will be curved and side 'X' will be straight, and the magnitude of curvature will be equal to that of a square 'Y by Y' laminate.

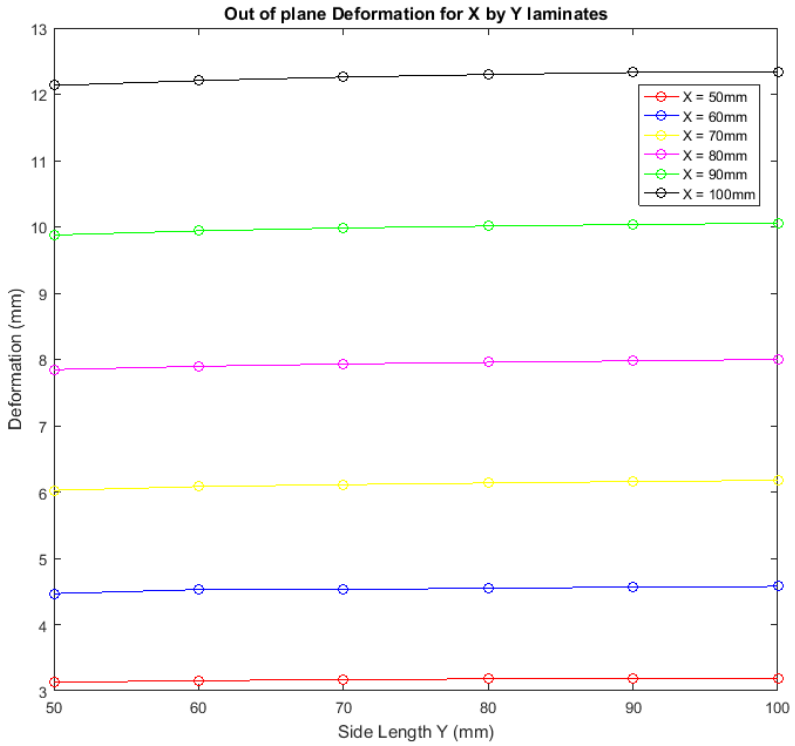

Figure 3.31. Out of plane deformation of 'X by Y' laminates (FEA).

Experimental Approach

The same approach is followed experimentally but with different values of X and Y. The values of X and Y are increased to allow for human error in lay-up, and the loss of curvature due to the reasons explained in section 2 of this chapter. The values of X and Y are as shown in table 3.6 and the fabricated laminates are shown in figure 3.32. The figure shows 21 laminates, with the rectangular laminates giving two different shapes and data points. Therefore, in total we obtain 36 data points from the laminates to match the 36 shapes given in table 3.5.

2.5 x 2.5	3.0 x 2.5	3.5 x 2.5	4.0 x 2.5	4.5 x 2.5	5.0 x 2.5
2.5 x 3.0	3.0 x 3.0	3.5 x 3.0	4.0 x 3.0	4.5 x 3.0	5.0 x 3.0
2.5 x 3.5	3.0 x 3.5	3.5 x 3.5	4.0 x 3.5	4.5 x 3.5	5.0 x 3.5
2.5 x 4.0	3.0 x 4.0	3.5 x 4.0	4.0 x 4.0	4.5 x 4.0	5.0 x 4.0
2.5 x 4.5	3.0 x 4.5	3.5 x 4.5	4.0 x 4.5	4.5 x 4.5	5.0 x 4.5
2.5 x 5.0	3.0 x 5.0	3.5 x 5.0	4.0 x 5.0	4.5 x 5.0	5.0 x 5.0

Table 3.7. List of rectangular laminates for experiment (All dimensions in inches)

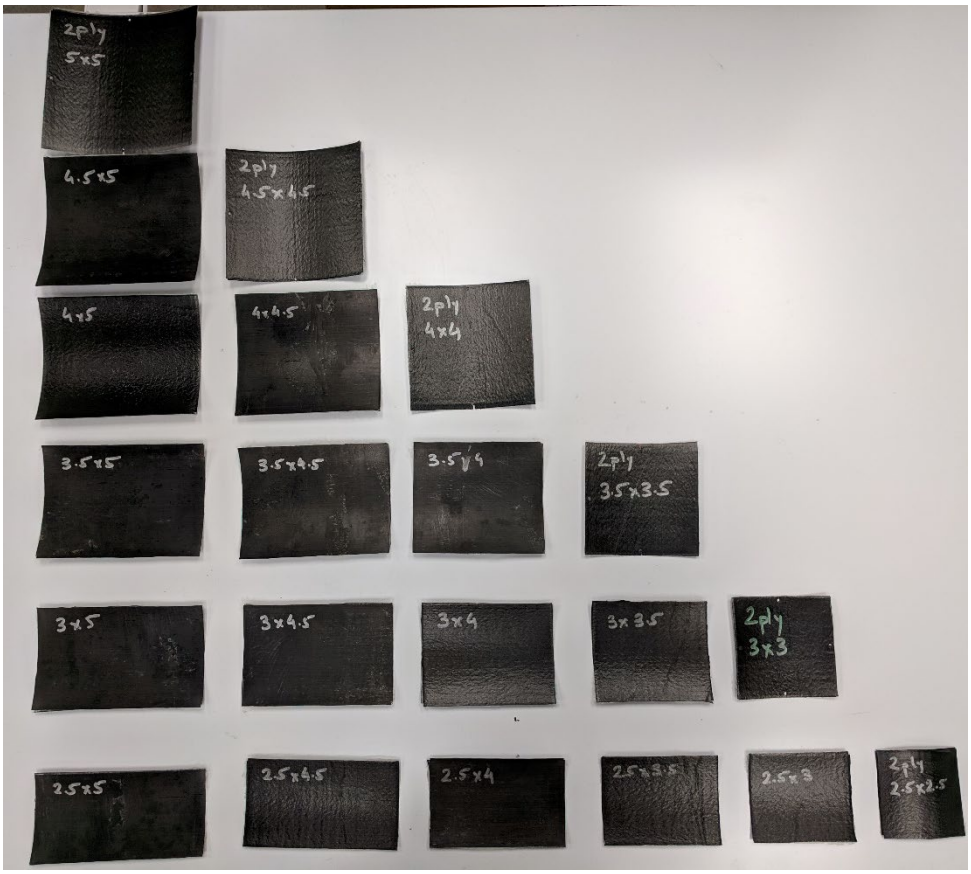

Figure 3.32. Fabricated laminates for dimensions given in table 3.2.

The out of plane deformation is measured using the profilometer and the results are plotted as shown in figure 3.33.

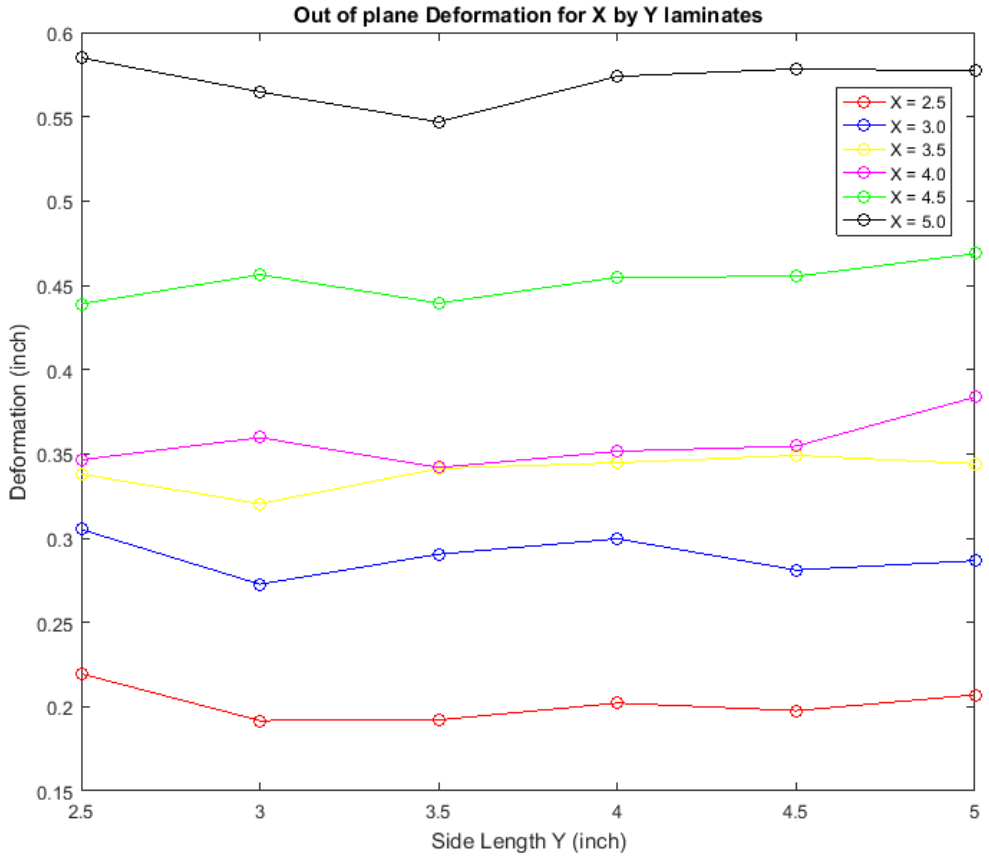

Figure 3.33. Out of plane deformation of 'X by Y' laminates (Experiment).

Discussion

A method was developed to be able to predict the curvature of square and rectangular laminates. Using the graph shown in figure 3.30, it is possible to predict the

curvature of square laminates. For rectangular ‘X by Y’ laminates, it was proven that there exist two shapes such that:

1. The side ‘X’ will be curved and side ‘Y’ will be straight, and the magnitude of curvature will be equal to that of a square ‘X by X’ laminate.
2. The side ‘Y’ will be curved and side ‘X’ will be straight, and the magnitude of curvature will be equal to that of a square ‘Y by Y’ laminate.

V. Prediction of snap-through force for bistable laminates

For bistable laminates, a simple form of actuation between the two shapes is to apply a point force in the center of the laminate. For a functioning application of bistable composites, it is necessary to be able to predict the required force of actuation. The scope here is limited to square laminates, since rectangular laminates require a change in boundary conditions for large values of aspect ratio, as demonstrated in the aspect ratio section.

FEA Approach

The FEA method of calculating the necessary snap-through force was presented by [18] and is used here. The force vs displacement data for the snap-through step is extracted from FEA, as shown in figure 3.34.

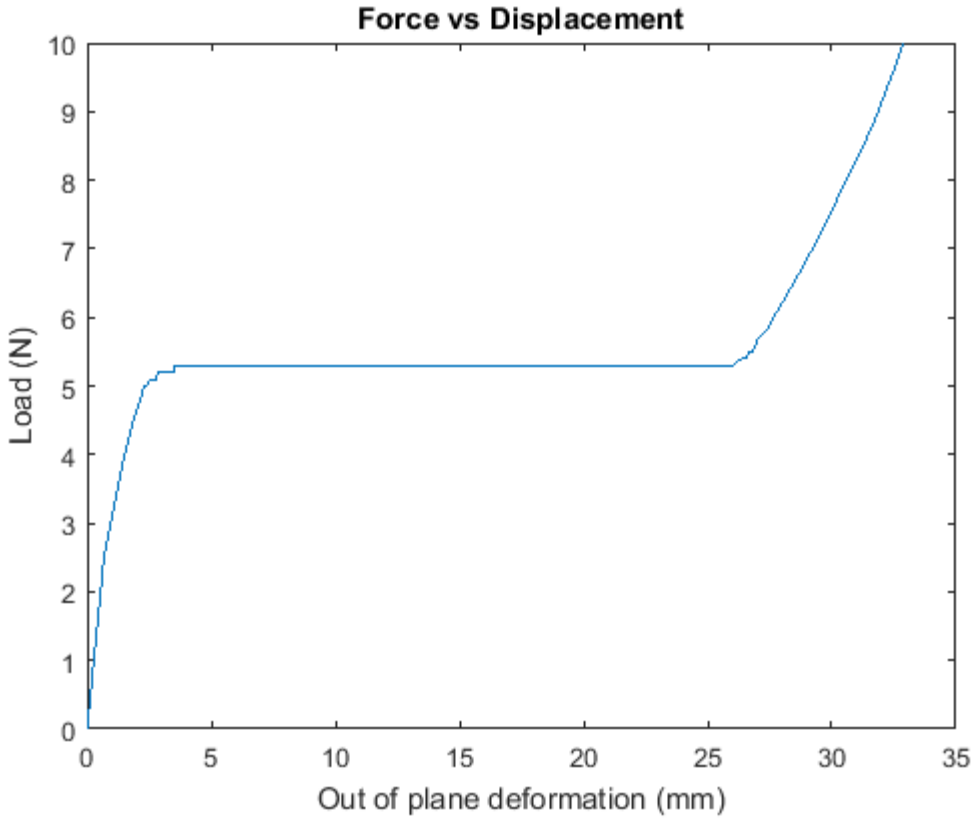

Figure 3.34. Force Vs Displacement for a [0/90], 100 x 100 mm^2 laminate. Snap-through occurs at a force of 5.30N.

It can be seen that the laminate center, which is the point of application of force, goes through huge displacement for a constant value of force. This force is the critical snap-through force and has a value of 5.30N for the given example. For laminates with a stacking sequence of [0/90], the side length is varied starting from the critical length of 24mm up to a maximum side length of 150mm. The snap-through is found for each laminate and the results are as shown in figure 3.35.

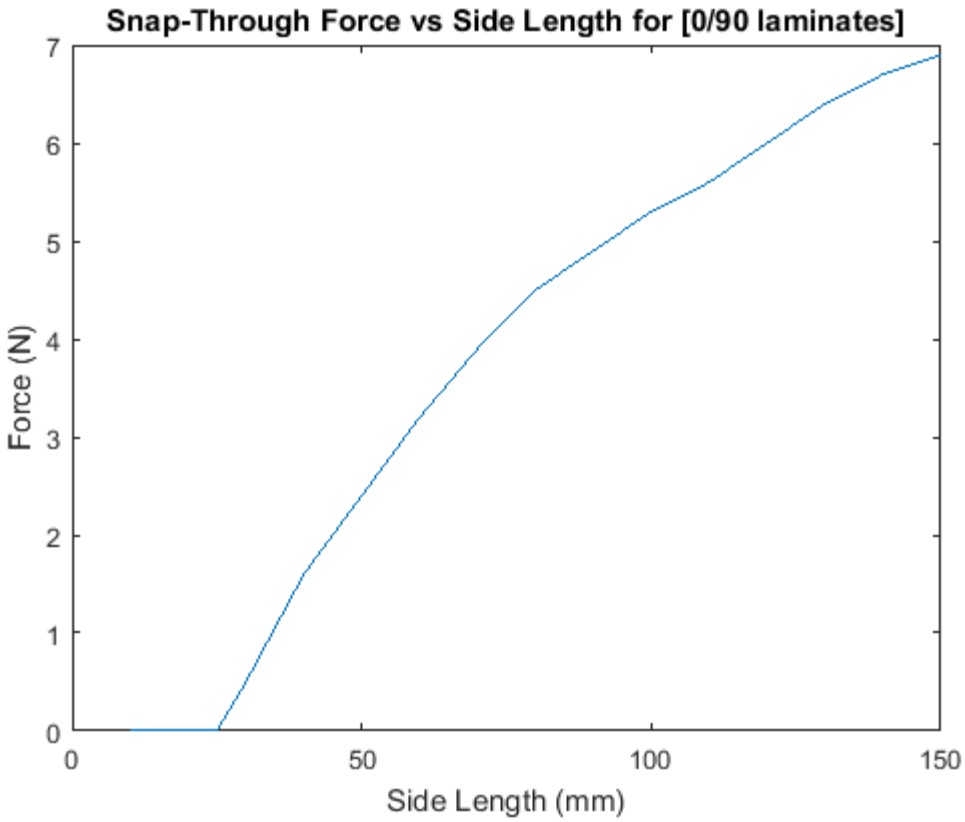

Figure 3.35. Snap-Through Force Vs Side Length for [0/90] laminates.

Further, the thickness is changed to 4 plies, i.e. a stacking sequence of $[0_2/90_2]$, and length is varied from the critical length for 2 plies of 47mm up to a maximum length of 150mm. Also, for 6 plies, i.e. a stacking sequence of $[0_3/90_3]$, the length is varied from 70mm up to 150mm. Results for 2 plies, 4 plies, and 6 plies are plotted on a graph shown in figure 3.36. It can be seen that there is no clear relation between the thickness and force for the data shown in the figure. For example, for a side length of 80mm, the snap-through forces are 4.5N for 2 plies, 6.4N for 4 plies, and 2.1N for 6 plies. Which means that the force for snap through has the relation $F_{4\ plies} > F_{2\ plies} > F_{6\ plies}$. But, for a side length of

100mm, the snap-through forces are 5.3N for 2 plies, 9.8N for 4 plies, and 7.7N for 6 plies giving a relation of $F_{4\ plies} > F_{6\ plies} > F_{2\ plies}$ This suggests that thickness alone is not affecting the snap-through force, and curvature difference between two stable shapes also plays a role since the curvature reduces as thickness is increased.

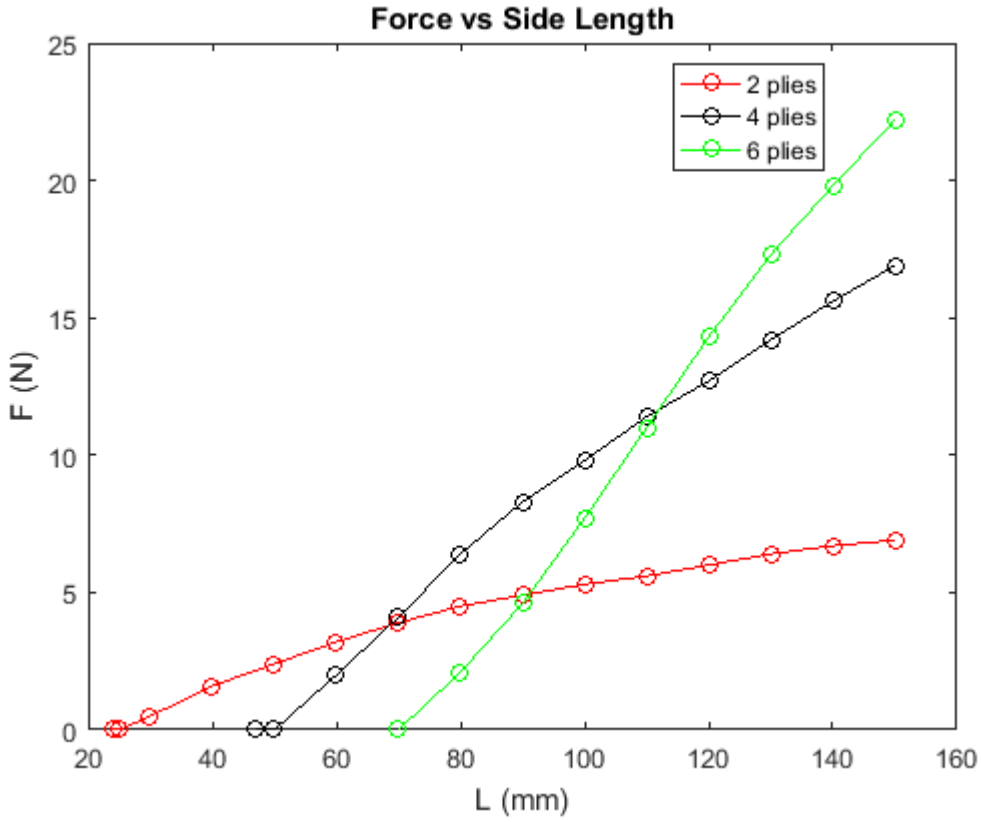

Figure 3.36. Force vs Side Length for 2, 4, and 6 plies (FEA).

Therefore, we introduce non-dimensional parameters. The length is divided by the thickness, and the force is divided by the square of the length and also divided by E_1, which is the Young's modulus in the direction of the fibre orientation. This is given in equations 3.3 and 3.4.

$$L^* = \frac{L}{t} \tag{3.3}$$

$$F^* = \frac{F}{E_1 L^2} \tag{3.4}$$

Where L* is the non-dimensional side length and F* is the non-dimensional snap-through force. We choose E_1 to make the parameter unitless. Since E_2 is the Young's modulus perpendicular to the fibre direction, the amount of epoxy affects its value. Therefore, since E_1 is fairly constant, it is used to make the force non-dimensional. Plotting these non-dimensional parameters gives us the results shown in figure 3.37.

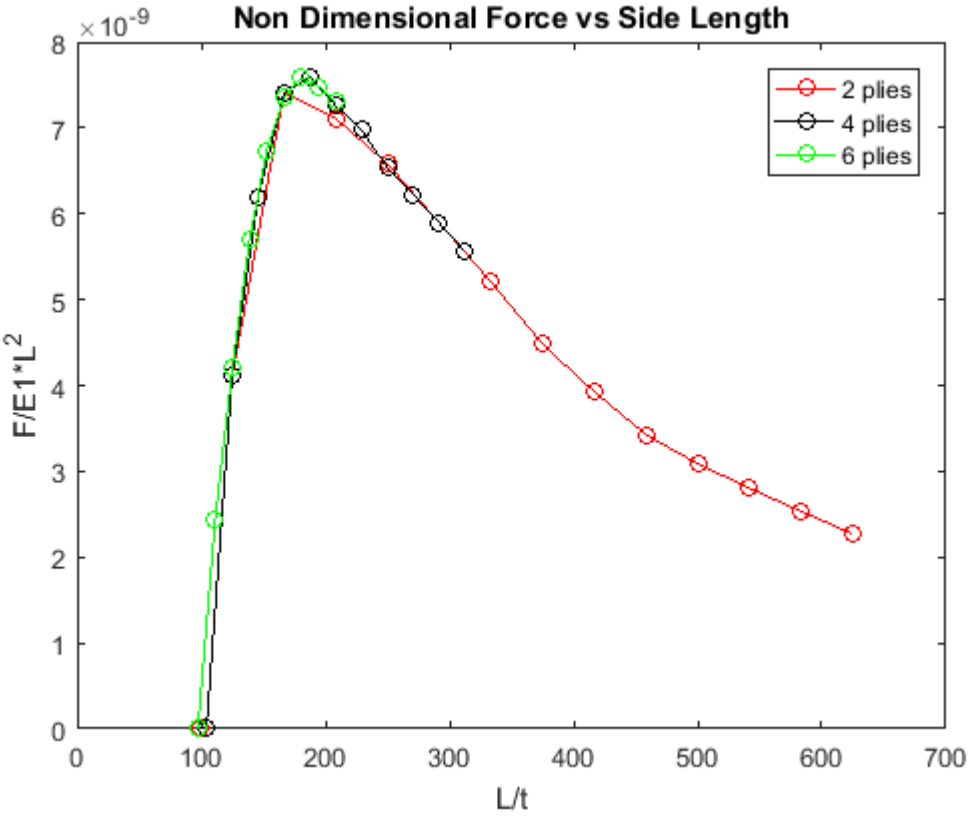

Figure 3.37. Non Dimensional Force Vs Side Length. (FEA)

Using this graph, it is possible to predict the required force of actuation for any square laminate. For example, a square laminate with 50 plies and a side length of 50 inches would have a 'L/t' ratio of 211.667, giving a 'F/E_1L^2' ratio of $7.11e^{-9}$. This allows us to calculate the force to be 2.4N.

It should be noted that E_1 is a constant and does not affect the nature of the graph presented in figure 3.37. It is included in the equation to make the force perfectly non-dimensional. If the force is divided by the square of the length alone, the curves for the different number of plies still collapse into a single curve, as shown in figure 3.38.

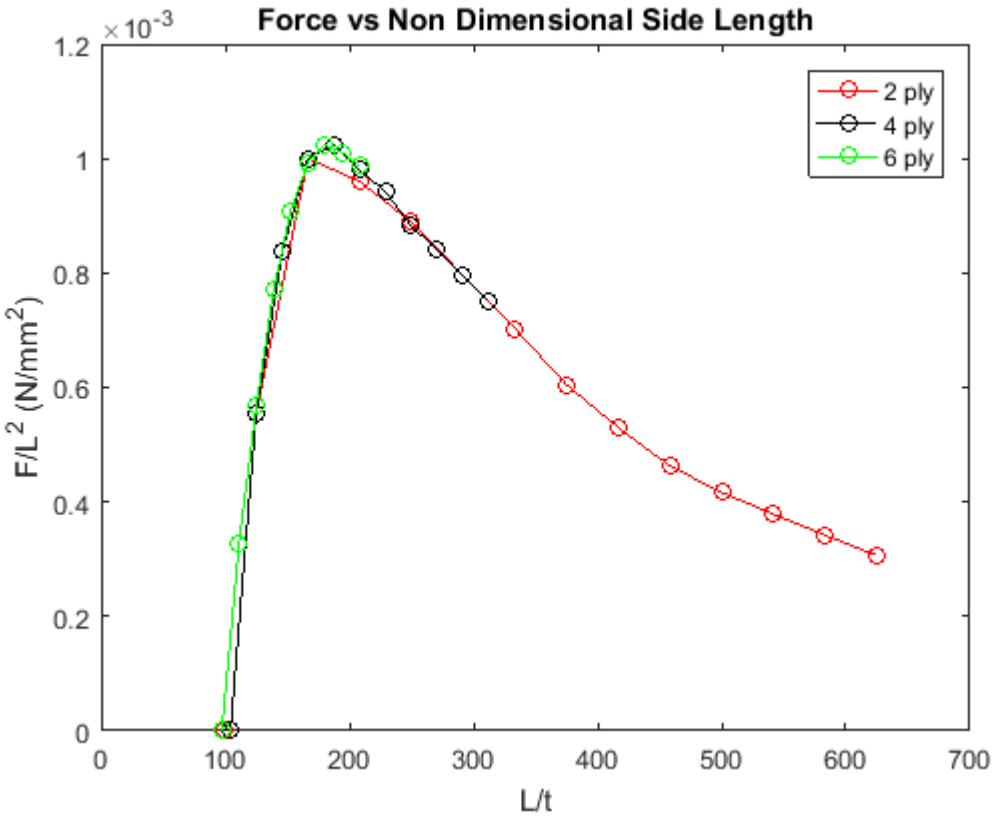

Figure 3.38. Force vs Non Dimensional Side Length.

Experimental Approach

The ADMET Universal test set up explained in the first section of this chapter is used to conduct experimental snap-through tests. Tests are conducted for laminates with 2, 4, and 6 plies. The data points include 9 laminates for 2 plies ranging from 3 inches to 9 inches, 7 laminates for 4 plies ranging from 4 inches to 10 inches, and 5 laminates for 6 plies ranging from 6 inches to 10 inches. The maximum length is 10 inches because of the size limitations of the ADMET test up. The minimum length is set by the critical length found in the second section of this chapter. Plotting the snap-through forces for each laminate gives us the results shown in figure 3.39. Logarithmic trend lines are added for easier comparison with the FEA results shown in figure 3.36. The same non dimensional parameters given in equations 3.3 and 3.4 are used, and the results are shown in figure 3.40.

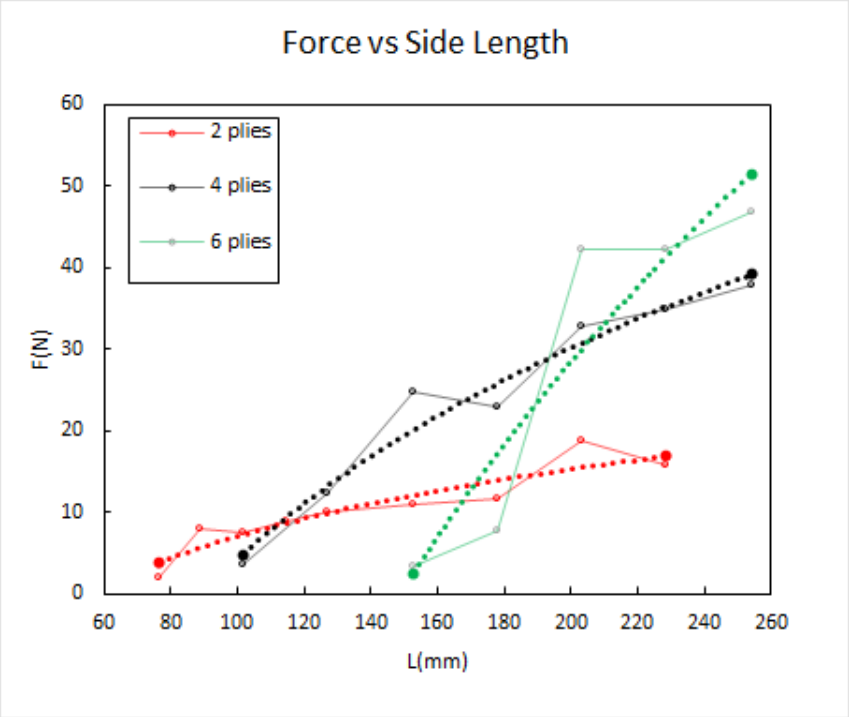

Figure 3.39. Force vs Side Length for 2, 4, and 6 plies (Experiment).

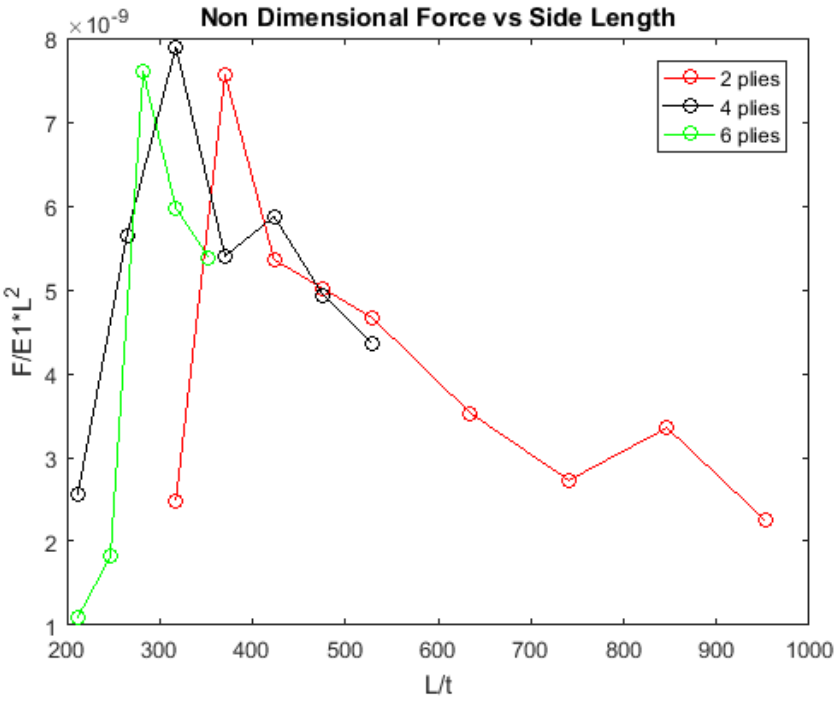

Figure 3.40. Non Dimensional Force Vs Side Length. (Experiment)

Discussion

As established in the second section of this chapter, there is a difference between the magnitude of curvature predicted by FEA and the curvature that is found in fabricated laminates. More specifically, the critical length found from FEA is lower than the critical length found from experiment. Because of this, it is not possible to directly compare the FEA results for the prediction of snap-through force with the experimentally obtained values. There are two reasons for this:

1. For the FEA analysis, there is a higher limit on the side length of the square laminates for conducting a snap-through test. Beyond this limit, the laminate has a very high value of curvature and starts to coil around itself, making an application of point force in the center of the laminate ineffective. This was shown in figure 3.25 for rectangular laminates.
2. For the experimental approach, there is a lower limit on the side length of the square laminates imposed by the critical length.

Therefore, it is not possible to conduct a snap-through test using FEA and experiment on a laminate of the same size and stacking sequence. However, using different sizes of laminates, it was possible to prove that the trend seen in the FEA results is also found in the experimental results, giving us two conclusions:

1. The magnitude of force necessary for snap-through is a function of thickness, and the square of the side length.
2. Introducing non dimensional parameters by dividing the side length on the X axis by the thickness and diving the force on the Y axis by the square of the side length and the

Young's modulus E_1, the curves for the force Vs side length for different number of plies collapse into a single curve.

Based on this, it is possible to predict the force of actuation for a square laminate for which the side length and thickness is known.

CHAPTER FOUR

CONCLUSION AND FUTURE WORK

Conclusion

There were four objectives in this research:

1. To find the relation between the side length and thickness of square laminates necessary for achieving bistability.
2. To find the relation between the length and width of rectangular laminates necessary for achieving bistability.
3. To predict the curvature of square and rectangular bistable laminates based on the size and stacking sequence.
4. To predict the force of actuation of square bistable laminates based on the size and stacking sequence.

The results obtained from the FEA and experimental approach are given below:

1. Relation between side length and thickness of square laminates: A non-dimensional critical length of 95.833 was found using FEA. Using this value, the minimum side length for square laminates of any thickness required to achieve bistability can be predicted. Experimentally, the non-dimensional critical length was found to be 199.99. There are many possible reasons for this difference, including incorrect material properties in the

FEA analysis and fabrication defects caused by inaccurate hand lay-up. Using this non-dimensional critical length and taking into account the effect of moisture absorption, two thick bistable laminates were fabricated: one, with a stacking sequence of $[0_{10}/90_{10}]$ and side length of 24 in, and two, with a stacking sequence of $[0_{15}/90_{15}]$ and side length of 36 in.

2. Relation between length and width of rectangular laminates: It was found that aspect ratio does not cause a rectangular laminate to lose bistability, as long as both sides are above the critical length. Laminates with aspect ratios of 1, 2, 4, 8, and 16 were simulated using FEA and it was found that the curvature slightly increased with an increase in aspect ratio, proving that laminates with even higher aspect ratios would be bistable. Experimentally, laminates with aspect ratios of 6, 8, 15, and 25 were fabricated and proven to be bistable.

3. Prediction of curvature: The graph of curvature Vs side length for different number of plies collapsed into a single curve upon introducing non-dimensional parameters. Using this graph, it is possible to predict the curvature of any square laminate for which the thickness and side length is known.

For any rectangular 'X by Y' laminate it was proven that there exist two shapes such that:

1. The side 'X' will be curved and side 'Y' will be straight, and the magnitude of curvature will be equal to that of a square 'X by X' laminate.

2. The side 'Y' will be curved and side 'X' will be straight, and the magnitude of curvature will be equal to that of a square 'Y by Y' laminate.

4. Prediction of force: A non dimensional study was performed on the relation between force and side length. It was found that the force is a function of thickness as well as side length. Introducing non dimensional parameters made the graph between force and side length to collapse into a single curve for different number of plies. Using this curve, it is possible to predict the force of actuation of any square laminate knowing its thickness and side length. This was validated by fabricating and testing laminates of various stacking sequences and thicknesses. It was found that while there was good correlation between FEA and experiment, there was a difference in the values obtained for both.

Future Work

While good correlation was found between numerical results and experimental results, the effects of manufacturing defects and environmental conditions were found to be the reasons for a mismatch between the results. Therefore, an analytical model must be used that would allow prediction of the behavior of a laminate with a variation in moisture content, temperature and material properties. A benefit of an analytical model will be that the volume fractions of the fibers and the epoxy can be varied, allowing an investigation into their effects on the curvature.

The prediction of bifurcation points and curvature was based on free edge boundary conditions. In any application, all edges will never be free and therefore the effect of clamping one or more sides on the curvature and/or the loss of bistability should be investigated.

The benefit of bistable composites is that they can be actuated from one state to the other. In an application where there is repeated actuation, fatigue stresses will have an effect on the behavior of the laminate. This should also be investigated.

APPENDICES

–Appendix A

Abaqus step-by-step guide

Open Abaqus and select “Create Model Database with Standard/Explicit Model”

Step 1: Our first step is creating the geometry of the laminate. This will be a 2-D sketch on Abaqus. If the geometry is complicated, it can be created on a separate CAD software and imported onto Abaqus.

Geometry is created using the following steps:

1. Click on “Parts” under the Model Tree. Modelling Space: 3D, Type: Deformable, Base Feature Shape: Shell, Type: Planar. Click “Continue”.

2. Draw the geometry using the Toolbox Area. For a 100 x 120 mm model, draw a rectangle and assign the dimensions as 100 x 120, click “done” in the prompt area.

Step 2: The second step is to create a material with the correct material properties.

We are going to assign Elastic properties and Expansion Properties. Click on “Materials”.

Elastic:

1. Select “Elastic” from the drop-down menu. Mechanical → Elasticity → Elastic, Type: “Lamina”.

2. The properties are as follows: E1 = 135000, E2: 9500, E3: 0.3, G12: 5000, G13: 7170, G23: 3970.

PS: Abaqus does not work with units. It is our duty to make sure that the same unit system is followed while assigning values. Here, we are using N and mm.

Expansion:

1. Mechanical → Expansion, Type: Orthotropic

2. alpha11: 2E-008, alpha22: 3E-005, alpha33: 3E-005

Click OK. Our Material is created.

Step 3: Third step is to assign the material properties to the geometry and to create the composite laminate.

To create a composite laminate, there are two methods.

One is to create a composite shell under the "Sections" tab and then assigning the created geometry to the section under "Parts". The second method is to create a "Composite Layup" under "Parts".

In our case, both methods work. To learn the difference between the two, refer to section 12.2.4 "Defining composite layups" in the Abaqus User's Guide. Here, we use the first method.

1. Sections → Category: Shell, Type: Composite, click continue. Material: Material-1, Thickness: 0.12, Orientation Angle: 0 for first one and 90 for the second, click OK.

2. Go back to Parts → Part-1 → Section Assignments → Select the geometry, click done and OK.

Step 4: Creating the mesh.

1. Assembly → Instances, Instance Type: Independent, click OK.

2. Assembly → Instances → Part 1-1 → Mesh (Empty).

3. Assign Element Type → Select the created geometry and click done. By default, the 4-node doubly curved shell element will be selected. Click OK.

3. Seed Part Instance, Approximate Global Size: 5, click OK.

4. Mesh Part Instance → Click Yes in the Prompt Area.

Our mesh is created. To check the convergence of the mesh, we use an iterative process. We run the simulation once and check the results. Then, after creating a finer mesh by reducing the Approximate Global Size, the results are compared. This is repeated and once the results start converging, we select the corresponding mesh for our simulations.

Step 4: Creating assembly and sets.

We create four sets as follows:

1. Assembly → Sets → Name first set as "Center Node", Type: Node, click continue. Manually select the node at the (approximate) geometric center of the laminate. While selecting the center manually, just count the number of elements on each side of the selected node. The number of elements on the left and right and on the top and bottom of the selected node should be equal.

2. Sets → Name "-X and +X", Type: Node, click continue. Manually select the two nodes on the left and right edges of the laminate. Select the nodes which are in line with the center node.

3. Sets → Name "-Y and +Y", Type: Node, click continue. Manually select the two nodes on the top and bottom edges of the laminate. Select the nodes which are in line with the center node.

We also create a set that includes the entire geometry:

4. Sets → Name: Laminate, Type: Geometry, click continue → Select the entire geometry (4 edges, 4 corners and middle surface) and click done.

Step 5: Applying Loading and Boundary Conditions by creating steps.

The simulation consists of three steps as follows:

"1. Simulation of the cured shape / first stable shape by applying the necessary curing conditions.

2. Simulation of the snap through behavior or shape change from the first stable state to the second stable state.

3. Simulation of the snap back behavior or shape change from the second stable state back to the first stable state." [1]

Initial condition: We assign the initial conditions:

1. Steps → Initial → BCs → Category: Mechanical, Type: Displacement/Rotation, click continue → Click on "Sets" in the prompt area → Select the "Center Node" → Assign 0 for U1, U2, U3, UR1, UR2, UR3 to eliminate all degrees of freedom for the center node by checking all the boxes. This way, the center is fixed.

2. To assign the initial elevated temperature, select Predefined Fields → Other → Temperature, click continue → Sets (Prompt Area) → Select "Laminate" (entire geometry) → Magnitude: 121, click OK.

Cooling: In the second step, we simulate the cooling process.

1. Click on steps → Name: "Cooling" → Procedure type: Static, General, click Continue. "Nlgeom" should be on, click OK.

PS: Nlgeom considers nonlinear effects of large displacement. The difference between the linear Classical Lamination Theory and Hyer's non-linear "Extended Classical Lamination Theory" is the same as a simulation with the Nlgeom off and with the Nlgeom on. This

means that with the Nlgeom off, we will get a saddle shape, but with the Nlgeom on, we will get the accurate cylinder shape.

The boundary condition (fixed center node) is propagated, while the predefined field is modified.

Click on Predefined Field → Status: Modified → Magnitude: 20, click OK.

Snap-through loading: The curing process has been created. Now we apply the loads for the snap-through.

1. Step → Name: STL (Snap Through Loading), type: Static, General, click continue. Automatic stabilization: Specify damping factor: 2.5E-007, click OK.

2. Deactivate BC-1 and create two new BC's:

   1. BC → Mechanical – Displacement/Rotation → Select "-Y and +Y" → Assign 0 for U3, UR1, UR2, UR3 so that those 4 dof are eliminated. The nodes at +Y and –Y are free to move in U1 and U2 (X and Y) direction.
   2. BC → Mechanical – Displacement/Rotation → Select "Center Node" → Assign 0 for U1, U2, UR1, UR2, UR3 so that those 5 dof are eliminated. The center node is free to move in U3 (Z) direction.

3. We now apply the loading conditions:

Loads → Mechanical, Concentrated Force, click continue → Select Center Node → CF3 = 10 (Force of 10N in Z direction).

Snap-through unloading: We release the load and keep the center fixed and check whether laminate is stable in the snap through position.

1. Step → Name : (STU) Snap-Through Unloading, Type: Static, General, click continue, click OK.

2. Deactivate BC's 1, 2 and 3. Create new BC: BC → Mechanical, Displacement/Rotation, click continue, select center → Eliminate all 6 dof's by assigning 0, click OK.

3. Deactivate Load-1.

Snap-back loading: A load is applied in the –Z direction. This is the exact reverse of the Snap-Through Loading step.

1. Step → Name: (SBL) Snap-Back Loading, type: Static, General, click continue. Automatic stabilization: Specify damping factor: 2.5E-007, check "Use adaptive Stabilization", click OK.

2. Deactivate BC's 1, 2, 3 and 4 and create two new BC's:

1. BC → Mechanical, Displacement/Rotation, → Select "-X and +X" → Assign 0 for U3, UR1, UR2 and UR3. Nodes at +X and –X are free to move in U1 and U2 (X and Y) direction.
2. BC → Mechanical – Displacement/Rotation → Select "Center" → Assign 0 for U1, U2, UR1, UR2, UR3. The center node is free to move in U3 (Z) direction.

3. Applying the load: Loads → Mechanical, Concentrated Force, click continue → Select Center Node → CF3 = -15 (Force of 15N in -Z direction).

Snap-back unloading: This process is the exact reverse of the snap-through unloading step. We fix the center load and release the forces and other boundary conditions.

1. Step → Name : (SBU) Snap-Back Unloading, Type: Static, General, click continue. Automatic stabilization: Specify damping factor: 2.5E-007, check "Use adaptive Stabilization", click OK.

2. Deactivate BC's 1-6. Create new BC: BC → Mechanical, Displacement/Rotation, click continue, select center → Eliminate all dof's by assigning 0, click OK.

3. Deactivate Load-2.

Step 6: Creating and submitting a job for analysis.

Jobs → Model-1, Name: 150x150_Two_Ply, Parallelization: Use Multiple Processors according to the computer specifications for faster processing.

Right click on "150x150_Two_Ply", click Submit.

Step 7: Viewing Results.

Right Click on "150x150_Two_Ply", click "Results".

From the toolbox area, click "Plot Contours on Deformed Shape"

To view the animation, click "Animate: Time History".

REFERENCES

[1] A. K. Kaw, *Mechanics of Composite Materials, Second Edition*. 2005.

[2] R. M.Jones, *Mechanics of Composite Materials.* 1983.

[3] M. W. Hyer, "Calculations of the Room-Temperature Shapes of Unsymmetric Laminates.," *Journal of Composite Materials*, vol. 15. pp. 296–310, 1981.

[4] M. W. Hyer, "Some Observations on the Cured Shape of Thin Unsymmetric Laminates," *J. Compos. Mater.*, vol. 15, no. 2, pp. 175–194, 1981.

[5] M. W. Hyer, "The Room-Temperature Shapes of Four-Layer Unsymmetric Cross-Ply Laminates," *J. Compos. Mater.*, vol. 16, no. 4, p. 318, 1982.

[6] H. Akira and M. W. Hye, "Non-linear temperature-curvature relationships for unsymmetric graphite-epoxy laminates," *Int. J. Solids Struct.*, vol. 23, no. 7, pp. 919–935, 1987.

[7] Y. Dang, J., Tang, "Calculation of the Room-Temperature Shapes of Unsymmetric Laminates," in *International Symposium on Composite Materials and Structures, People's Republic of China*, 1986, pp. 201–206.

[8] W. J. Jun and C. S. Hong, "Effect of residual shear strain on the cured shape of unsymmetric cross-ply thin laminates," *Compos. Sci. Technol.*, 1990.

[9] W. J. Jun and C. S. Hong, "Cured Shape of Unsymmetric Laminates with Arbitrary Lay-Up Angles," *J. Reinf. Plast. Compos.*, vol. 11, no. 12, pp. 1352–1366, 1992.

[10] L. J. B. Peeters, P. C. Powell, and L. Warnet, "Thermally-induced shapes of

unsymmetric laminates," *J. Compos. Mater.*, 1996.

[11] M.-L. Dano and M. W. Hyer, "Thermally-induced deformation behavior of unsymmetric laminates," *Int. J. Solids Struct.*, vol. 35, no. 17, pp. 2101–2120, 1998.

[12] F. Mattioni, P. M. Weaver, and M. I. Friswell, "Multistable composite plates with piecewise variation of lay-up in the planform," *Int. J. Solids Struct.*, 2009.

[13] A. Pirrera, D. Avitabile, and P. M. Weaver, "Bistable plates for morphing structures: A refined analytical approach with high-order polynomials," *Int. J. Solids Struct.*, 2010.

[14] M. Schlecht, K. Schulte, and M. W. Hyer, "Advanced calculation of the room-temperature shapes of thin unsymmetric composite laminates," *Compos. Struct.*, vol. 32, no. 1–4, pp. 627–633, 1995.

[15] M. Schlecht and K. Schulte, "Advanced calculation of the room-temperature shapes of unsymmetric laminates," *J. Compos. Mater.*, 1999.

[16] M. Gigliotti, M. R. Wisnom, and K. D. Potter, "Loss of bifurcation and multiple shapes of thin [0/90] unsymmetric composite plates subject to thermal stress," *Compos. Sci. Technol.*, 2004.

[17] F. Mattioni, A. Gatto, P. Weaver, M. Friswell, and K. Potter, "The application of residual stress tailoring of snap-through composites for variable sweep wings," in *47th AIAA/ASME/ASCE/AHS/ASC Structures, Structural Dynamics, and Materials Conference
 14th AIAA/ASME/AHS Adaptive Structures Conference
 7th*, 2006.

[18] S. Tawfik, Xinyan Tan, S. Ozbay, and E. Armanios, “Anticlastic stability modeling for cross-ply composites,” *J. Compos. Mater.*, 2007.

[19] F. Mattioni, P. Weaver, M. Friswell, and K. Potter, “Modelling and applications of thermally induced multistable composites with piecewise variation of lay-up in the planform,” in *48th AIAA/ASME/ASCE/AHS/ASC Structures, Structural Dynamics, and Materials Conference*, 2007.

[20] F. Mattioni, P. M. Weaver, K. D. Potter, and M. I. Friswell, “Analysis of thermally induced multistable composites,” *Int. J. Solids Struct.*, 2008.

[21] P. Portela, P. Camanho, P. Weaver, and I. Bond, “Analysis of morphing, multi stable structures actuated by piezoelectric patches,” *Comput. Struct.*, 2008.

[22] E. Eckstein, A. Pirrera, and P. M. Weaver, “Morphing high-temperature composite plates utilizing thermal gradients,” *Compos. Struct.*, 2013.

[23] S. Annamalai, “Design of Bistable Composite Laminates for Shape Morphing Applications,” no. August, 2016.

[24] J. Etches, K. Potter, P. Weaver, and I. Bond, “Environmental effects on thermally induced multistability in unsymmetric composite laminates,” *Compos. Part A Appl. Sci. Manuf.*, 2009.

[25] P. F. Giddings, C. R. Bowen, A. I. T. Salo, H. A. Kim, and A. Ive, “Bistable composite laminates: Effects of laminate composition on cured shape and response to thermal load,” *Compos. Struct.*, 2010.

[26] D. N. Betts, A. I. T. Salo, C. R. Bowen, and H. A. Kim, “Characterisation and modelling of the cured shapes of arbitrary layup bistable composite laminates,”

Compos. Struct., vol. 92, no. 7, pp. 1694–1700, 2010.

[27] C. J. Brampton, D. N. Betts, C. R. Bowen, and H. A. Kim, "Sensitivity of bistable laminates to uncertainties in material properties, geometry and environmental conditions," *Compos. Struct.*, vol. 102, pp. 276–286, 2013.

[28] M. Moore, S. Ziaei-Rad, and H. Salehi, "Thermal response and stability characteristics of bistable composite laminates by considering temperature dependent material properties and resin layers," *Appl. Compos. Mater.*, 2013.

[29] S. A. Tawfik, D. Stefan Dancila, and E. Armanios, "Planform effects upon the bistable response of cross-ply composite shells," *Compos. Part A Appl. Sci. Manuf.*, 2011.

[30] M. L. Dano and M. W. Hyer, "The response of unsymmetric laminates to simple applied forces," *Mech. Compos. Mater. Struct.*, 1996.

[31] K. Potter, P. Weaver, A. A. Seman, and S. Shah, "Phenomena in the bifurcation of unsymmetric composite plates," *Compos. Part A Appl. Sci. Manuf.*, 2007.

[32] C. G. Diaconu, P. M. Weaver, and A. F. Arrieta, "Dynamic analysis of bi-stable composite plates," *J. Sound Vib.*, 2009.

[33] M. R. Schultz, "A concept for airfoil-like active bistable twisting Structures," *J. Intell. Mater. Syst. Struct.*, 2008.

[34] S. Daynes, P. M. Weaver, and K. D. Potter, "Aeroelastic Study of Bistable Composite Airfoils," *J. Aircr.*, vol. 46, no. 6, pp. 2169–2174, 2009.

[35] F. Mattioni, P. M. Weaver, K. D. Potter, and M. I. Friswell, "The application of thermally induced multistable composites to morphing aircraft structures," vol.

6930, p. 693012, 2008.

[36] A. F. Arrieta, P. Hagedorn, A. Erturk, and D. J. Inman, “A piezoelectric bistable plate for nonlinear broadband energy harvesting,” *Appl. Phys. Lett.*, 2010.

[37] D. N. Betts, C. R. Bowen, H. A. Kim, N. Gathercole, C. T. Clarke, and D. J. Inman, “Nonlinear dynamics of a bistable piezoelectric-composite energy harvester for broadband application,” *Eur. Phys. J. Spec. Top.*, 2013.

[38] D. N. Betts, H. A. Kim, C. R. Bowen, and D. J. Inman, “Optimal configurations of bistable piezo-composites for energy harvesting,” *Appl. Phys. Lett.*, 2012.

[39] D. N. Betts, H. A. Kim, and C. R. Bowen, “Static and Dynamic Analysis of Bistable Piezoelectric- Composite Plates for Energy Harvesting,” *53rd AIAA/ASME/ASCE/AHS/ASC Struct. Struct. Dyn. Mater. Conf.*, 2012.

[40] Fibre Glast, “Vacuum Bagging Equipment and Methods | Fibre Glast,” *Fibre Glast Developments Corp.* 2015.